DYNAMIC MODELLING AND EXPERIMENTAL VALIDATION OF THE CYCLIC OPERATION AND LOADED PULL-DOWN OF A CONVENTIONAL DOMESTIC REFRIGERATOR

by

Salman Mustafa Husain

B.S., Mechanical Engineering, Middle East Technical University, 2018

Submitted to the Institute for Graduate Studies in
Science and Engineering in partial fulfilment of
the requirements for the degree of
Master of Science

Graduate Program in Mechanical Engineering
Boğaziçi University

2021

To my parents….

ACKNOWLEDGEMENTS

I would like to begin by expressing my sincerest gratitude to my Thesis Supervisor Assoc. Prof. Dr. Hasan Bedir, who helped me in all stages of the process and provided me with valuable guidance at all times. His patient effort and constant support made this possible. Indeed, it was a great pleasure and honour to carry out this work with him. I would also like to thank the other jury members: Prof. Dr. Kunt Atalık and Asst. Prof. Dr. Murat Çakan, for taking valuable time out for evaluating this thesis and being present at my thesis defence.

To my former manager at Arçelik, Dr. Tolga Nurettin Aynur, who acted as a mentor figure and helped me in many steps; to my current Manager Dr. Serdar Kocatürk, who always provided valuable and detailed feedback; to my project leader Mutlu İpek, who devoted countless hours in teaching me modelling and aiding me like an elder brother; to Gökmen Peker for helping me in experimentation; to Akın Çağlayan for aiding me in modelling and helping with the Turkish abstract; to Tayfun Atsız and Uğur Cesur for preparing the experimental setup; and to all my other colleagues at work who helped in one way or the other: Thank you very much. I would also like to thank TLK-GmbH for the support they provided in modelling.

To my sister Ramla, who played a large role in my academic and personal development. She taught me the love of books at an early age and improved my mathematical ability immensely. Had these two skills not developed, I would have hardly made it through high school, let alone write this M.S thesis in engineering. Thank you so much sister.

Finally, to my parents: Azra and Mustafa. No amount of thanks and gratitude can balance what they have done and keep doing. Their unflinching support, diligent effort and constant love have been absolutely indispensable for any milestone I have ever achieved. The least I can do is to dedicate this to them. May God give them long and happy lives.

ABSTRACT

DYNAMIC MODELLING AND EXPERIMENTAL VALIDATION OF THE CYCLIC OPERATION AND LOADED PULL-DOWN OF A CONVENTIONAL DOMESTIC REFRIGERATOR

A dynamic model of a top mounted, conventional, serial system domestic refrigerator is created in this thesis using the TIL library in Dymola. The compressor is modelled semi-empirically using loss parameters obtained by model fitting simulation results and data from calorimeter experiments, while the capillary tube is modelled by incorporating both friction and momentum pressure drop. Heat exchangers (condenser and evaporator) are modelled as tubes divided into finite volume cells. The capillary tube-suction line heat exchanger is treated by connecting part of the capillary tube to the suction line via a heat resistor. As for the cabinet, the walls, air and items present inside the cabinet are connected to each other in a network, such that heat gained by the surroundings is transmitted to each component.. All the components are then arranged in a cycle, and several simulations are carried out. The cyclic operation is validated at 32 °C and 25 °C using a fixed speed compressor. To test the sensitivity of the model to a different compressor and different compressor speeds, simulations are carried out at 32 °C using a different compressor operated at three different speeds. As the second part of this thesis, the model is modified to include the effect of placing a warm load of water in the refrigerator and simulating the subsequent pull down. This model is also validated using an experiment in which 20 L of water at 27 °C is placed inside the Fresh Food compartment. Results show that the power consumption value is captured well, with the average power consumption deviating less than 10 % for all tests except for the loaded pull-down case. The energy consumption yielded even better results, with deviation lying within ±5% for all tests. For the loaded pull down, the deviation in water temperature was a maximum of 1.2 °C for the whole cooling period.

ÖZET

EV TİPİ KONVANSİYONEL BİR BUZDOLABININ DÖNGÜSEL ÇALIŞMA VE YÜKLEME SONRASI SOĞUTMA DAVRANIŞININ DİNAMİK MODELLENMESİ VE DENEYSEL VALİDASYONU

Bu tez çalışmasında, dondurucu bölmesi üst kısımda olan iki bölmeli, doğal taşınım ile çalışan, seri sistemli soğutma yapısına sahip ev tipi bir buzdolabının dinamik modeli oluşturulmuştur. Kompresör modeli, kalorimetre sonuçları kullanılarak istatiksel mantıkla çalışan bir program aracılığıyla parametrelere ait değerlerin hesaplanması ile elde edilmiştir. Kapileri tüp, modele hem sürtünme hem de momentum basınç kayıpları dahil edilerek modellenmiştir. Isı değiştirici (kondenser ve evaporatör) modelinde, sonlu hacimler yaklaşımıyla çözüm yapılmaktadır. Kapileri tüp ve dönüş borusu arasındaki ısı transferi mekanizması, ısıl portları arasına termal direnç elemanı eklenerek modellenmiştir. Buzdolabı kabin modelinde, her bir duvar elemanı, hava hacimi, kabin içerisindeki kütleler ve ortam arasındaki ısı transferi mekanizması gerçekleştirilmiştir. Tüm modelleme işlemi gerçekleştirilen modeller birbirine bağlanarak soğutma çevrimi modeli oluşturulmuştur. Buzdolabın döngüsel davranışı, sabit devirli kompresör kullanılarak 25 °C ve 32 °C ortam sıcaklıklarında gerçekleştirilen deneylerle doğrulanmıştır. Modelin değişen durumlara deney ile benzer hassasiyette davranıp davranmadığı anlamak için 32 °C ortam sıcaklığında farklı kompresör kullanılarak çeşitli devirler üzerinden karşılaştırma yapılmıştır. Tez çalışmasının ikinci kısmında ise, dolap içerisine yerleştiren daha yüksek sıcaklığa sahip su yüklerinin kabin sıcaklığına etkisi ve devamında su yüklerinin soğuma karakteristiği modellenmiştir. Hazırlanan model, 27 °C sıcaklığında 20 litre su kütlesi buzdolabının taze gıda bölmesine yerleştirildiği durum için yapılan deney ile doğrulanmıştır. Güç tüketim değeri için, yüklü test durumu harici diğer yapılan tüm karşılaştırmalarda %10'dan az fark görülmüştür. Enerji tüketim değeri ise, tüm karşılaştırmalarda ±%5 aralığı içinde uyumludur. Yüklü durum testinde, su kütlelerinin soğuma sürecinde maksimum fark 1.2 °C dir ve model ile deney benzer karakteristikte davranmıştır.

TABLE OF CONTENTS

LIST OF FIGURES

LIST OF TABLES

LIST OF SYMBOLS

A	Area *(m^2)*
d	Displacement *(m^3)*
D	Diameter *(m)*
E	Energy *(Wh/24h)*
g	Acceleration due to gravity *(m/s^2)*
G	Mass flux *(kg/m^2s)*
h	Enthalpy *(J/kg)* or Convective heat transfer coefficient *(W/m^2K)*
k	Thermal conductivity *(W/mK)*
L	Length *(m)*
m	Mass flow rate *(kg/s)*
n	Rotational speed *(Hz)*
p	Pressure *(Pa)*
P	Power *(W)*
Q	Heat transfer rate *(W)*
r	Pressure ratio
R	Heat resistance *(K/W)*
T	Temperature *(°C or K)*
U	Overall heat transfer coefficient *(W/m^2K)*
w	Uncertainty
Pr	Prandtl number
Re	Reynolds number
Ra	Rayleigh number
Nu	Nusselt number

α	Heat transfer coefficient for compressor shell (W/m^2K)
β	Thermal expansion coefficient (K^{-1})
γ	Specific heat ratio
ε	Emissivity or tube roughness (m)
λ	Thickness of tube (m)
ν	Kinematic Viscosity (m^2/s)
ρ	Density (kg/m^3)
τ	Shear Stress (Pa)

LIST OF ACRONYMS/ABBREVIATIONS

1-D	One Dimensional
ABS	Acrylonitrile butadiene styrene
ANN	Artificial Neural Network
CFD	Computational Fluid Dynamics
COP	Coefficient of Performance
CT-SL HX	Capillary tube-Suction line Heat Exchanger
FF	Fresh Food compartment
FRZ	Freezer compartment
RT	Compressor Run-Time

1. INTRODUCTION

One of the most important global issues facing us today is global warming and depletion of the earth's energy resources. It is therefore imperative that these valuable resources are used as efficiently as possible, so that further human progress does not come at the expense of future generations. One of the most effective ways to make use of natural resources is to make domestic appliances more energy efficient, since they are ubiquitous in households, and account for a large portion of the global energy consumption. The domestic refrigerator alone, for example, accounts for 6% of the world's electrical energy consumption [1].

The upper limit to the Coefficient of Performance (COP) of a refrigerator is set by the Carnot refrigerator, which is both externally and internally reversible. A Carnot refrigerator requires isothermal heat transfer and isentropic expansion/compression, both of which cannot be practically sustained by modern domestic refrigerators. Hence, the full Carnot COP can never be realised in reality. Enhancement of a refrigerator's COP therefore more often revolves around selecting the best system specifications such as capillary tube length and diameter, refrigerant charge amount, compressor type, cabinet wall thicknesses and heat exchanger dimensions in order to maximise cooling capacity and minimise average power consumption- in other words, maximise the COP, which is the ratio of the former two.

The bulk of such optimisation has been traditionally carried out using time consuming experiments, since they provide a "slow-but-(arguably) sure" way of reaching the best operating point (to this end, many manufactures have adopted sophisticated six sigma approaches which include carefully planned Design of Experiment (DOE) methods). For example, in one study by Diniz et al. [2], the performance of a refrigerator's compressor under different ambient and compartment temperatures was examined. Optimisation of the compressor speed, capillary tube flow capacity, and charge amount was studied by Yan et al. [3]. Tosun and Tosun [4] analysed the effect of capillary tube geometry and evaporator type and geometry on the energy consumption of a refrigerator. Fatouh and Ziyan [5] tested a refrigerator for different charge amounts of a refrigerant blend consisting of three different refrigerants. They did experiments for different capillary tube lengths, and, among other

important outcomes, found that the COP increases as the subcooling degree increases but decreases as the capillary tube length, pressure ratio and superheat increases. In another study by the same authors [6], the same blend was used to carry out experiments in order to determine the cyclic and transient characteristics of the refrigerator and compare it with the case of a single refrigerant (R-134a). It was found that a combination of 5.5 m of capillary tube length and 70g of the blend gives a COP about 3% greater compared to that of R-134a. To study the effect of the ambient temperature on refrigerator energy consumption, Harrington et al. [7] compiled experimental data conducted previously and plotted the energy consumption values at different ambient temperatures. They then noted that depending on the type of refrigerator, the power consumption at 16 °C is 30% to 50% lower compared to that at 32 °C. These two ambient temperatures are particularly important because the new International Standard requires testing at those two temperatures. As a final experimental study, Choi et al. [8] examined the effect of an oil-less compressor by removing oil from the system and measuring the energy. It was found that the power consumption of oil-less systems is actually reduced by about 4% compared to conventional systems.

Experimentation is time consuming and very costly and runs the risk of not reaching an optimum value if all the factors are not examined. Modelling of the refrigeration cycle can speed up the optimisation process greatly, since simulations can be run much faster, and can eliminate unwanted noise factors inherent in experimentation. Moreover, many important system parameters such as capillary tube length and charge amount can be tweaked in the model without the risk of increased cost. This “free” tweaking of system factors can reveal a great deal of information regarding the optimum operating point, allowing the production of much more energy efficient refrigerators. While experiments will still be needed to reach a conclusive decision, reliable models can drastically reduce the total number of experiments required otherwise. It is thus no wonder that many studies have started focusing on different modelling approaches over the past two decades. Such studies range from very basic steady state models to full-fledged transient models including 3-D CFD based cabinet models.

This thesis involves modelling a *top-mounted, conventional and serial system* refrigerator dynamically. While details will be presented in later sections, a few words about the type of refrigerator are in order. “Top-mounted” refers to the common type in which the

Freezer compartment (used to store frozen food around -18 °C) is situated at the top while the Fresh Food compartment (used to store unfrozen food at around 2-6 °C) is at the bottom of the cabinet. “Conventional” refers to refrigerators not equipped with a fan and defrost heater inside. That is, they operate solely by natural convection and radiation heat transfer. Finally, “serial” system refers to the refrigeration circuit, with the implication that the evaporators present in the Fresh Food and Freezer compartment are connected to each other in series.

This study thus focuses on creating a dynamic model of the above type of refrigerator to model the cyclic behaviour of the appliance as the compressor turns on and off according to a thermostat. The cyclic behaviour is validated for different ambient temperatures and compressor types and speeds. Moreover, the addition of warm water into the Fresh Food compartment and its subsequent pull down to a cooler temperature is modelled and validated. Chapter 2 includes a detailed literature review regarding refrigerator modelling, after which the gaps are identified, and the objective of this thesis reiterated in Chapter 3. A brief description of refrigeration is included in Chapter 4 as a refresher, followed by a detailed description of the modelling methodology for both the cyclic operation and warm water pull down in Chapter 5. The details of the experimental method used for validation are described in Chapter 6. Finally, the simulation and experimental results are presented for both cyclic operation and loaded pull down in Chapter 7. Conclusion and References form the last two chapters of this thesis.

2. LITERATURE REVIEW

There have been many different approaches to modelling over the past years in the field of refrigeration. These can generally be classified into steady state and dynamic models. In the former, the transient nature of all the components of the refrigerator (compressor, capillary tube, heat exchangers and cabinet) is neglected, while in the latter, details of the time-varying nature of all the components are captured in as much detail as possible.

The main advantage of the steady state approach is that it has low computational cost and can give faster results. However, it does not show the transient behaviour of all the components, which is a serious shortcoming because the time-varying nature of the components is needed to improve the system. For example, the actual heating and cooling durations of the air temperature give useful information regarding the thermal inertia of the cabinet, which may be increased by placing a Phase-Change Material (PCM) inside [9]. Another case where transient behaviour is important is in the case of pull down (i.e., when a warm refrigerator is first turned plugged in, and the cabinet cools down with time, often taking several hours before reaching cyclic state), which cannot be captured by a steady state model. All of these drawbacks are handled by a transient model, which gives information regarding the dynamic behaviour of the components. Of course, a transient model is more expensive computationally, but the cost is justified considering the useful insight it offers.

The level of detail for each component model depends on the resources available for the study, its scope and the specific objective at hand. For instance, if the study is only focusing on the final energy consumption value, there is no need to capture the detailed 3-D temperature distribution of the cabinet. Conversely if the main objective is to assess the air flow and temperature contours inside a compartment, the cabinet model might be modelled in full detail, while the other compartments may be treated using very simplistic relations using the first law of thermodynamics.

Section 2.1 presents two review papers regarding refrigerator modelling. In the next two sections (Section 2.2 and 2.3), keeping in mind the above classification, steady state and

transient modelling literature is presented. Finally, some other important papers not exactly fitting in these two sections are included in Section 2.4.

2.1. Review Papers

As the first paper, it is worth mentioning Ding's [10] excellent review paper explaining the progressive development in simulation techniques for vapor-compression refrigerant systems. The types of models available for each component were described. For example, for the compressor it was mentioned that both steady state and dynamic models are available although steady state is preferred in most studies. For the capillary tube, the "homogeneous" and "separated" approaches were explained. Homogeneous implies the treatment of the two phase region as a uniform mixture of liquid and gas, and this approach often underestimates the mass flow rate. In the separated approach, the two phases are treated as two separate regions consisting of liquid and gas, with a slip ratio defined where they interact. While being more accurate, the separated approach can give different results under different runs, since the method used to reach the solution becomes important in this technique (in the homogeneous approach only the working conditions are important). The review paper also described various modelling approaches for the cabinet (referred to as "envelope structure" in the paper). Details about the various techniques falling under control theory, such as the Z-transfer function method and state space methods were explained.

Another review paper was by Flores et al. [11]. Although that was a more general review regarding enhancing refrigerator performance, a whole section was devoted to modelling studies carried hitherto. Major studies were described, and it was noted that both steady state models and dynamic models have their advantages. The use of Artificial Neural Network in modelling was also mentioned briefly. Approaches used to model some of the components were also presented, such as the various empirical models used for calculating the mass flow rate of capillary tubes.

2.2. Steady State Approaches

Davis and Scott [12] laid out general guidelines for refrigerator modelling in what may be termed as the earliest attempt at modelling. The authors described losses inside the compressor and showed how to calculate the mass flow rate using volumetric efficiency. The volumetric efficiency is the ratio of the amount of refrigerant successfully compressed and discharged to the total compressor displacement. The two are not equal because of leakages that occur as valves open and close, and re-expansion of the refrigerant trapped in the clearance volume at the end of the stroke (i.e., when the compressor reaches top dead centre). The authors thus multiplied the efficiency by the total compressor displacement (divided by the refrigerant specific volume at the inlet) to get the mass flow rate. The use of empirical data to calculate unknown parameters was also suggested. The other component the authors focused on was the heat exchanger. It was suggested to divide it into two (for evaporator) or three (for condenser) zones, with one zone being two-phase while the others being single phase (both superheated vapor and subcooled liquid occur in the condenser-hence two single phase zones are needed for a condenser; in contrast, only superheated vapor occurs in the evaporator). For modelling heat transfer in each zone, correlations were suggested for the single phase region, while empirical constants were advised for the two phase region (understandably, since two-phase heat transfer is much more complex). This study only focused on these two components; however, it deserves mention since it was the first real attempt at a detailed model for refrigerators.

In another early study, Chen et al. [13] presented a generalized model of the refrigerator by taking into account both external and internal irreversibilities. The approach was fully analytic, in which the authors started with the Carnot efficiency, and then introduced external irreversibilities by defining heat transfer between the evaporator and cabinet, and the condenser and surroundings. After handling this external irreversibility, internal irreversibilities such as friction and turbulence were introduced. Finally, the heat gain entering the cabinet via conduction through the walls was also considered using heat transfer relations. These relations were combined with the first and second law of thermodynamics to get a formula for the COP for different cases (fully reversible, externally reversible, fully irreversible) in terms of the cooling capacity. The cooling capacity was then graphed against the COP, and it was noted that the relation is parabolic for internally

irreversible cycles- in contrast to internally reversible ones, for which the COP decreases monotonically as cooling capacity increases.

Gupta et al. [14] obtained the temperature and velocity distribution in the Freezer and Fresh Food compartment using CFD. A 3-D unstructured mesh was used and solved for steady state. The temperature and velocity profiles across different cross sections (height-wise and width-wise) were obtained in both the compartments, and the model was validated through experimentation by keeping the compressor running until the cabinet got cold enough to be balanced by the heat gain and thereby attain steady state. The deviations in the results were attributed to lack of knowledge of the exact air flow and heat leakage into the compartment due to the gasket and hot compressor present at the back.

To predict the energy consumption of household refrigerators, Hermes et al. [15] used a steady state approach. The compressor was modelled using control volume relations, with the mass flow rate obtained using volumetric efficiency and the power obtained using isentropic efficiency. The capillary tube-suction line heat exchanger as well as other heat exchangers (evaporator and condenser) were modelled using heat exchanger effectiveness relations. The cabinet model was more interesting; the heat gain into the cabinet was equated to the total cooling capacity minus the fan work. This cooling capacity was found by multiplying the air flow rate through each compartment by the evaporator's heat transfer rate. The air pressure drop across the fan was calculated using fan characteristic curves. To calculate the condenser and evaporator pressures, the saturation pressure at a given evaporation/condensation temperature was adjusted for superheat and subcool and the resulting value was obtained from refrigerant data. The final solution algorithm was as follows: the evaporation, condensation, subcool, superheat and desired cabinet temperatures were taken as inputs, and the algorithm solved for the final energy consumption. Engineering Equation Solver (EES) was used, with RefProp 7 to obtain refrigerant data. The model was validated against experiment, and the results were 5% off. In addition, a sensitivity analyses for different compressor speeds, compressor stroke, number of condenser tube rows and number of evaporator fins was carried out. All in all, this was comprehensive steady state modelling study.

In a similar study to the previous one, Gonçalves et al. [16] used a steady state model to predict the cooling capacity and power consumption. The compressor was again modelled using efficiency, although the efficiencies themselves were obtained using empirical relations. The heat exchangers were treated by using different overall heat transfer coefficient values for the subcool, superheat and saturated phases. The pressure drop through the heat exchangers was calculated using Moody friction factor. For the capillary tube, a set of π-groups were used. These groups were basically dimensionless parameters obtained using the length and diameter of the capillary tube, subcool temperature, superheat temperature and evaporation and condensation pressures. The coefficients of these parameters were found empirically using experimental data. These parameters were used to calculate the mass flow rate. The final results for compressor power and internal air temperature showed 5% and 4.5 °C deviation respectively.

2.3. Transient and Quasi-Steady State Approaches

Ding et al. [17] created a dynamic model of a natural convection bypass cycle refrigerator. In this study, the component models were presented in detail. The compressor model was comprised of two parts: the shell and the cylinder. The latter was basically where the compression took place, and for this, the mass flow was calculated using volumetric efficiency while the power was calculated using a polytopic compression relation. The shell model was used to model the convective heat transfer between the shell and the ambient. For the heat exchangers, a multizone model was used. The zones were basically divided according to the phase the refrigerant was in (single phase vs two-phase). The capillary tube was modelled into two parts; the adiabatic part-in which the capillary is fully insulated, and heat transfer from capillary tube to any other component can be neglected- was treated as a simple steady state tube, while the diabatic part – in which the insulation is removed and the capillary tube is in contact with the suction line so that heat exchange can occur- was modelled by introducing extra subcool. Finally, for the cabinet model the heat gain was calculated, and the transient nature was modelled by using expressions for the thermal capacitance of the lumped volume inside.

As a continuation of the above study, Lu et al. [18], carried out the actual simulation and validation in this study. The predictor-corrector method and adaptive integration time-step method were used as the solution methods for the system algorithm. The simulation results were compared to experimental data obtained by testing a Haier BCD-188 RF model refrigerator and the agreement was good except for the first start-up process. This was imputed to the poor lubrication of the compressor at first start-up.

In a study by Hermes and Melo [19], the heat exchangers were divided into control volumes (pressure drop was neglected). Single phase and two phase heat transfer correlations were used to model heat transfer. The capillary tube was treated as 1-D, quasi-steady flow, and homogenous. The friction factor for flow through the capillary tube was obtained using Churchill's relation (the relation used to draw the Moody chart). The compressor was divided into two domains: the compressor shell and the compression process. As for the cabinet model, it comprised of wall layers, with the inner air mass being treated as a lumped mass. Final results showed a deviation of 10% in the energy consumption.

The model of the previous study was used by Hermes and Melo [20] in a subsequent study to carry out a sensitivity analysis for the capillary tube-suction line heat exchanger, compressor speed, internal air flow rate and temperature range of the thermostat. It was found that the energy consumption could be reduced by 8% by changing the capillary tube inner diameter to 0.6 mm and the heat exchanger length to 2.34 m and using a charge of 80g. Another interesting finding was that the energy consumption decreases when the temperature range of the thermostat increased but only if the cut-out temperature is not extremely low. The cut-out temperature is the lower threshold of the thermostat range; the compressor turns off upon reaching this value. The finding implied that for greater thermostat ranges energy consumption decreases since the compressor runs longer and peak power values occurring at start-up are minimized. But too low a cut-out temperature leads to the compressor running for very long periods, so much so that the advantage from reduced start-up losses is offset by the increased duration for which the compressor does work.

Borges et al. [21] used a somewhat different approach by creating a quasi-steady state model. This was done to have reasonable computation time while capturing the transient behaviour of the air temperature at the same time. In this approach, the system components

(namely, compressor, condenser, capillary tube and evaporator) were modelled as steady state, whilst the cabinet was modelled as transient, by treating the compartments as lumped masses. Results were not bad, with a maximum deviation of 2% in the compressor run-time and energy consumption. A sensitivity analysis was also carried out for the evaporator and condenser conductance values.

Lin et al. [22] created a very detailed dynamic model of the refrigerator. The most striking feature of the study was the cabinet model, which was created using the Z-transfer function method. The method was used to model the heat gain and transient temperature behaviour of the air inside the cabinet. In this method, equations were written in state space, and then converted into the Z domain, and solved thereafter. It was claimed that this method is quicker (40000 times faster!) than conventional difference equation methods to model the dynamic behaviour of air in the cabinet. Besides the cabinet, the other models were simple; the compressor was modelled semi-dynamically, with the outputs yielding the power and discharge temperature. The heat exchangers once again were divided into zones. For the capillary tube-suction line heat exchanger, an “effective enthalpy” method was used, in which the capillary tube’s inlet enthalpy was adjusted by adding extra subcooling to account for the heat exchanger

A study done specifically for heat exchanger validation was carried out by Bergera et al. [23], in which a transient 1-D model was made. The heat exchanger was divided into cells, and the first law of thermodynamics was solved for each cell. Two-phase region was treated using the void fraction approach. In this, the vapor and liquid phases are treated separately, and a slip ratio is defined based on the separate velocities each phase. The slip ratio is in turn used to define the so-called void fraction, which is then used to calculate pressure drop and other significant quantities The general model was then extended for a wire-on-tube condenser, by considering the wire as simply part of the conduction resistance of the tube (the tubes themselves were modelled directly just as straight tubes). For validation, a special experimental rig for wire-on-tube condensers was used. The start-up transients were captured well by the model, with deviations attributed to errors in mass flow rate measurement and uncertainties in heat transfer coefficient.

Heimel et al. [24] aimed to create a reliable simulation tool for examining the energy consumption and cycle efficiency. To do this, they studied the transient refrigerant distribution and the impact of a component's thermal inertia as well as the time dependant heat transfer. The compressor was modelled semi-empirically, with parameters used in polytropic relations coming from experimental data. It was mentioned that this approach is much better than using experimental data directly to create a regression-based model, which is limited in the sense that it does not allow extrapolation. The capillary tube was treated as homogeneous (i.e., not void fraction) and 1-D. The code was used to generate data for Artificial Neural Network (ANN). More than 30000 data points were used to train the algorithm. Finite volume distributed parameter approach was used to model the heat exchangers (evaporator and condenser). In this approach, the heat exchangers are treated as 1-D tubes, divided into volumes. The mass and energy conservation equations are applied to each volume. The cabinet model was comprised of 6 walls divided into 20 layers. Air inside was treated as a lumped mass. All the models were then coupled to each other, and simulations were run. A mean deviation of 7% was observed in the energy consumption and run-time ratio.

As a final study for the transient modelling approach, Egger et al. [25] created models for each component and then combined the models in a software. The heat exchangers were divided into a finite number of control volumes and the heat transfer and friction factor was calculated using relevant correlations. The compressor model was divided into three parts: housing, oil reservoir and the compressor itself. The parameters were fitted according to calorimeter measurements. To model the capillary tube, a previously validated 1-D model was used in conjunction with ANN: Around 40000 simulations were used to train the ANN, so that the model could be used for various boundary conditions. The overall cycle was then simulated; results for the power consumption and run time were in good agreement.

2.4. Other Studies

Some other relevant studies are now presented.

Relatively few refrigerator modelling studies related to Modelica could be found, hence this particular one by Heinrich and Berthold [26] deserves mention. In this study, a Modelica library was created using component models. A detailed compressor model was prepared, including heat transfer into the oil, which forms a significant portion of the compressor. Refrigerant sorption in the lubricant oil was also modelled. For the heat exchangers, Shah's correlation was used for the heat transfer coefficient at the refrigerant side. Moreover, the void fraction approach (explained previously) was used to model two phase flow. The capillary tube was modelled as discretized finite volumes.

Avcı et al. [27] used CFD and ANN to optimise the parameters affecting the total cooling capacity in the cabinet (at steady state). The CFD model for the cabinet was 3-D, and the mesh structure had a total of 1768081 tetrahedral elements. Inlet and outlet regions of the fan box were densely meshed. Turbulent air flow, natural convection, forced convection and radiation were included. The ANN model was then created by using 50 data points to train the algorithm. The model was used to predict the optimum values for the evaporator height, average air velocity at fan outlet, and placement of the fan box on the rear wall.

In another CFD study, Bayer et al. [28] carried out a 3D discretization of the refrigerator cabinet to model the turbulent, coupled and non-linear flow of air in the cabinet. The main aim was to simulate the fluid flow and temperature distribution in the cabinet. Experimentally determined temperature values were used as constant wall temperature boundary condition.

So far, all the studies focused on an empty cabinet, that is, a cabinet which has no food or other load inside it. In a study by Laguerre and Flick [29], however, a steady state model of the cabinet with load placed inside was created. The main equations were the usual heat transfer equations between cold wall and air and the load and air. Radiation was also taken into account. After the physical model had been established, a matrix equation was formed,

containing all the various temperatures as unknowns, including the room temperature and thermostat temperature. These latter two were taken as stochastic inputs (that is, they were treated as random variables having a normal distribution) to the model, and the resulting simulation gave the air and load temperatures as stochastic outputs (again, normally distributed). The results were in very good agreement, with the approximately 1 °C deviation in air and load temperature attributed to heat transfer coefficients.

3. OBJECTIVE

3.1. Gaps in Literature

The above literature review section shows several gaps not addressed by any study to the best of the author's knowledge. Firstly, no study could be found which handles all the losses present in the compressor using empirical parameters. The closest semi-empirical compressor model was the study by Heimel et al. [24], who used experimental data to fit weighing parameters used to calculate the volumetric and electric efficiency of the compressor. But even in that study other losses such as pressure drop at the inlet and frictional losses were not modelled, and empirical data was not used to calculate parameters which lead to an accurate calculation of the cooling capacity. Secondly, most refrigerators run according to an algorithm which has information regarding the so-called cut-in and cut-out temperatures, which are set-point temperatures governing the on-off operation of the compressor. No model could be found which enables a user to define these set-point temperatures, so that the compressor performs the cycles as it would in reality. Finally, and possibly the biggest void in present literature is the simulation of a warm load as it is pulled down after having been placed inside a previously cool refrigerator. Assessing the performance of this load pull-down is important because it is a realistic measure of how quickly a refrigerator can cool down a certain mass of warm water. This test, referred to as the "Water Pot Test" in this study, may be used in determining the size of the evaporator, and is a requirement for some manufacturers, especially in tropical countries where hot summers are more prevalent and obtaining cold water quickly is extremely desirable. Thus, it is about time a model is created which can simulate this test.

To summarize, the following gaps are present in refrigerator modelling literature:

i) A semi-empirical compressor model with all the loss parameters treated explicitly.
ii) An appropriate algorithm allowing temperature feedback to the compressor (through cut-in and cut-out temperatures).
iii) Modelling and validation of loaded pull-down.

3.2. Thesis Objective

The first objective of this thesis is to create a dynamic model of top-mounted, conventional refrigerator with serial cooling system and validate the cyclic behaviour of the refrigerator using experiments. A sensitivity analysis for different compressor speeds and ambient temperatures is also performed and validated. The second objective is to model and validate the loaded pull-down behaviour of the refrigerator. This directly fills the third gap mentioned above, while the first two gaps are addressed by using a compressor model treating all the loss parameters and embedding an algorithm which enables input of the set-point temperatures.

4. BRIEF THEORY ABOUT REFRIGERATION

A refrigerator comprises various components, each of which may be modelled using different methodologies. An adequate model must ensure that the main features of all the individual components are captured so that the final refrigerator model gives reliable results.

A serial system refrigeration cycle consists of a compressor, condenser, capillary tube, evaporator and a capillary tube-suction line heat exchanger (CT-SL HX). Refrigerant, which is commonly Isobutane (also known as R600a) passes through all these components in a loop, thereby enabling heat to be transferred from the lower temperature in the cold storage cabinet to the higher temperature of the surroundings. Of course, as per the Clausius Statement of the second law, work must be done in order to accomplish this, and indeed electrical work is supplied to compressors in order to compress the refrigerant after it passes through the evaporator.

The compression process raises both the temperature and pressure of the refrigerant. This high-temperature vapor then flows into the condenser, where it loses heat to the ambient and thereby condenses into liquid. Although the main aim is to convert vapor into saturated liquid, oftentimes large condensers are designed to further cool the refrigerant so that it becomes sub-cooled. Subcooling increases the efficiency of the cycle. After passing thorough the condenser, the fluid then passes through a very narrow (~1mm diameter) capillary tube, where, it drops in pressure and temperature and exits as low-quality two-phase fluid. Most refrigerators use a CT-SL HX to sub-cool the refrigerant even more. Another important function of the CT-SL HX is to ensure that the refrigerant exiting the evaporator is fully vaporized before entering the compressor (this is often referred to as superheating). This is vital because liquid can greatly damage the internal components of a compressor. The refrigerant exiting the capillary tube enters the evaporator. In a serial system refrigerator, the evaporators for both compartments (Fresh Food and Freezer) are connected in series- that is, the refrigerant directly enters the second evaporator after passing through the first one. Heat is transferred from the warm cabinet air to the evaporator, thereby maintaining cool conditions inside the cabinet.

Other details pertaining to each component are discussed in later sections. At this point, however, it will be worthwhile to present a schematic of the serial system refrigeration cycle:

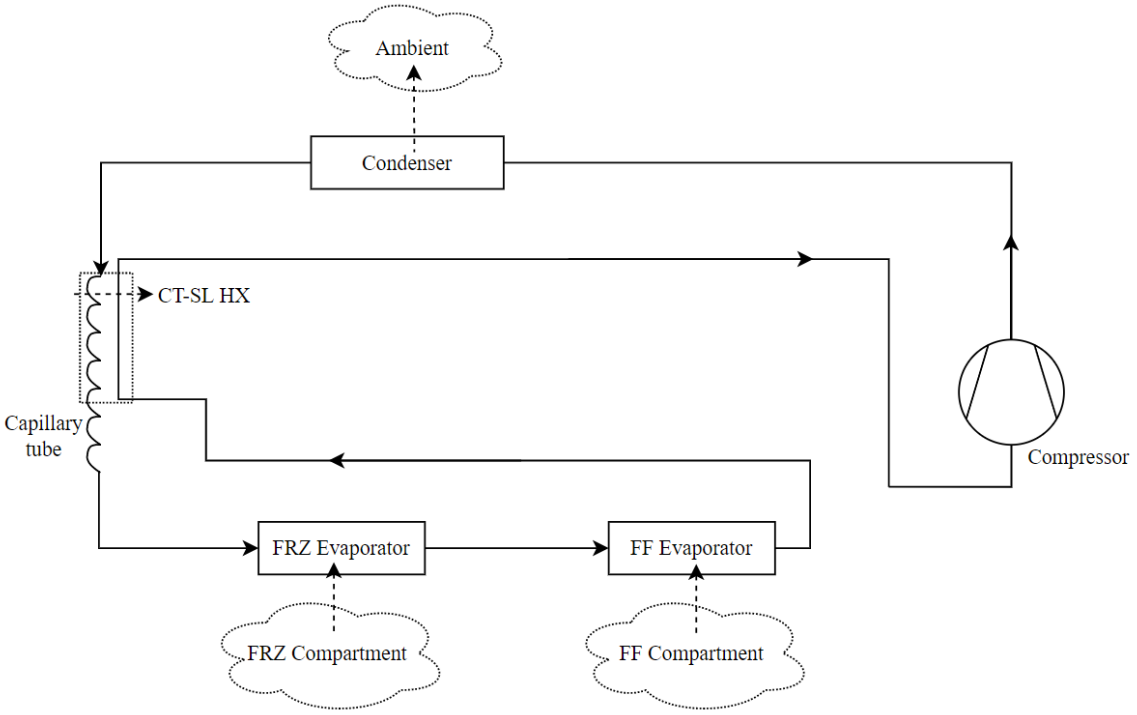

Figure 4.1. Serial System Refrigerator Circuit.

As Figure 4.1 above shows, the Fresh Food (FF) compartment evaporator and Freezer (FRZ) compartment evaporator are connected in series, hence the name “serial cycle”. The solid arrows show the direction of fluid flow, while the dashed arrows show heat transfer.

5. MODELLING DETAILS

Having discussed the theory, the details of each component model, followed by the full cycle model, and finally the modified model for simulating the loaded cabinet will be described in the following sections. A software called Dymola (by Dassault Systems), based on the object-oriented programming language Modelica, was used for modelling. Almost all of the base classes were taken from a thermodynamic systems library called TIL, created by TLK-GmbH.

5.1. Compressor Model

A compressor forms the heart of a refrigerator, since it maintains the pressure difference between condenser and evaporator and thereby ensures that the refrigerant keeps on flowing. Moreover, it directly determines the energy consumption of the refrigerator, and should therefore be modelled as accurately as possible. For domestic refrigerators, the positive-displacement and reciprocating type compressor is used most widely.

It is usually assumed that a compressor performs the compression process isentropically. For such an ideal compressor, the power can be given simply by the first law relation:

$$P_{isentropic} = m\,(h_{2s} - h) \tag{5.1}$$

where m is the mass flow rate, h_{2s} is the outlet enthalpy assuming isentropic compression, and h is the inlet enthalpy.

However, real compressors are anything but ideal, and several losses are therefore present which introduce irreversibility and make the compression process non-isentropic. These losses, along with brief descriptions, are listed as follows:

• Pressure drop at suction side: As the refrigerant moves into the compressor through the inlet valve, some pressure drop occurs. This reduces the inlet pressure, and therefore increases the pressure ratio of the compressor.

• Pressure drop at discharge side: Similarly, pressure drop occurs as high pressure refrigerant is discharged through the discharge valve.

• Friction as the piston moves: Mechanical friction between the piston and cylinder.

• Re-expansion of the refrigerant: This occurs due to the presence of a clearance volume at the end of the compressor stroke. The clearance volume is deliberately kept to allow for thermal expansion and tolerances in manufacturing. Due to this clearance volume some amount of refrigerant is left in the compressor at the end of the discharge stroke. This implies that once the suction stroke starts, the suction valve cannot open immediately since there is high pressure refrigerant inside the cylinder at the discharge pressure. Only when the volume increases and the pressure of the refrigerant inside drops does the suction valve open and fresh low-pressure refrigerant is able to enter the compressor. Thus, there is a certain amount of re-expansion of the refrigerant after the discharge stroke. This means that the full swept volume of the compressor cannot be utilized to pressurize the refrigerant; a certain amount of volume must be forgone to allow for re-expansion, and this causes the mass flow rate to be lower than the ideal case with no re-expansion. This gives rise to a volumetric efficiency, as was explained in Section 1.1 while discussing a previous study.

• Internal Leakage: Refrigerant leakage across the cylinder walls and piston.

• Heat transfer at suction and discharge side: heat transfer from the compressor to the ambient at the discharge side and vice versa for the suction side.

A schematic showing the above losses is shown in Figure 5.1.

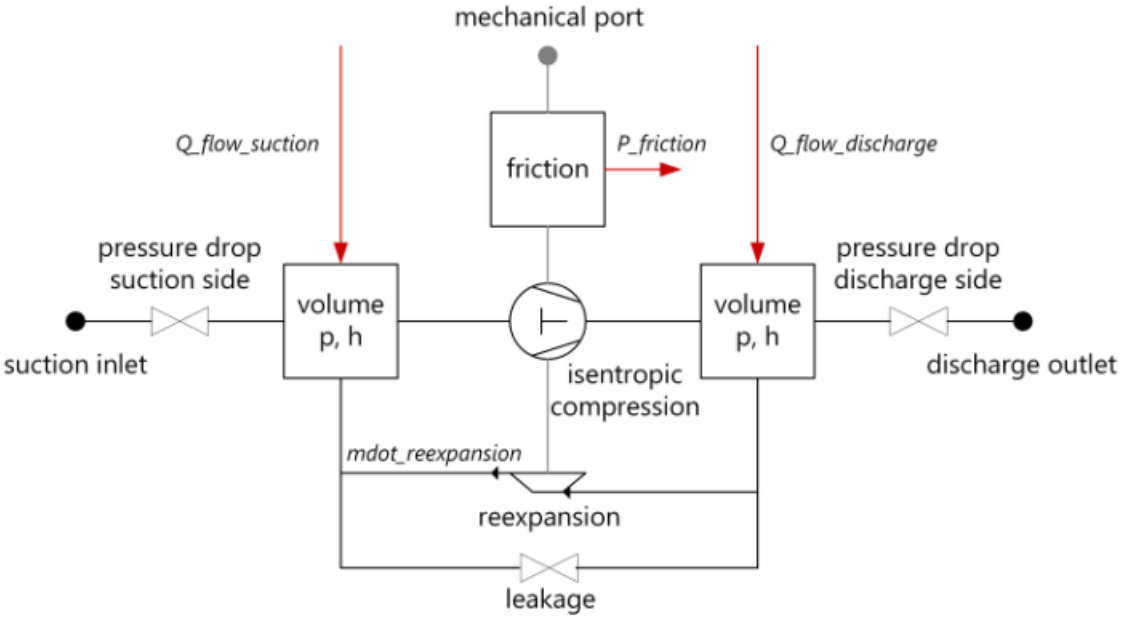

Figure 5.1. Losses in a compressor.

Due to the above losses, a real compressor is not isentropic. To calculate the aforementioned losses, several equations are used in the compressor model present in TIL library. These will be shown next.

5.1.1. Compressor Model Equations

A reciprocating compressor model is already present in the TIL library of Dymola. This model handles all of the losses mentioned above, except for the heat loss at the suction side, which is neglected. This is reasonable since the refrigerant temperature at the suction side is not very different from the ambient (except during initial start-up). These losses are used in conjunction with the transient form of the mass and energy balances to obtain the actual mass flow rate and power values. The equations used to calculate each loss are presented next.

5.1.1.1. Pressure drop and internal leakage

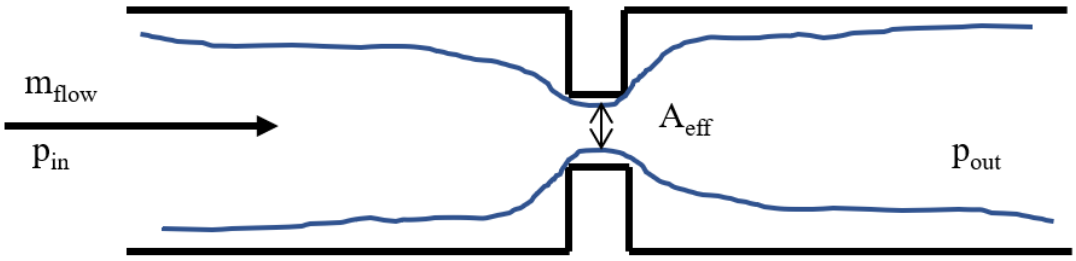

Figure 5.2. A schematic showing the loss of pressure across a narrow constriction. This is the logic upon which Saint Venant-Wentzel equations are based.

The Saint Venant-Wantzel [30] equation (Equation 5.2 below) is used to calculate the pressure loss at the suction and discharge sides, as well as the mass flow leakage (i.e. leakage from discharge to suction side due to the pressure difference):

$$m_{flow} = \varphi A_{eff}\sqrt{2p_{in}\rho_{in}} \tag{5.2}$$

where m_{flow} is the internal leakage flow rate, shown in Figure 5.2 above, φ is a factor calculated using Equations 5.3 or 5.4 below, A_{eff} is the effective area and is one of the 9 parameters to be found empirically (all the parameters are listed at the end). p_{in} is the pressure at the inlet (may be suction or discharge depending on the case), and ρ_{in} is the inlet density (which again may be the suction or discharge side).

The pressure ratio $r = \frac{p_{out}}{p_{in}}$ is critical in the calculation of φ. If $r > \left[\frac{2}{\gamma+1}\right]^{\frac{\gamma}{\gamma-1}}$,

$$\varphi = \frac{\gamma}{\gamma-1}\sqrt{\left[\frac{p_{out}}{p_{in}}^{\frac{2}{\gamma}} - \frac{p_{out}}{p_{in}}^{\frac{\gamma+1}{\gamma}}\right]} \tag{5.3}$$

However, if $r < \left[\frac{2}{\gamma+1}\right]^{\frac{\gamma}{\gamma-1}}$,

$$\varphi = \left(\frac{2}{\gamma+1}\right)^{\frac{1}{\gamma-1}} \sqrt{\frac{\gamma}{\gamma+1}} \tag{5.4}$$

where γ is the specific heat ratio of the refrigerant.

The pressure loss at the suction and discharge sides is calculated using Equation 5.2 by taking the mass flow rate through the compressor as the input (this will change according to the compressor on and off state).

Once the pressure drop at both the suction and discharge sides is known, the mass flow leakage is found by simply using the discharge pressure plus the associated pressure drop as the inlet, and suction pressure minus the associated pressure drop as the outlet pressure in Equation 5.2. (Note: leakage occurs from high pressure to low pressure side, or from right to left in Figure 5.2).

5.1.1.2. Friction loss

$$P_{friction} = fn + n^2 f_{piston} \tag{5.5}$$

where $P_{friction}$ is the power loss due to friction, f is the friction factor, n is the rotational speed, and f_{piston} is the friction factor associated with the piston, and d is the displacement (note: the friction factors are not dimensionless)

5.1.1.3. Re-expansion of compressed fluid

$$m_{re-expansion} = \left(S_{dead} + t_{delay}\right) n \rho d \tag{5.6}$$

where S_{dead} is the relative dead space, which is the clearance volume on top of the piston after compression expressed as a percentage of total displacement, t_{delay} is a measure of the delay in the closing of the valve at high speeds, ρ is the outlet density of the refrigerant vapor

under isentropic conditions, d is the displacement, and n is the rotational speed of the compressor.

5.1.1.4. Heat transfer loss at the discharge side

$$Q_{flow,dischage} = P_{friction} + \alpha A\left(T_{ambient} - T_{discharge}\right) \quad (5.7)$$

where $Q_{flow,dischage}$ is the net heat transfer into the compressor, $P_{friction}$ is the friction loss (can be considered as a heat generation term), α is the heat transfer coefficient, and A is the area of the compressor shell.

5.1.2. Semi-empirical parameters

As may be observed from the above equations, several of the terms are not known and cannot be calculated using theoretical calculations. To this end, the required 9 parameters are obtained semi-empirically by using a model fitting technique. The parameters are:

- d
- A_{eff} (3 different for suction, discharge, and leakage)
- f
- f_{piston}
- S_{dead}
- t_{delay}
- αA

To perform model fitting, compressor map data is compared with simulation results from a compressor "tester" model. Compressor map data is obtained by carrying out calorimeter experiments in which the compressor is connected to a condenser and evaporator maintained at specified temperatures. Refrigerant flows through the circuit as it would in a refrigerator, but the conditions are controlled by keeping the evaporator at a desired temperature using heaters powered externally. The subcool and superheat temperatures are also kept at fixed values. Using various values of the evaporation, condensation, subcool and superheat temperatures as inputs, corresponding values for the mass flow rate, power

consumption, cooling capacity and discharge temperature are obtained as outputs. To get simulation results for these outputs, the same evaporation, condensation, subcool and superheat temperatures are supplied to the model, along with guess values for the nine parameters listed above. Note that one of the outputs is cooling capacity, which may seem misplaced considering that the compressor does not directly provide the cooling in a refrigerator. However, the compressor is the major component which determines the mass flow rate through the refrigeration circuit, and since cooling capacity is given by Equation 5.8, the cooling capacity (Q_c) is also included as a major parameter which governs compressor performance:

$$Q_c = m\left(h_{evaporator,outlet} - h_{evaporator,inlet}\right) \tag{5.8}$$

where m is the mass flow rate through the evaporator, and h denotes enthalpy. The inlet and outlet evaporator enthalpies are obtained using thermodynamics tables, since the state points are fixed by the subcool, superheat, condensation and evaporation temperatures.

Model fitting is performed using least squares minimization. In this method, initial values for the above parameters are utilized by the model to create an initial set of outputs, which are then compared to their experimental counterparts. The resulting residuals are compared to a minimum desired value set by the user, and the difference is used by an algorithm to predict new parameter values. This process is repeated until the minimum residual level is reached. The algorithm employed in this study is the Levenberg-Marquardt Algorithm [31]. This is a combination of the more popular Gradient Descent and Gauss-Newton methods. Gradient descent is more effective when the results are far off from the optimum, whereas Gauss-Newton is better when the results are close to the optimum. Levenberg- Marquardt utilizes the benefits of both, by defining a parameter whose value is adjusted based on the distance from the optimum. Detailed equations are not presented here, since this is a very deep topic in and of itself. Nonetheless, further information can be found in [31].

The model fitting algorithm is embedded in a macro excel file written by TLK-GmbH (named “Modelfitter”). The experimental data is entered in this file, while simulation results are obtained using the tester model described above. A functional mock-up unit (fmu) of the

model is used to store the simulation outputs in the excel macro file. The fmu file is part of the functional mock-up interface (fmi), a cross-platform interface which allows models from one platform to be read by another platform. This fmu file is thus read by Modelfitter, and the algorithm then finds the best parameter fits to match the experimental data.

A schematic of the process can be seen in Figure 5.3. Note that the evaporation, condensation, subcool and superheat temperature are inputs, while the discharge temperature, power input, cooling capacity and mass flow rates are outputs. As explained above, these specific inputs and outputs are in line with those coming from compressor map data.

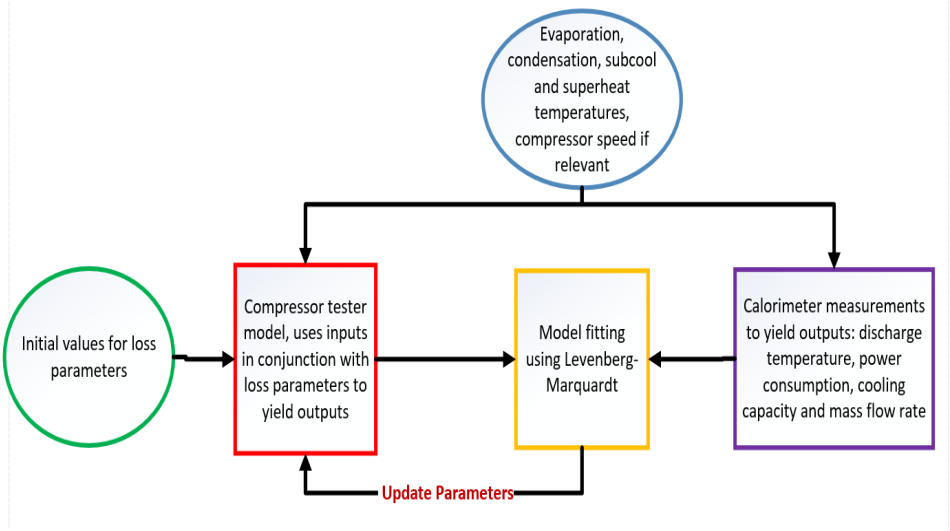

Figure 5.3. Flow chart to determine the compressor loss parameters.

Simulation results of all four outputs obtained using the fitted parameters are shown together with experimental results in Figures 5.4-5.7. It can be seen that the deviation between experimental and simulation results is less than 1 °C for the discharge temperature and less than 5% for the power input, cooling capacity and mass flow rate.

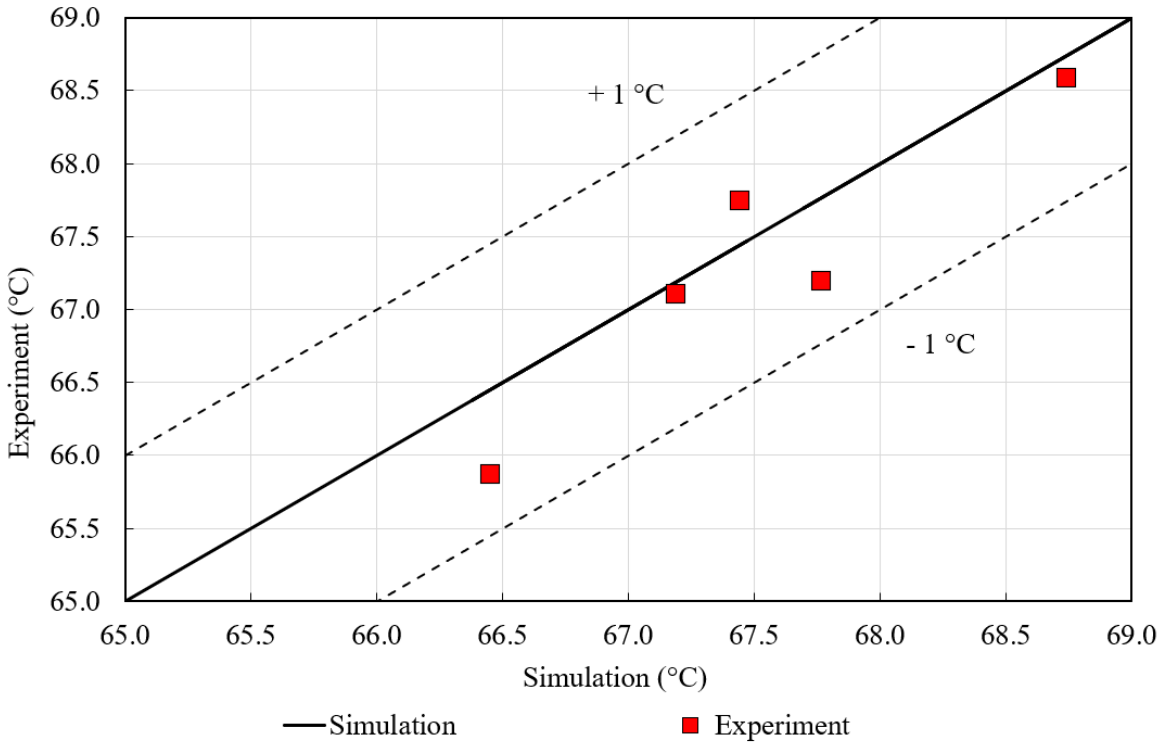

Figure 5.4. Discharge Temperature-Experiment vs Simulation.

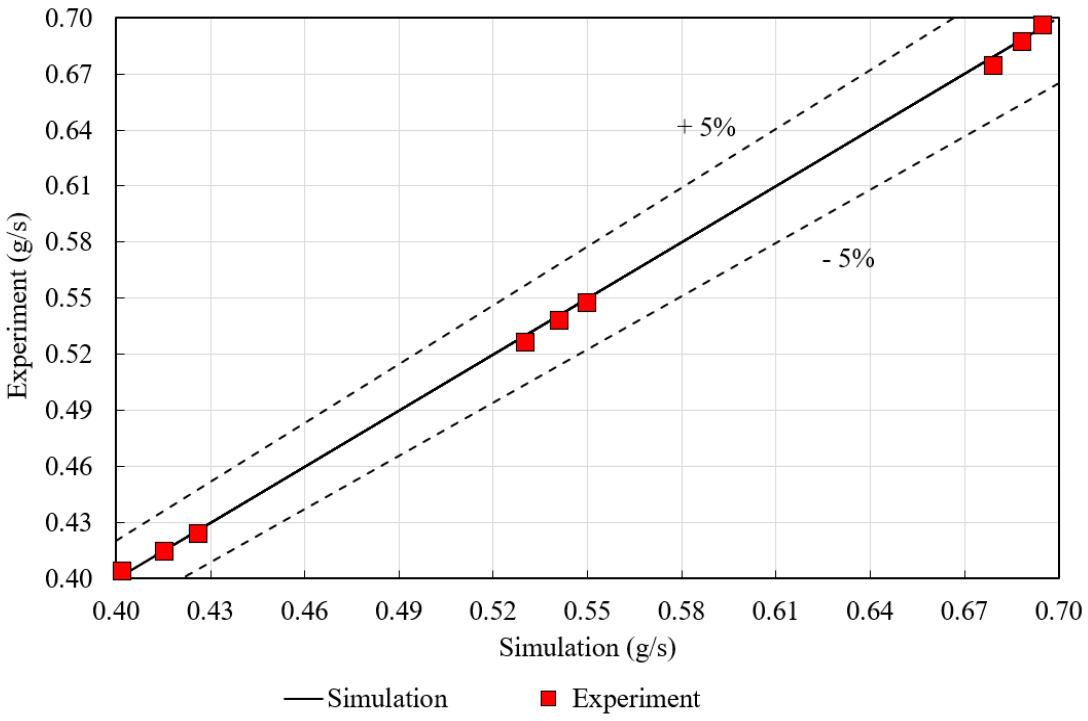

Figure 5.5. Mass Flow Rate- Experiment vs Simulation.

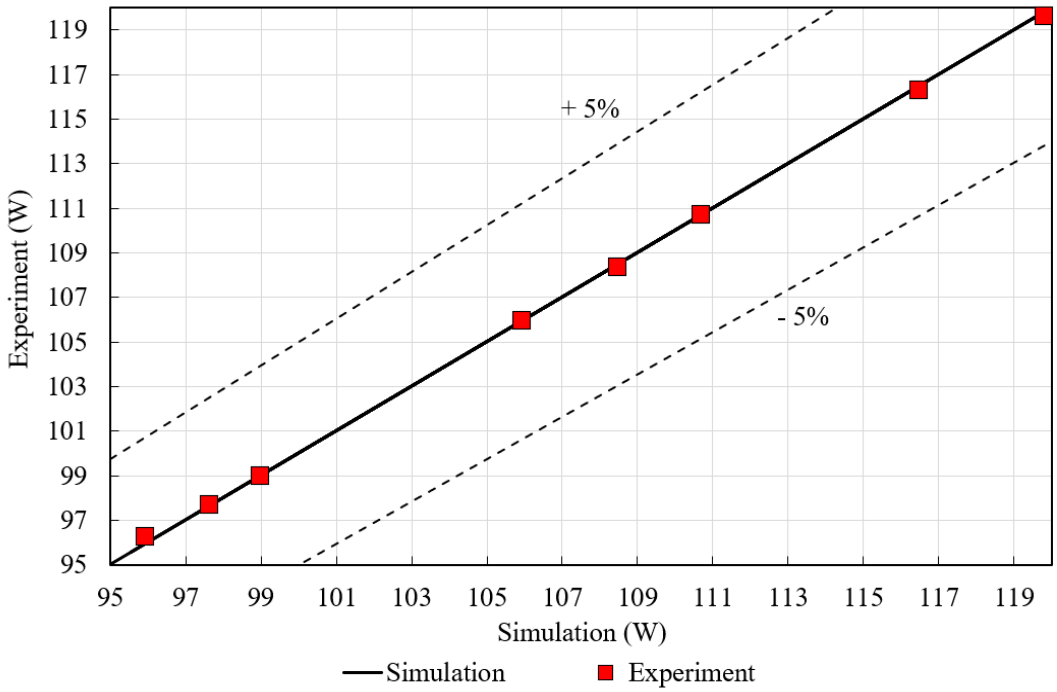

Figure 5.6. Input Power- Experiment vs Simulation.

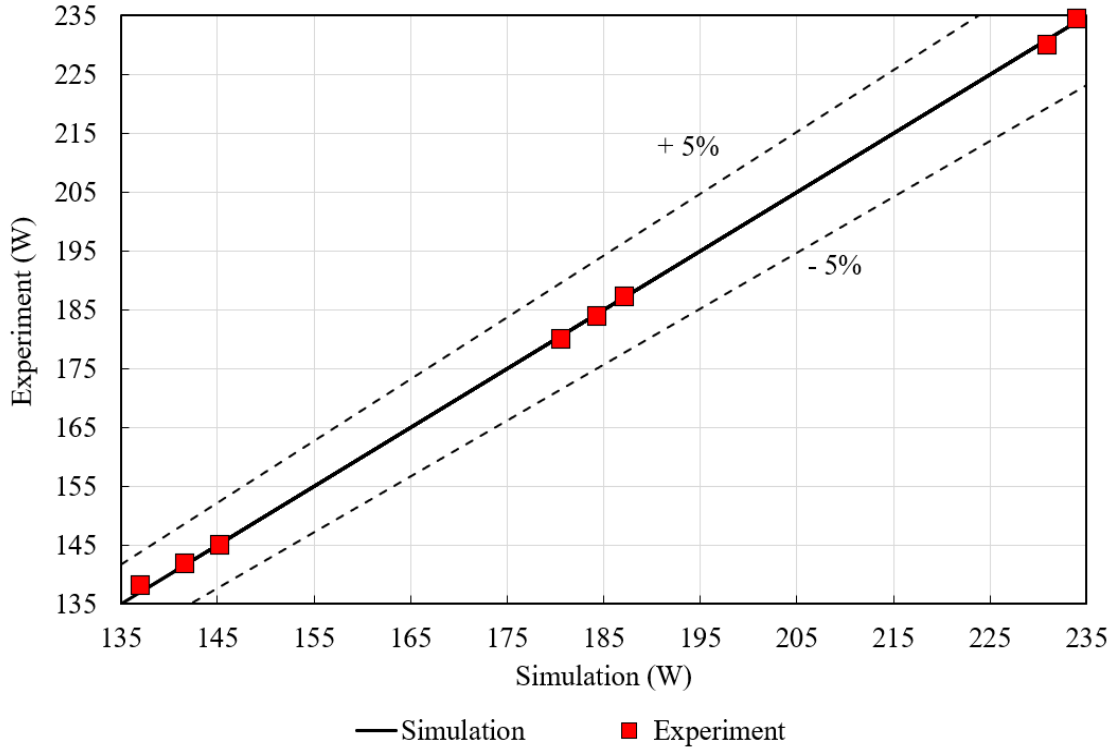

Figure 5.7. Capacity- Experiment vs Simulation.

5.2. Condenser and Evaporator

Two main heat exchangers are present in a refrigerator: condenser and evaporator. Several types are available for each, such as the hot-wall, wire-on-tube, coil and mini-channel types for condensers, and fin-and-tube, roll-bond, plate-on-tube, and skin types for evaporators. In the refrigerator used for validation in this study, the condenser was wire-on-tube, whilst the evaporator was plate-on-tube and skin for Fresh Food and Freezer respectively. Figures 5.8 and 5.9 show schematics of the FF and FRZ Evaporator respectively, while Figure 5.10 shows the actual condenser located at the back of the refrigerator.

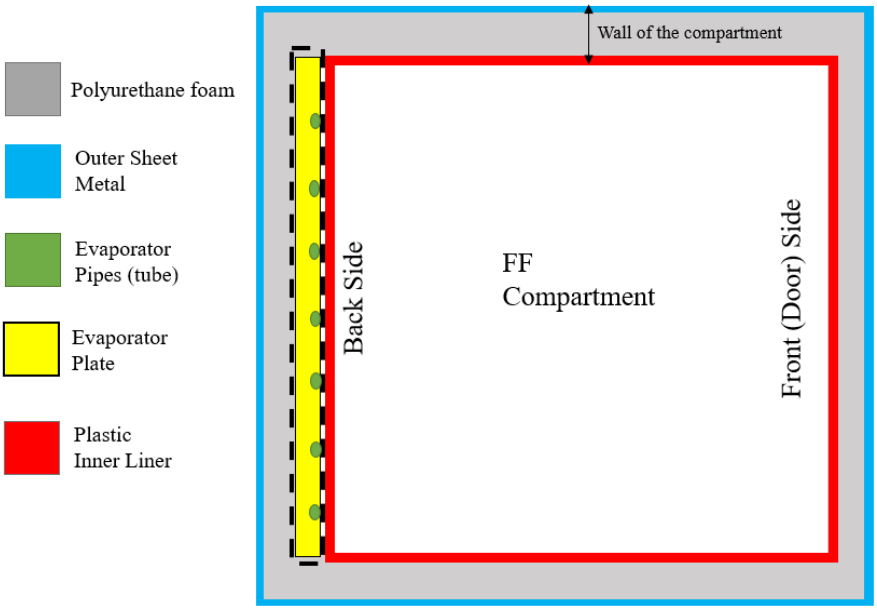

Figure 5.8. FF Evaporator Schematic.

Figure 5.8 shows the side view of the refrigerator. The evaporator (boxed by the dashed black lines) is located at the back wall of the FF compartment, behind the plastic inner liner (denoted by red lines). The green circles represent the cross section of the tube which is attached to the evaporator plate.

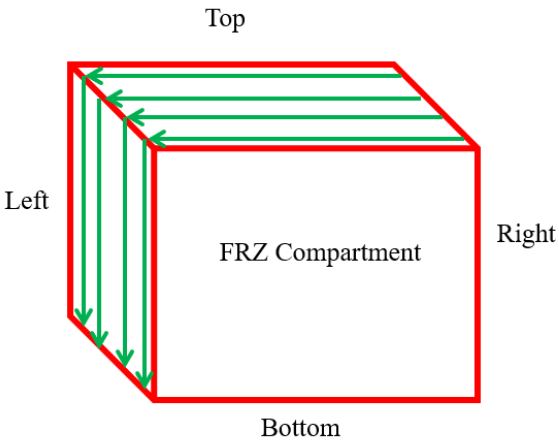

Figure 5.9. FRZ Evaporator Schematic.

An isometric schematic of the inner liner of the FRZ compartment is show in Figure 5.9. The “skin-type” evaporator is named so because the evaporator pipe is attached to the innermost layer (i.e., “skin”) of the compartment. The green arrowed lines actually denote the evaporator pipes, which run parallel to the top, left, bottom and right walls of the compartment. The pipes are not shown at the bottom and right wall for clarity.

Figure 5.10. Wire-on-tube condenser.

Finally, Figure 5.10 shows the wire-on-tube condenser, located at the exterior of the back wall of a refrigerator. Long, thin wires are attached to the tube to increase the heat transfer area.

In TIL library, these heat exchangers are modelled as diabatic tubes (i.e., heat transfer can occur across the tubes). Figure 5.11 below shows a cross section of the tube where the inner and outer heat transfer coefficients (h_{in} and h_{out}) and the wall thermal conductivity (λ) are depicted. These parameters are the main factors which govern the heat transfer rate through the heat exchangers.

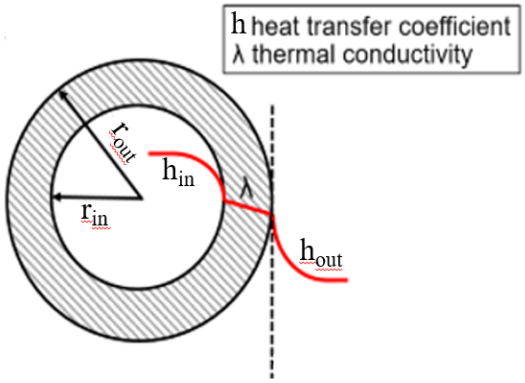

Figure 5.11. Cross-section of a tube.

The total length and tube outer and inner radii are entered as geometric parameters in the model. The tube is discretized into a number of finite volume cells, and the mass, momentum and energy balance equations are solved for each cell. Although pressure drop correlations are present in the library, a zero pressure drop model is used, since the pressure drop in the condenser and evaporator is not very significant, as previous experimental data has shown. A major provision provided by the tube model is the inclusion of a heat port, which allows the tube to be connected to another outer element. This is important for the refrigeration cycle since the ultimate purpose is to transfer heat to the ambient (for a condenser) or from the cabinet (for an evaporator). The heat port allows such a connection to be made.

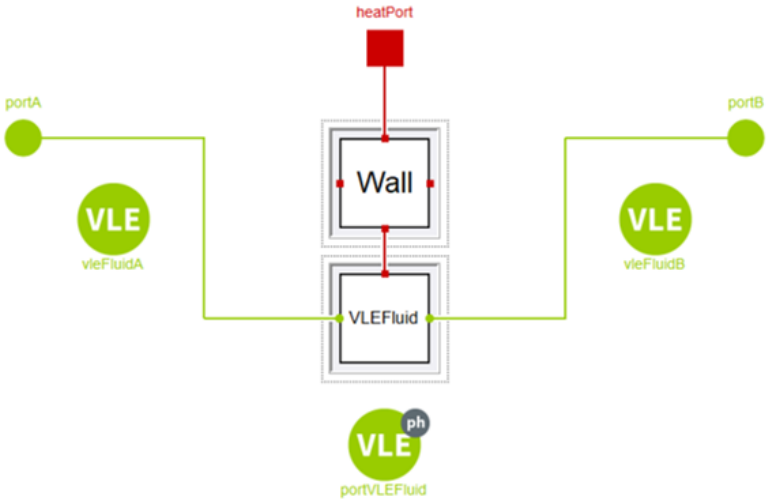

Figure 5.12. Major components of the tube model.

Figure 5.12 shows the heat port, along with other details of the tube model. The green circle to the left, labelled "portA" is the inlet of the tube, while the corresponding right circle labelled "portB" is the outlet. The "Wall" and "Vapor Liquid Equilibrium Fluids (VLEFluid)" blocks actually consist of a discretized number of cells (Figure 5.13). The green circles labelled "vleFluidA" and "vleFluidB" represent the thermo-physical properties at the inlet and outlet, while the bottom circle labelled "portVLEFluid" represents the pressure and enthalpy of the VLEFluid element.

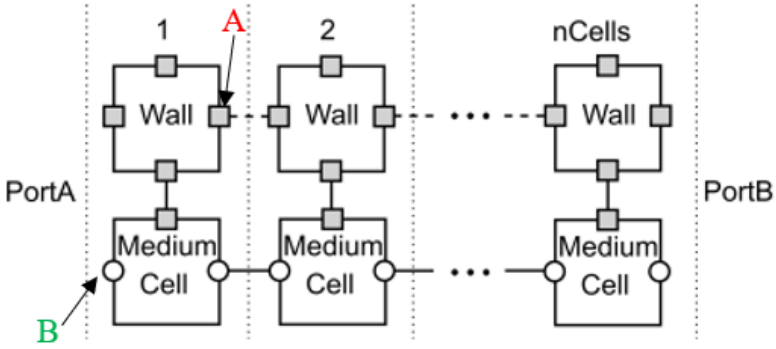

Figure 5.13. Discretized cells comprising the tube model.

Figure 5.13 basically zooms in on the Wall and VLEFLuid blocks. Each block consists of an equal number of finite volume cells, connected to each other. The grey squares (one of which is labelled as A) at each joint represent heat ports, between which heat transfer occurs, while the white circles (one labelled as B) running left-right on each "medium" cell represent fluid ports, between which refrigerant flows. The medium cells contain the properties of the working fluid (isobutane- R600a in this case), while the wall cells contains the properties of the tube wall material. That is, steel for the condenser and aluminium for the evaporators.

As explained above, heat transfer through the tube is modelled using a heat transfer coefficient at the fluid side, which may be calculated using any of the several correlations present in the model.

For the single-phase region, the well-known Dittus-Boelter correlation is used:

$$Nu = 0.023 Re^{\frac{4}{5}} Pr^{\frac{1}{3}} \tag{5.8}$$

where Nu: Nusselt Number, Re: Reynolds Number, Pr: Prandtl number.

Note that in some textbooks a more accurate version of Equation 5.8 is reported, in which the exponent of the Prandtl number is taken as either 0.3 or 0.4 (instead of 1/3) depending upon heating or cooling. This introduces only a minor change in the final simulation results, and the simpler version (Equation 5.8) is therefore used in the model.

For the two-phase region, other correlations can be used. For example, for condensation, Shah's correlation [32] is used:

$$h_{in} = h_{liq}\left[(1-x)^{0.8} + \frac{3.8x^{0.76}(1-x)^{0.04}}{{p_r}^{0.38}}\right] \tag{5.9}$$

where h_{liq} is the single-phase heat transfer coefficient which can be calculated using the Dittus-Boelter correlation above, x is the quality, p_r is reduced pressure (= p/p_c), and p_c is critical pressure.

The thermal conductivity values for the solid is predefined in the libraries for many common materials. Finally, the outer heat transfer coefficient can again be declared by the user. This is calculated using natural convection correlations for the evaporator-cabinet area (details will be described in a later section), while values form the ASHRAE Handbook [33] are used for the condenser.

5.3. Capillary Tube

One of the most obscure parts of a refrigerator, the capillary tube is a vital component to ensure correct functioning of the cycle. It is the capillary tube which allows the liquid refrigerant from the condenser to expand and thereby drop in pressure and temperature so that cold liquid-vapor mixture can enter the evaporator.

At the inlet of the capillary tube, the refrigerant enters as a subcooled liquid. As it flows, the refrigerant pressure and temperature drops, causing it to eventually reach the two phase region. Pressure continues to drop in this region until the end of the capillary tube. Flow in a capillary tube can therefore be divided into two parts: single phase and two-phase. According to [34], pressure drop in the single phase region is linear and is caused by friction only, whereas that in the two phase region is non-linear, and is caused by both friction and momentum. Momentum changes occur in the two phase region because as the liquid vaporises, the overall density decreases, causing the fluid to accelerate. This acceleration causes a rapid drop in pressure. A qualitative representation of the pressure drop, based on [34], can be seen in Figure 5.14:

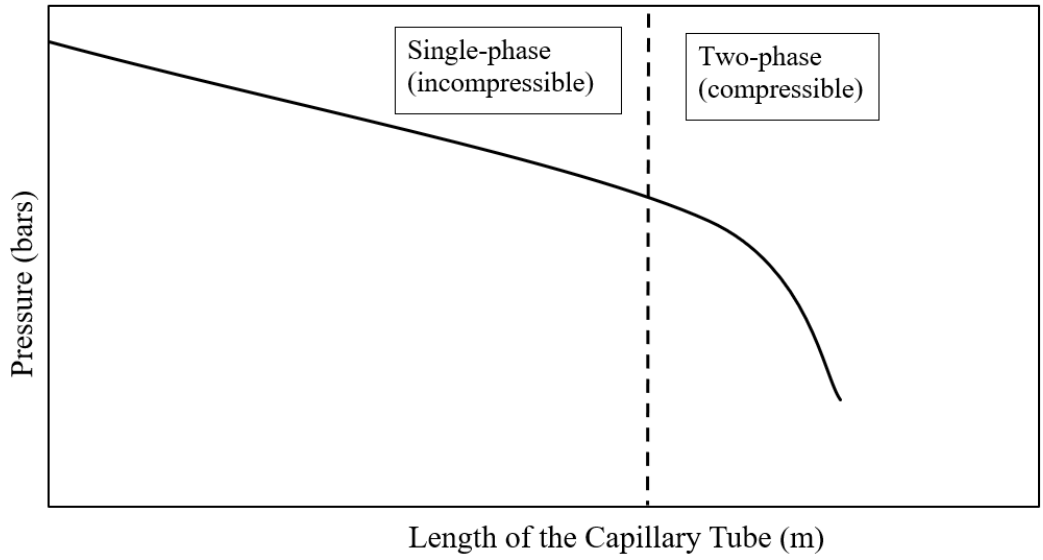

Figure 5.14. Capillary tube pressure drop- theoretical results.

In the single-phase region, assuming fully developed flow, the integrated form of the 1-D momentum balance reduces to the following (since the inertia terms disappear, and the body force terms are also neglected):

$$p.\pi.\frac{D^2}{4} - (p + \Delta p).\pi.\frac{D^2}{4} - \tau_w.\pi.D.\Delta L = 0 \tag{5.11}$$

where p is pressure, D *is* tube diameter, Δp is pressure drop, τ_w is shear stress, and ΔL is length of the cell.

Note that the inertia term is absent. The pressure drop Δp is then related only to the viscous shear stress term. Thus, only frictional pressure drop is present in single phase, which can be found using the well-known formula:

$$\Delta p = \left(f\frac{G^2}{2\rho_L D}\right)\Delta L \tag{5.12}$$

where f is the Darcy friction factor, G is the mass flux, and ρ_L is the density

The friction coefficient can be found using the Colebrook correlation [35]:

$$\frac{1}{f^{0.5}} = -2\log\left(\frac{\varepsilon/_D}{3.7} + \frac{2.51}{Ref^{0.5}}\right) \tag{5.13}$$

where ε is tube roughness and Re is Reynolds Number.

Since Colebrook is implicit in *f*, an explicit version such as the Swamee-Jain [36] correlation may be employed instead, which is given as:

$$f = \left[-2\log\left(\frac{\varepsilon/_D}{3.7} + \frac{5.74}{Re^{0.9}}\right)\right]^{-2}. \tag{5.14}$$

Now, for the two-phase region, pressure drop is more complicated. This is because the density changes in this regime, due to which fluid acceleration occurs. The reduced and integrated form of the momentum balance this time contains the inertia term:

$$p.\pi.\frac{D^2}{4} - (p + \Delta p).\pi.\frac{D^2}{4} - \tau_w.\pi.D.\Delta L = m.\Delta U \tag{5.15}$$

where *m* is the mass flow rate and ΔU is the change in velocity.

The pressure drop is thus composed of two components, friction and momentum. While extensive correlations are available in literature for each component, such as Lin's correlation [37] for friction pressure drop and various other approaches for the momentum drop [38], the model uses Swamee-Jain again, albeit with two-phase properties (this is done to simplify the process). Since the capillary tube will be modelled as a discrete number of cells, the pressure drop can be calculated by rearranging Equation 5.15 above for each cell:

$$\Delta p = \left[\left(\frac{f}{2D}\right)\Delta L + \frac{\rho_{in} - \rho_{out}}{\rho}\right].\frac{G^2}{\rho} \tag{5.16}$$

where ρ_{in} is density at inlet, ρ_{out} is density at outlet, ρ is average density of cell. Thus, by solving for this in each cell, the pressure drop for two-phase flow region is obtained

To validate the capillary tube model, simulations were carried out on a tester model, and the resulting pressure drop graph was compared with the expected theoretical result (shown in Figure 5.14). Simulation results are shown in Figure 5.15. The similarity in the characteristic can be seen clearly. Note that the x-axis is labelled as number of cells, because the capillary tube was divided into 50 cells of equal length.

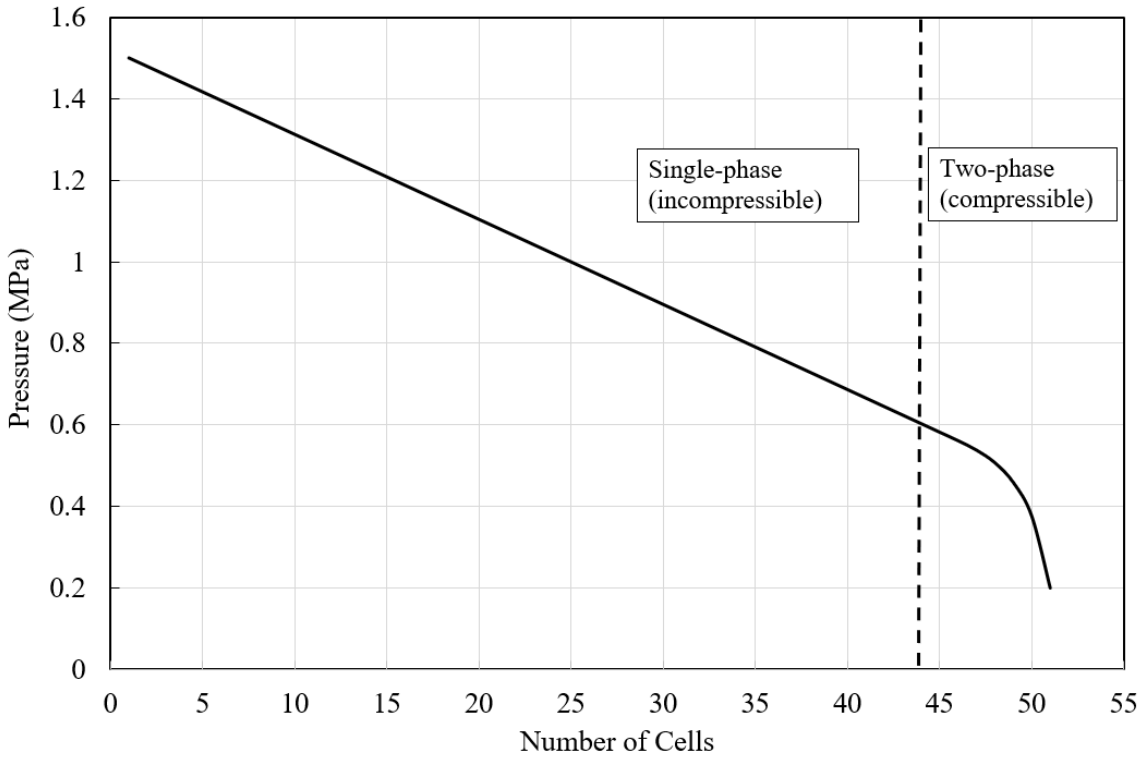

Figure 5.15. Simulation results of capillary tube tester model in this study.

Note that the pressure drop is linear in the single phase region, where only viscous friction causes the pressure drop. As the refrigerant evolves into two-phase, however, change in the density causes momentum pressure drop in addition to frictional pressure drop, which causes the total pressure drop to plummet steeply.

5.4. Capillary tube-Suction Line Heat Exchanger (CT-SL HX)

A CT-SL HX is used to ensure that sufficiently low-quality refrigerant enters the evaporator, and no liquid enters the compressor. This is done by attaching part of the capillary tube to the pipe exiting the evaporator so that a heat exchanger is formed, and heat is transferred from the hot refrigerant in the capillary inlet to the cold refrigerant in the suction line. To model this heat exchange between two tubes, tube models similar to the ones used for evaporator and condenser are used. A resistance element is used to connect the two tubes. For validation, a "tester" CT-SL HX model was created, as shown in Figure 5.16. In this model, the input parameters (condensation pressure, capillary tube length and diameters and CT-SL HX length) were used to calculate the mass flow rate, suction outlet temperature and enthalpy, and the total heat transfer between the capillary tube and suction line.

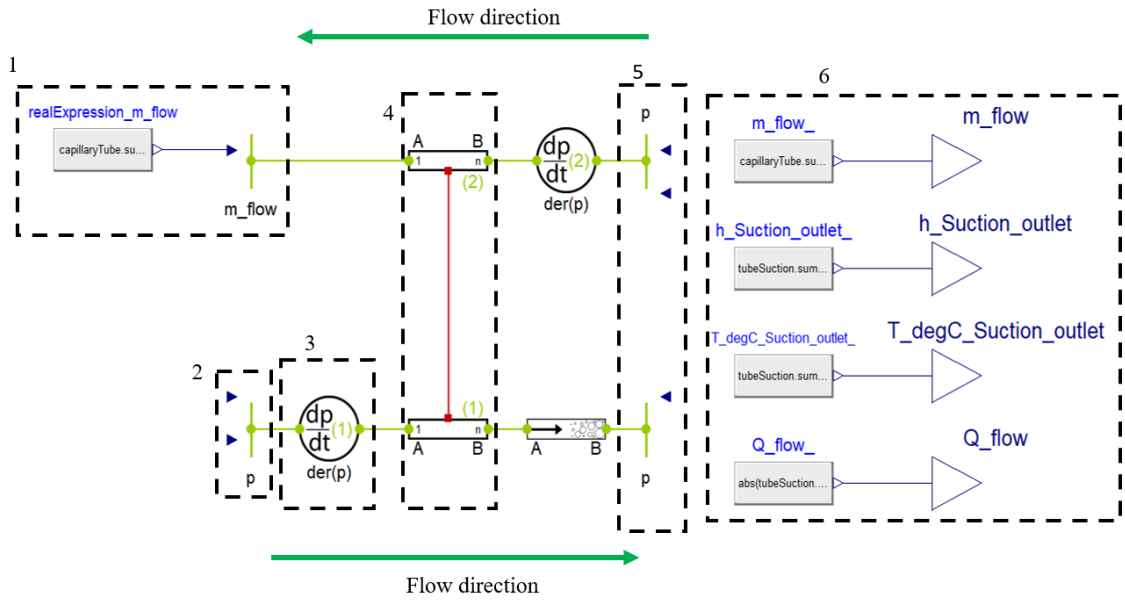

Figure 5.16. CT-SL HEX Tester Model.

Several key features of the tester model are enclosed in dashed boxes and numbered. These are explained as follows:

i) The m_flow denotes mass flow rate. An initial guess value is used by the model to start simulations, and then iterations are carried out until convergence is reached
ii) The condensation pressure is entered here
iii) This is placed at each line with a unique pressure level. Hence, it is placed at the high pressure line, as well as the low pressure suction line. The component makes the dp/dt term constant, thereby improving simulation performance. Note that this is the time derivative of pressure- pressure still decrease along the flow (unless the zero pressure drop assumption is explicit invoked in the model).
iv) The connection between the capillary tube and suction line can be seen. This is basically the CT-SL HX.
v) These pressure boundaries are the evaporation pressures
vi) All the outputs yielded by the model are shown: mass flow rate, suction outlet enthalpy and temperature, and CT-SLHX heat transfer rate.

The model was compared to experimental results obtained by Apaydın [39], in which the mass flow rate through and output temperature of the CT-SL HX were examined in a full-factorial experiment carried out for two different capillary tube lengths (2.6 m and 4 m), diameters (0.8 mm and 0.6 mm), HX length (2 m and 1 m) and condensation temperatures (32 °C and 40 °C). Using the same length, diameter, inlet and outlet conditions, results for the HX outlet temperature and mass flow rate were less than 2 °C and 10% different than those of [39] respectively, as Table 5.1 shows.

Table 5.1. CT-SL HEX- Simulation vs. Literature.

Apaydın [31]		Simulation		Comparison	
$T_{HEX,O}$ (°C)	m (g/s)	$T_{HEX,O}$ (°C)	m (g/s)	$\Delta T_{HEX,O}$ (°C)	Δm (%)
29.7	0.64	28.0	0.65	-1.7	1.6
23.0	0.54	22.0	0.53	-1.0	-0.6
23.8	0.49	23.6	0.47	-0.2	-4.7
26.6	0.54	27.9	0.59	1.3	8.3

5.5. Cabinet

The cabinet is a very important part of the refrigerator, where the actual load is placed. It has two compartments, a Freezer (FRZ) compartment and a Fresh Food (FF) compartment. The Freezer compartment, which is reserved for frozen food, operates around -18 °C. In the refrigerator used for this study, the Freezer is located on top of the cabinet (hence the term "Top-Mounted") The fresh-food compartment is used to keep everyday food stuff at ~5 °C and is located below the Freezer compartment in this refrigerator.

5.5.1. Walls of the Cabinet

The walls comprising a cabinet are arguably the most important part of the structure, since they control the heat gain through a refrigerator. For this refrigerator, the walls of the cabinet are made up of three layers: steel, polyurethane and ABS plastic. The outer steel layer is very thin, around 0.5mm. The middle layer is the thickest (ranging from 40mm to 90mm) and is the most important to minimize heat gain. It is made of Polyurethane, which is an excellent insulator, having a thermal conductivity (k) value of 0.0205 W/m^{2}K [40]. The innermost layer is made up of ABS plastic and has a k value of 0.17 W/mK [40]. This layer is also thin, around 1.5mm on average. The schematic below shows the layers:

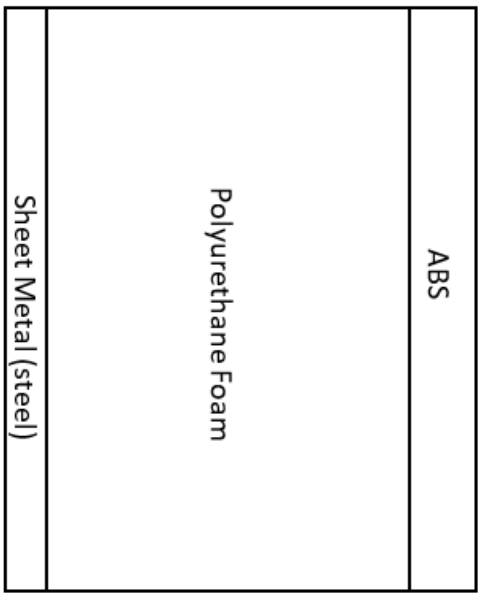

Figure 5.17. Schematic of the wall showing the three layers it is comprised of.

Since the thickness of each layer is much smaller compared to the length and width, the wall may be modelled as 1-D with minimal loss in accuracy.

To model the thermal capacity of each layer, the layers are divided as shown in Figure 5.18 below. The relevant heat flows and temperature values are also labelled:

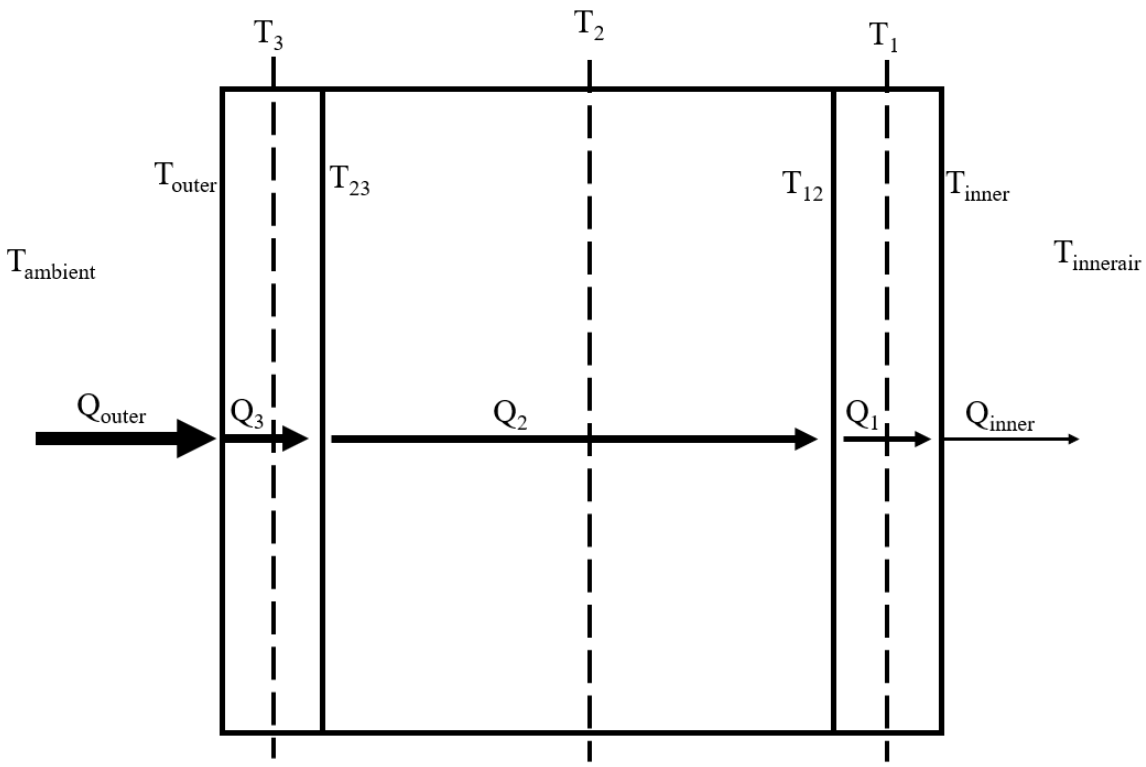

Figure 5.18. Heat transfer across and temperature of each layer in the wall model.

As can be seen, each layer is divided into two parts (shown by the dashed line) so that the heat entering the layer is not equal to the heat leaving it. This naturally implies that each layer has a thermal capacitance associated with it. Each layer is treated as a lumped mass, and the temperature is therefore given by the 1st Law energy equation for lumped masses:

$$m_j c_j \frac{dT_j}{dt} = Q_j \tag{5.17}$$

where *j* denotes the subscript attached to each layer and takes values from 1 to 3, m is the mass of a layer, *c* is the specific heat, *T* is the temperature, *t* is time, and *Q* is the heat transfer across a layer.

The net heat transfer across each layer is by conduction, and, using Fourier's law:

$$Q_j = -k_j A_j \frac{T_r - T_j}{t_j/2} + k_j A_j \frac{T_j - T_l}{t_j/2} \tag{5.18}$$

where *j* again denotes the layer in question whilst *r* denotes the side to the right of the layer and l to the left. For instance, for layer 1, *r* = 23 and l = o. *k*, *A* and *t* are a layer's thermal conductivity, area and thickness respectively.

Finally, at the extreme ends of the wall, heat transfer occurs through convection, and Newton's Law of Cooling gives:

For the left side (layer 3 side):

$$Q_{outer} = h_{outer} A_{outer} (T_{ambient} - T_{outer}). \tag{5.19}$$

For the right side (layer 1 side):

$$Q_{inner} = h_{inner} A_{inner} (T_{inner} - T_{innerair}). \tag{5.20}$$

5.5.2. Convection Coefficients Used in the Cabinet Model

As explained above, the cabinet model uses inside and outside heat transfer coefficients. The outside heat transfer coefficient is taken from ASHRAE's handbook [33] as 9.26 W/m^2 K. This value includes the effect of radiation as well. For the inside combined heat transfer coefficient, an appropriate way to treat the natural convection and radiation inside both the compartments is required. For natural convection, two main approaches were found in literature ([41-44]): treating the compartment as a 2D cavity or applying the vertical and/or horizontal wall natural convection correlations on the cold evaporator wall, by

treating the core air as stagnant. The latter approach was found to yield better results according to [44]. Laguerre et al. [45] again validated this claim in an experimental study in which the air velocity was measured at various locations. It was found that the air is indeed almost stagnant at the core. Therefore, this approach is used for both compartments, albeit with some differences, as explained next.

For the Fresh Food compartment, the coldest wall is the back wall, where the evaporator is located. Hence, that wall was treated as the vertical wall in concern. For the Freezer compartment, the situation is different since the evaporator is wrapped around the compartment such that the top, right, bottom and left walls all are all in contact with the evaporator. In this case, both vertical and horizontal wall correlations are used, and the maximum value obtained for the heat transfer coefficient is used as the final value. This was done to offset the underestimation stemming from the assumption of a completely stagnant core region.

To be able to use the wall correlations the first step is to calculate the Rayleigh number, given by Equation 5.21:

$$Ra_L = \frac{g\beta(T_{air} - T_{wall})L^3}{\nu^2} Pr \tag{5.21}$$

where β is the thermal expansion coefficient, L is the characteristic length and ν is the kinematic viscosity. Previous experimental data was used to get the wall and air temperatures, so that the Rayleigh Number could be calculated. With the Rayleigh number known, the correlations as presented by Cengel [46] were used, as shown in Equations 5.22-5.25.

For vertical walls and entire Rayleigh number range:

$$Nu = \left\{ 0.825 + \frac{0.387 Ra_L^{\frac{1}{6}}}{\left[1 + (0.492/Pr)^{\frac{9}{16}}\right]^{\frac{8}{27}}} \right\}. \tag{5.22}$$

For lower surfaces of a cold horizontal plate:

$$Nu = 0.54Ra_L^{\frac{1}{4}}. \tag{5.23}$$

Ra range: 10^4 - 10^7

$$Nu = 0.15Ra_L^{\frac{1}{3}}. \tag{5.24}$$

Ra range: 10^7 – 10^{11}

For the upper surface of a cold horizontal plate:

$$Nu = 0.27Ra_L^{\frac{1}{4}}. \tag{5.25}$$

Ra range: 10^5 – 10^{11}

After calculating the Nusselt number, the convective heat transfer coefficient is obtained using Equation 5.26:

$$h_c = \frac{kNu}{L}. \tag{5.26}$$

When the only mode of convection is natural convection, radiation also plays a major role in heat transfer, and cannot be ignored [47]. Hence, the radiation heat transfer coefficient is also calculated for both the compartments, according to Stefan-Boltzmann Law (Equation 5.27):

$$h_r = \frac{\sigma\epsilon(T_{hot}^4 - T_{cold}^4)}{T_{hot} - T_{cold}} \tag{5.27}$$

where $\epsilon = 0.9$ according to [40].

In this equation T_{hot} and T_{cold} are two wall temperatures. For the Fresh Food compartment, the natural choice is the back wall (the coldest wall behind which the evaporator is placed) and the wall directly opposite, namely, the door, since the view factor is maximum in this way (the evaporator does not "see" the other side walls). For the Freezer, the top and bottom wall are used, since previous experimental data showed that the temperature difference between those walls is much higher compared to the two side walls and back and front walls, which have very similar temperatures (at low temperature differences, radiation ceases to be particularly important).

Once both h_r and h_c are calculated, the final step is to combine both using the resistor network approach. Again, [44] used a similar approach, in which the network shown in Figure 5.19 is used. In the Figure, the reciprocal of the heat transfer coefficients represents the resistance values. These resistances are combined in parallel by taking the sum of the reciprocals, as given by Equation 5.28 (the resulting equivalent network is shown in the bottom part of Figure 5.19):

$$h_{combined} = \frac{1}{R_{equivalent}} = \frac{1}{\frac{1}{h_c} + \frac{1}{h_r}}. \tag{5.28}$$

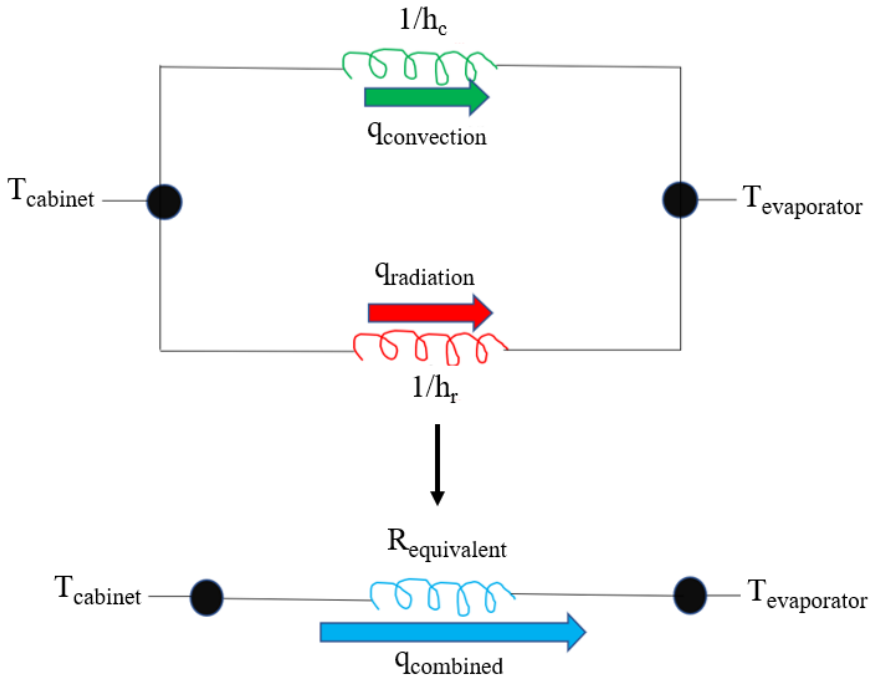

Figure 5.19. Equivalent Resistant Network.

Table 5.2 shows the quantities calculated to obtain the final combined heat transfer coefficient values. Note that calculations were done for both compressor on and off states, since the air and evaporator temperatures are different during these stages. The near 100-fold reduction in Rayleigh number from on to off state for both FF and FRZ can be seen.

Table 5.2. Calculation of combined heat transfer coefficient.

PHYSICAL PROPERY	FF ON	FF OFF	FRZ ON	FRZ OFF
Temp Difference [ΔT] (K)	25.7	3.2	5.4	0.8
Film Temperature (°C)	-10.5	3	-19.8	-14.3
Thermal Expansion Coefficient x ΔT	0.1	0.01	0.02	0.000624
Thermal Diffusivity (x10-5 m^2/s)	1.87	1.87	1.72	1.72
Kinematic Viscosity (x10^{-5} m^2/s)	1.35	1.35	1.22	1.22
Thermal Conductivity (W/mK)	0.0242	0.0242	0.0234	0.0234
Characteristic Length (m)	0.67	0.67	0.46	0.37
Rayleigh Number	1.13 x 10^9	6.71 x 10^7	1.10 x 10^8	1.5 x 10^6
Nusselt Number	133.6	56.6	71.9	19.2
Convective Heat Transfer Coefficient (W/m^2K)	4.9	2	3.7	1.2
Radiative Coefficient (W/m^2K)	3.5	3.98	3	3.3
Combined Heat Transfer Coefficient (W/m^2K)	8.4	6	6.7	4.5

5.5.3. Masses Inside the Cabinet

The cabinet model also includes a provision to enter the total mass of all materials present inside the cabinet. These include plastic shelves and drawers, glass shelves, gasket, and aluminium evaporators (which are embedded inside the cabinet). These items (henceforth referred to as “goods”) are treated as lumped masses, and heat transfer from these goods to the cold air occurs through convection. The total mass, surface area and specific heat capacity of each type of material is entered in the model as a parameter. In the refrigerator used in this study, the details of the goods is as shown in Table 5.3.

Table 5.3. Goods present in the refrigerator.

Compartment	Property	Plastic	Glass	Evaporator	Gasket
FF	Mass	6.2 kg	10.8 kg	0.76 kg	0.51 kg
	Surface Area	1.85 m^2	1.53 m^2	0.23 m^2	0.15 m^2
FRZ	Mass	0.31 kg	2.1 kg	0.85 kg	0.34 kg
	Surface Area	0.21 m^2	0.88 m^2	0.46 m^2	0.12 m^2

In addition to the above "solid" goods, air itself is also treated as a lumped mass inside the cabinet. This is represented by an air cell block in the cabinet model, as will be shown in Section 5.5.5. The air cell is directly connected to the evaporator at one end, and to the goods and wall models at the other.

5.5.4. Other Details of the Model

In a real refrigerator, some air infiltration occurs through the gasket region of the cabinet door even when the door is closed, since the sealing provided by the gasket is not perfect. The infiltration rate is determined though a "gasket" heat transfer coefficient which is determined experimentally. Using this coefficient, Equation 5.29 can be used to determine the total heat gain through the gasket:

$$Q_{gasket} = U_{gasket} L_{gasket} \left(T_{ambient} - T_{compartment}\right). \quad (5.29)$$

5.5.5. The Model in Dymola

The cabinet model in Dymola is as shown in Figure 5.20. The important parts of the model are labelled using dashed black boxes. As the Figure shows, the cabinet is divided into two compartments, Freezer and Fresh Food. The bulk of both compartments is comprised of wall models (a), which control the heat gain into the compartment as explained in Section 5.5.1. In addition, several goods (b) can be seen, which represent the different materials present inside each compartment. The total mass, length and gasket heat transfer coefficient can be entered in the gasket model (c). The air cell model (d) represents the

lumped air mass and is connected to the evaporator through a heat port (e). The other end of the air cell is connected to the walls, goods and gasket. Finally, (f) shows the fan model, where the desired combined heat transfer coefficient values (as calculated in Section 5.5.3) can be entered for both compressor on and off states.

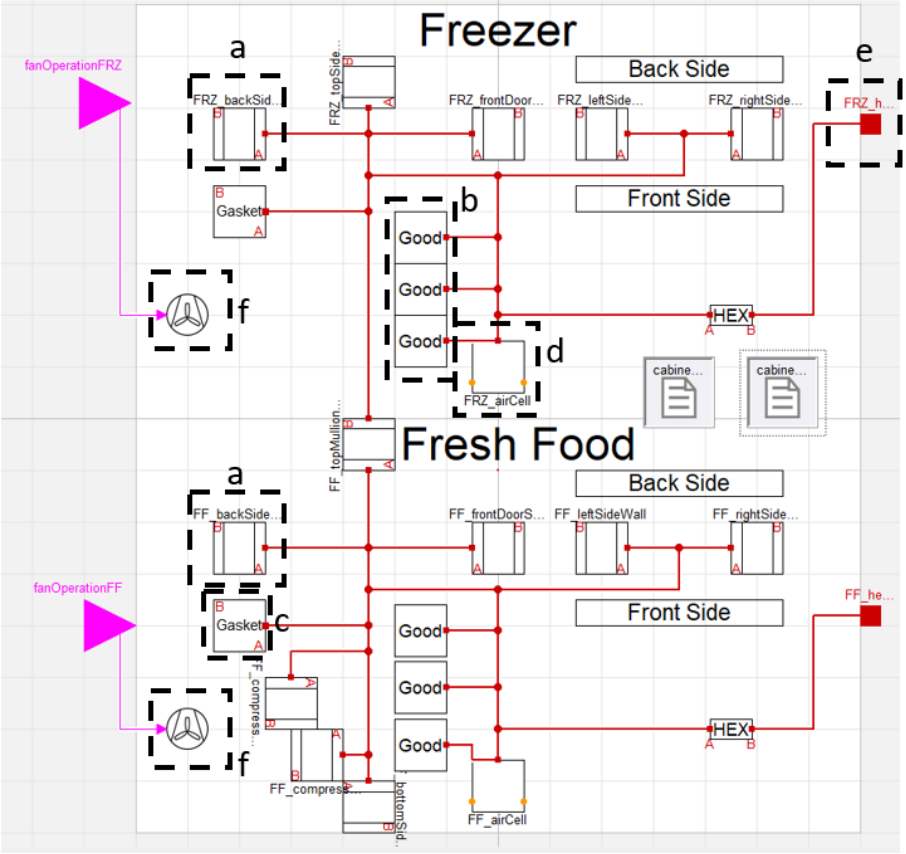

Figure 5.20. The Cabinet Model in Dymola.

5.5.6. Cabinet Model Validation

To validate the cabinet model, a temperature rise test was carried out on the refrigerator. In this test, a refrigerator is left to cool to a certain temperature, after which the appliance is unplugged, and the temperature rise curve is obtained. This experimental data was compared to the simulation results for both compartments. The results can be seen in Figures. 5.21 and 5.22. A deviation of less than 2 °C was obtained, which is quite acceptable considering the thermocouple uncertainty itself is 0.5 °C.

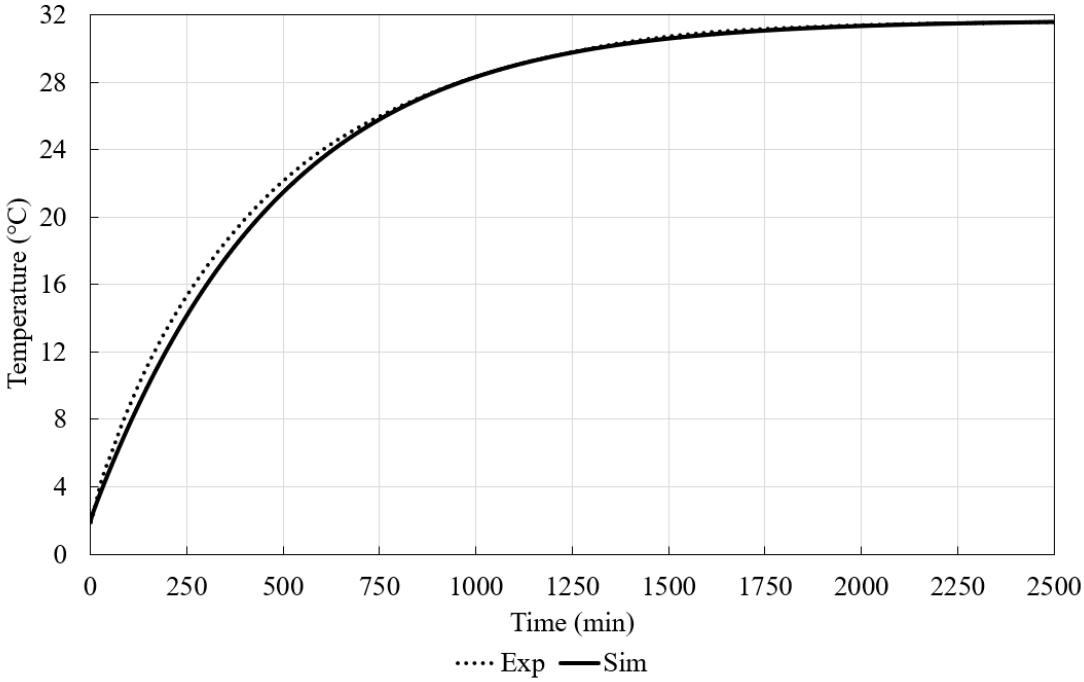

Figure 5.21. FF Temperature Rise- Sim vs Exp.

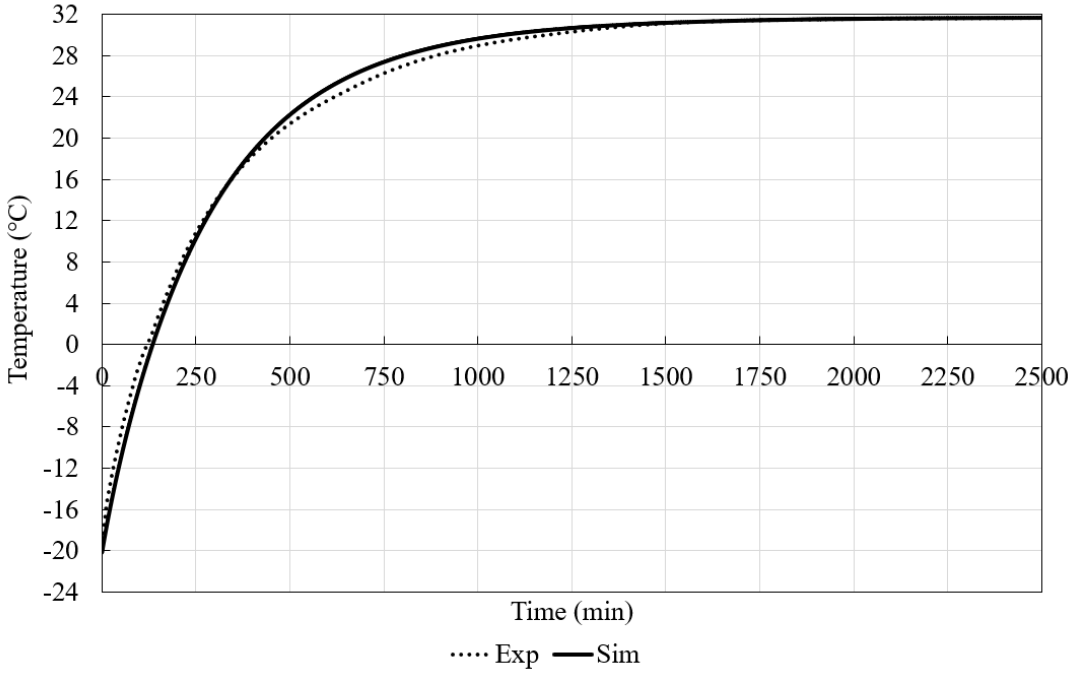

Figure 5.22. FRZ Temperature Rise- Sim vs Exp.

5.6. Complete Cycle Model

All of the components described above were used to create the serial system refrigeration cycle in Dymola. Figure 5.23 shows the cycle structure.

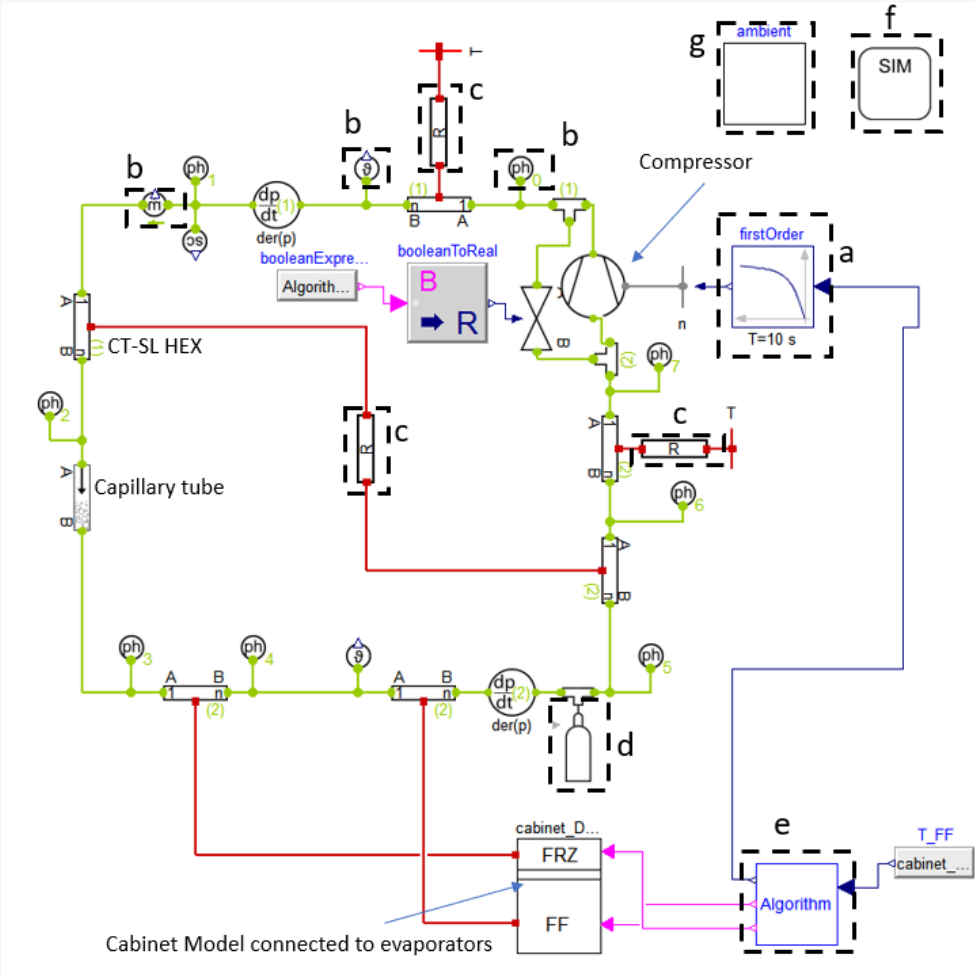

Figure 5.23. Full Cycle Model.

The components described above can be seen connected in a loop. Several other component models not explained above will be addressed now:

a. firstOrder: element used to smooth the transition of the compressor from on to off or vice versa
b. ph, v, m sensors: these exhibit the instantaneous values of the pressure, enthalpy, volume and mass flow rate at a particular port during simulation.

c. Resistors (seen as tubes labelled R): Heat resistance elements used to allow finite heat transfer between two tube components or a tube and a heat port.
d. filling station (tube labelled with a right-pointing grey arrow): controls the amount of refrigerant charge in the system. The user can enter the real charge amount in this component.
e. Algorithm: The algorithm block may be deemed as the core structure in a cycle model, since it governs when the compressor will be turned on and off. The conventional type refrigerator used in this study works according to high and low FF evaporator temperatures. The specific set point temperatures depend on the thermostat position (which ranges from 1-warmest to 7-coldest). Corresponding to the set point evaporator temperatures, the FF air temperature naturally operates at its own pair of threshold values called cut-in and cut-out values. These values are entered in this algorithm. When cooling starts, the FF air temperature is monitored continuously and once the cut-out value is reached, the compressor stops. This warms up the compartment, and the temperature is monitored again until the warmer cut-in temperature is reached. The compressor starts again, and the cycle continues. The connection to the FF air cell is evident through the T_FF input block to the right of the algorithm.
f. SIM: The working fluid is entered here (Isobutane R600a in this case).
g. Ambient: Block controlling ambient temperature and pressure.

Compressor loop with orifice valve: The valve, T-junctions and algorithm block to the left of the compressor (shown in Figure 5.24 below) were added during the fine-tuning stage of the study. Due to numerical limitations of the model, the compressor speed cannot be set to zero during off time, because the model cannot sustain zero mass flow rate in the loop. However, it is well known that in actual conditions refrigerant migration occurs during the first 3-4 minutes of the off time, after which the flow stops due to pressure equalization. While migration cannot be modelled at this stage, to at least stop flow in the system and indirectly equate pressures, the loop shown in Figure 5.23 was added. The algorithm controls the orifice valve such that it is open during off time and closes during on time. The effective flow area during off time is set to a high value, namely, 5×10^{-6} m^2, which was found by trial-and-error. This value is large enough to allow most of the flow to occur within the compressor loop, causing only a negligible mass flow rate through the actual refrigeration loop during off time. The off

time evaporation and condenser pressures are able to equalize, just as in real life conditions. By using this structure, the off time evaporation temperatures are also captured extremely well. During on time, since the orifice valve is closed, no flow occurs through this loop, and the refrigerant is able to flow through the actual refrigeration loop normally.

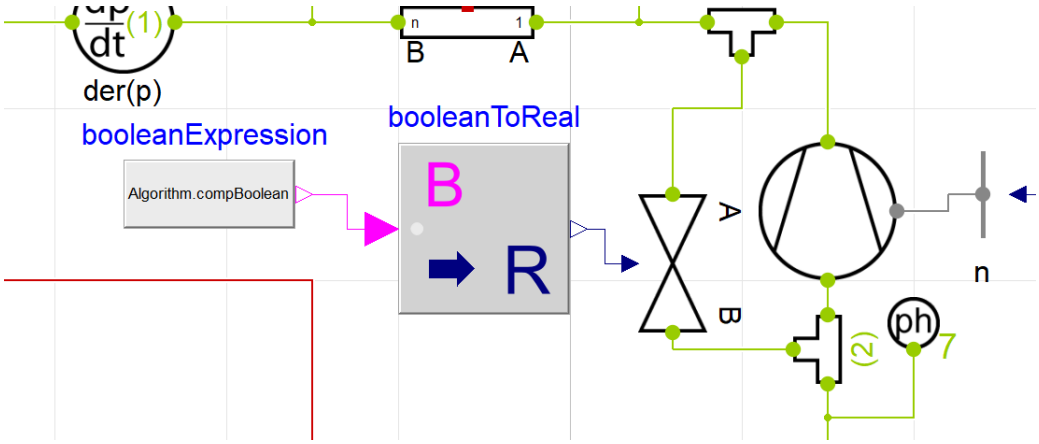

Figure 5.24. Valve Structure to model off time.

5.7. Modified Cabinet Model for Water Pot Test

As explained in the objective section, the second part of this study involved simulating the putting and subsequent cooling down of a warm load of water inside the cabinet. To perform this simulation, the cycle model was left unchanged, since the nature of those components do not change with the addition of goods in the cabinet (the operating conditions, however, do change since the inclusion of warm goods increase the evaporation temperature, thereby increasing the mass flow rate and also the compressor power input). The cabinet model, however, had to be modified to represent the following phenomena:

i) Opening of the Fresh Food compartment door for a specified time
ii) An increase in the amount of plastic goods (since the water were stored in plastic containers) and “water” good when the water was placed inside

The approach used to model the two phenomena will now be described.

5.7.1. Modelling Door Opening

As described in the wall model above, all the walls of a refrigerator, including the door, are made up of plastic, polyurethane and steel, each of which provide a certain resistance to heat conduction from the ambient to the inside of the refrigerator. During door opening, all three solid layers become, in effect, non-existent, and conduction resistance drops to zero. This principle was incorporated in the model by attaching a "table" function to each layer of the door of the cabinet. These tables, shown in Figures 5.25-5.27, map time against conductivity values of polyurethane, plastic and sheet metal. The left column represents time in minutes, while the right column shows the conductivity values in W/mK. As can be seen, until a certain desired time (in this case 365 minutes- when the door was opened in the validation experiment) the conductivity values are the standard values from [40]. From 365 min to 372 min (the door was opened for 6 minutes) the conductivity values are entered as excessively large numbers (10000 W/mK-approaching infinity) so that the corresponding resistances approach zero and heat gain through the door is maximised. After the door is closed, the values are returned to those before the door was opened.

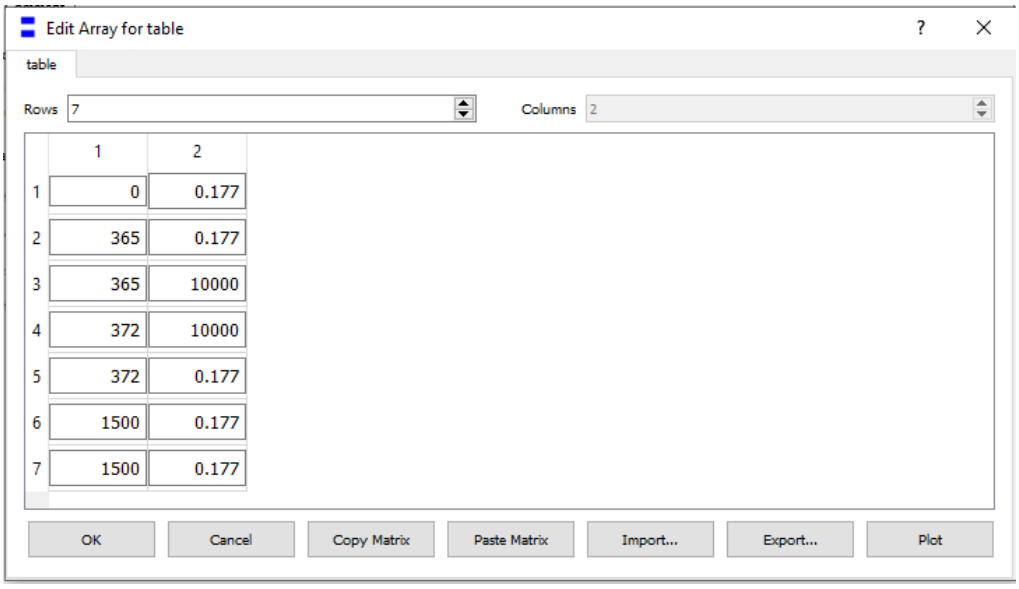

Figure 5.25. Table for inner plastic layer.

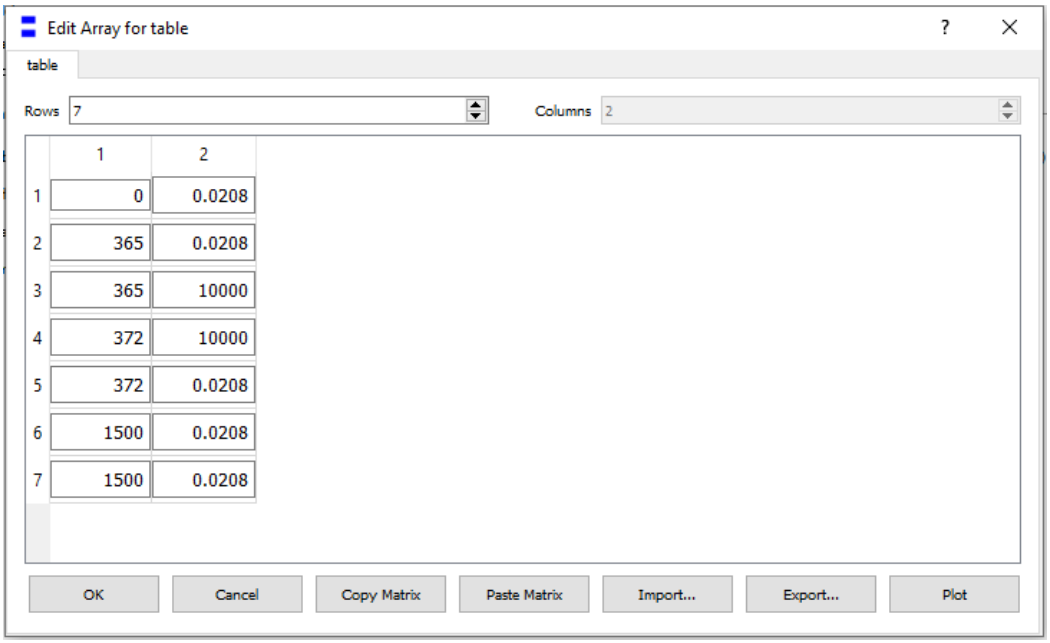

Figure 5.26. Table for polyurethane layer.

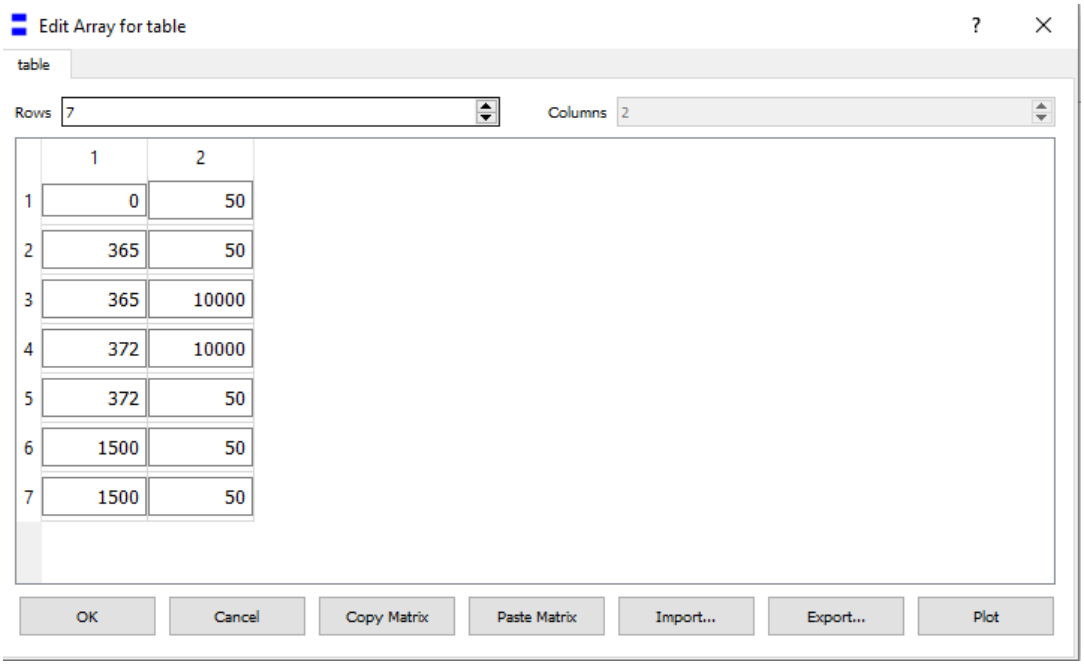

Figure 5.27. Table for outer sheet metal layer.

Besides conduction, there is a certain convective heat transfer coefficient inside and outside the refrigerator which sustains convection at both ends (the calculation of this was shown in Section 5.5.2). When the door opens, air infiltration occurs as well, and the increased mixing between the cold interior air and the warm exterior air causes the heat

transfer coefficient to increase. To capture this, tables are used, as shown in Figures 5.28 and 5.29, where the convective heat transfer coefficient is increased at both the inside and outside. Due to a lack of viable correlations available for the calculation of this type of convective heat transfer coefficient, the value was fine-tuned to match the experimental data. In this case, the best approximation turned out to be 50 W/m^2K. After the door is closed, the values are returned to those before the door was opened.

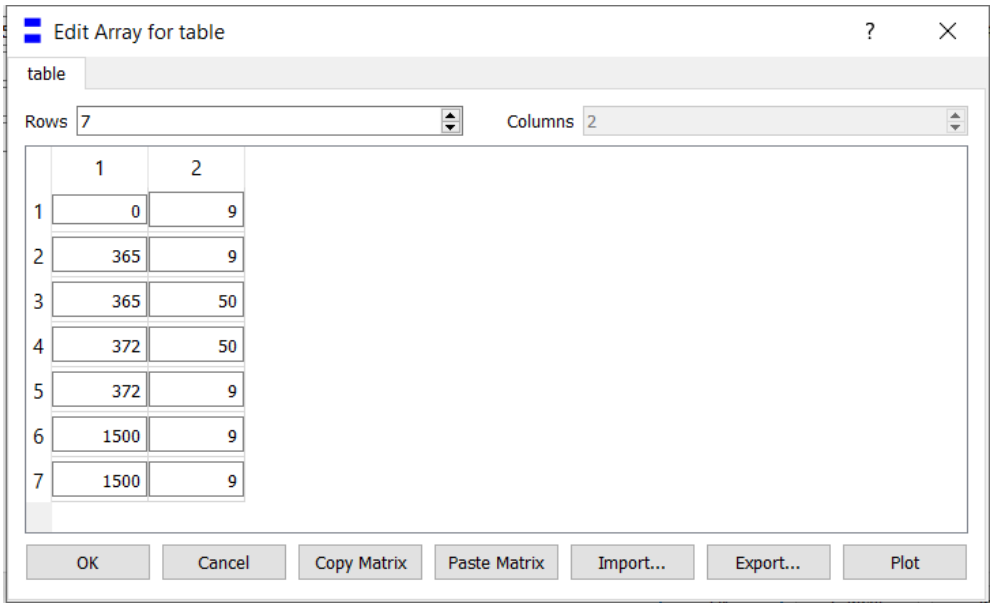

Figure 5.28. Cabinet Inside Heat Transfer Coefficents.

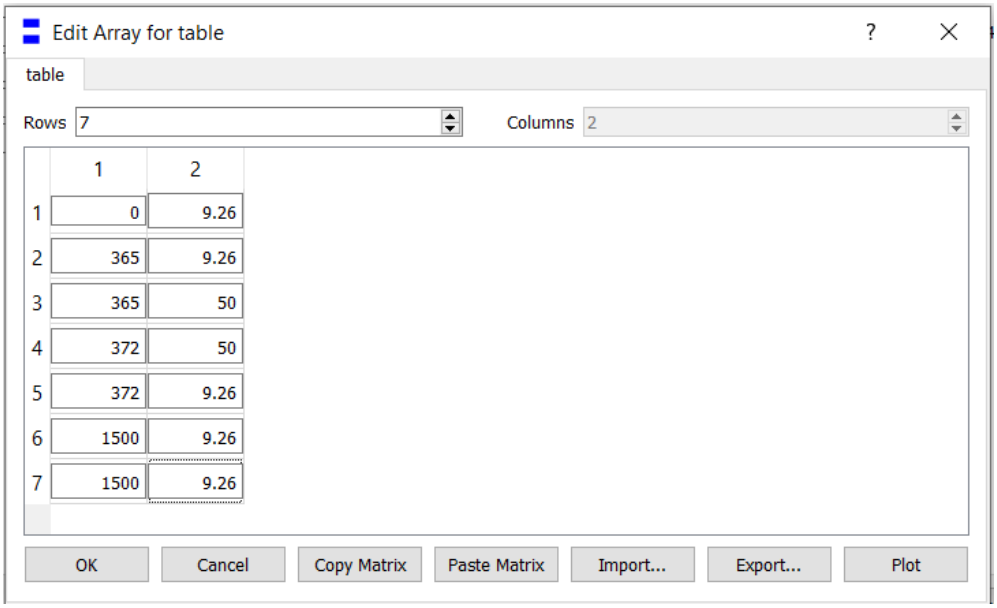

Figure 5.29. Cabinet Outside Heat Transfer Coefficents.

5.7.2. Modelling the Increase in Goods

Recall that the plastic containers filled with water are placed inside the refrigerator after it has been running for around 6 hours. This implies that the total mass inside the cabinet increases after 6 hours. This change in total mass becomes all the more important considering that water has a very high specific heat capacity (4180 J/kg K) compared to other materials such as plastic (1400 J/kg K) and glass (840 J/kg K), and the sudden inclusion of 20L of warm water will therefore significantly affect the transient behaviour of the cabinet.

The aforementioned phenomenon is modelled by including the total amount of water and additional plastic in the model as “goods”. These goods, however, are connected to the air cell through a resistor with a variable resistance value. This variable resistance value acted as a control switch, effectively turning “off” the effect of goods during the initial cooling of the refrigerator (i.e., when the additional load is not present). This is done by setting the resistance value to a very high value, approaching infinity. As the resistance approaches infinity, the heat transfer rate approaches zero, thereby suppressing the presence of additional goods. After the load is placed and the door is closed, the resistance value is set such that it approaches zero, so that the heat transfer rate between the goods and air returns back to the value governed by the original convective heat transfer coefficient defined for the air (and calculated using the approach outlined in Section 5.5.2). This effectively turns “on” the effect of goods. The table of values for the resistors is shown in Figure 5.30. It can be seen that the resistance value is essentially infinite upto 365 minutes (~ 6 hours) and is set to near-zero thereafter.

Edit Array for table

table

Rows 5

	1	2
1	0	10000
2	365	10000
3	365	0.0001
4	1500	0.0001
5	1500	0.0001

Figure 5.30. Table of values for resistance connected between air and additional goods.

The final modified cabinet can be seen in Figure 5.31. The additional components described above are labelled and defined below:

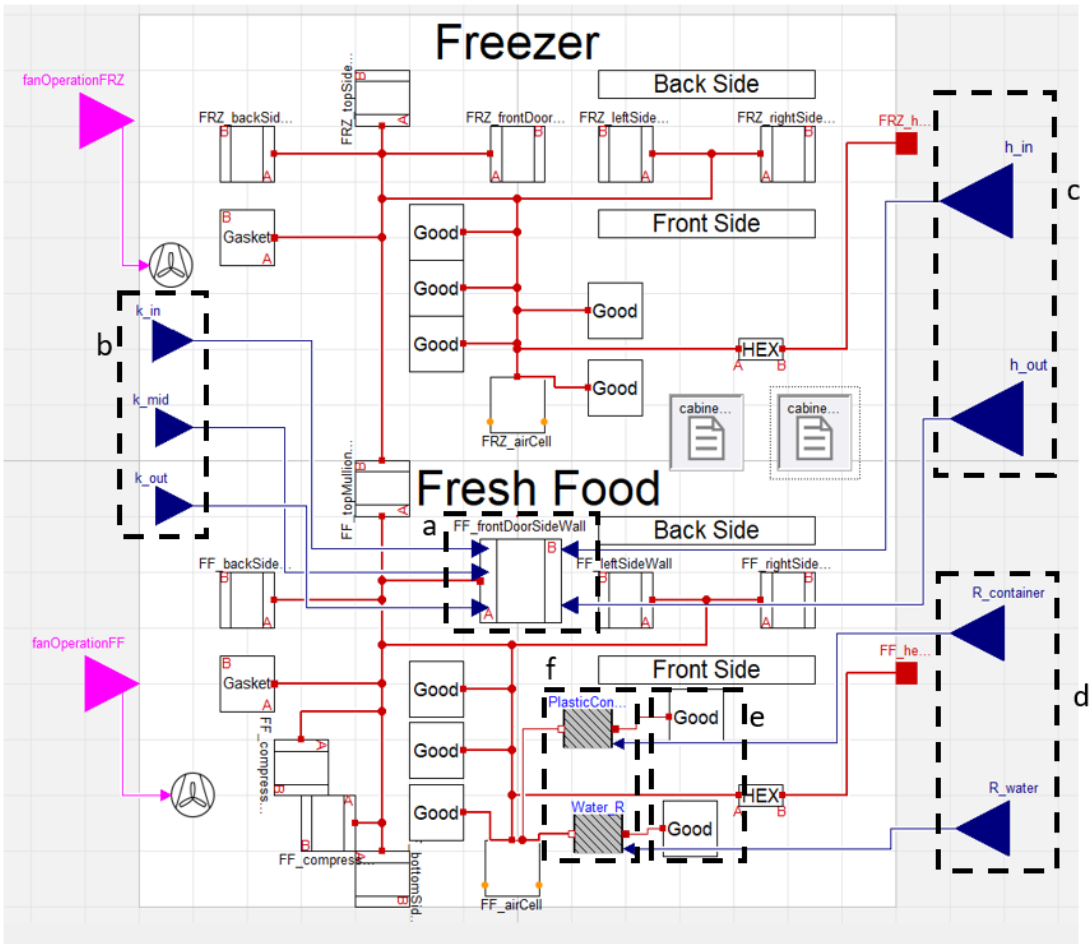

Figure 5.31. Modified Cabinet Model for Water Pot.

a. The FF door, which is connected to various inputs
b. Thermal conductivity inputs for each wall layer. These are connected to the table of values shown in Figures 5.25-5.27
c. Convective heat transfer inputs for inside and outside the cabinet. These are connected to the table of values shown in Figures 5.28 and 5.29.
d. Resistance inputs for the resistor between goods and air. These are connected to the table of values shown in Figure 5.30.

The final cycle model incorporating the modified cabinet model can be seen in Figure 5.32.

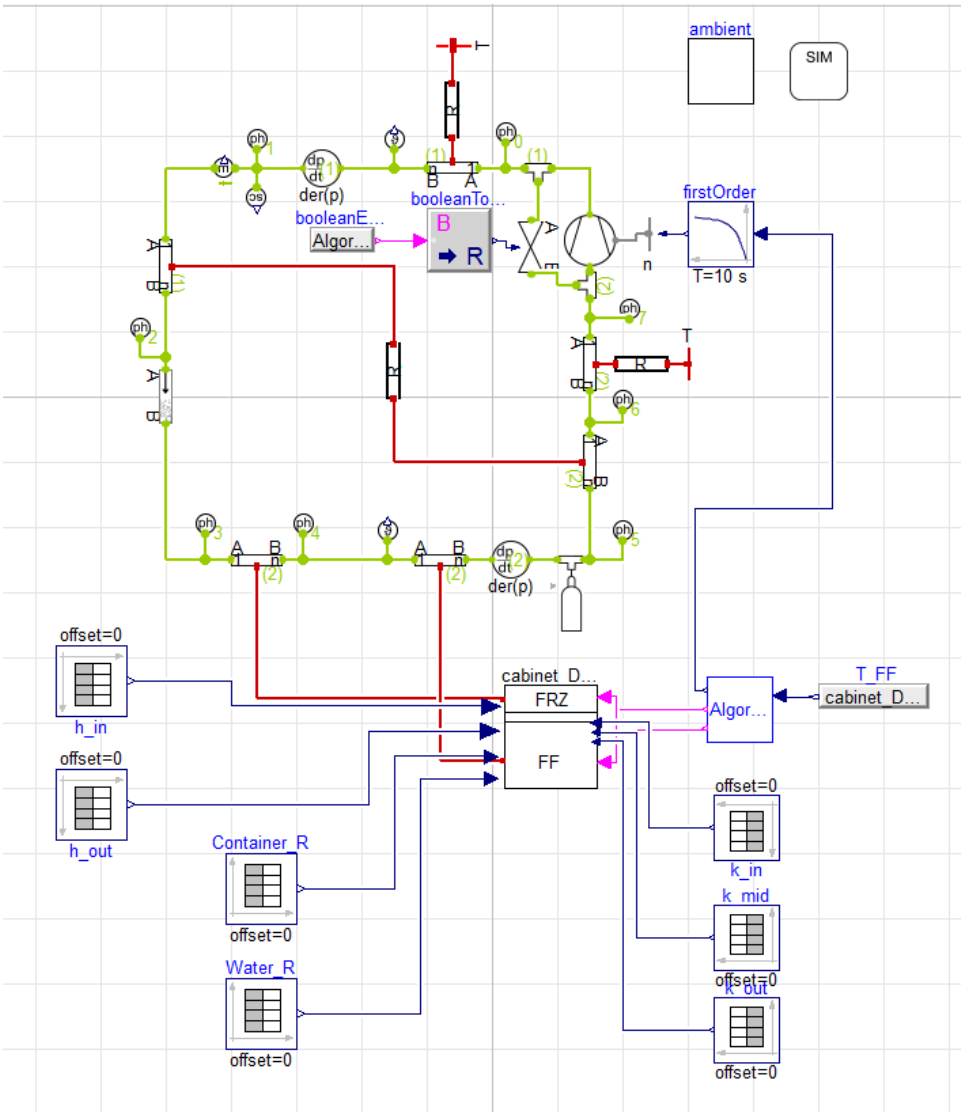

Figure 5.32. Complete cycle model.

6. EXPERIMENTAL DETAILS

To validate the model and to gather data for calculating empirical parameters such as the heat transfer coefficient (as explained in Section 5.5.2), experiments were carried out on a top-mounted conventional refrigerator. Details of the refrigerator, the experimental setup, and the method used to obtain data are now presented.

6.1. Details of the Refrigerator

The refrigerator consisted of a Freezer compartment and a Fresh Food compartment. The Freezer compartment was located at the top, while the Fresh Food was located at the bottom of the cabinet. Figure 6.1 shows the refrigerator from the front, with the compartments labelled. Figure 6.2 shows the inside view of the refrigerator.

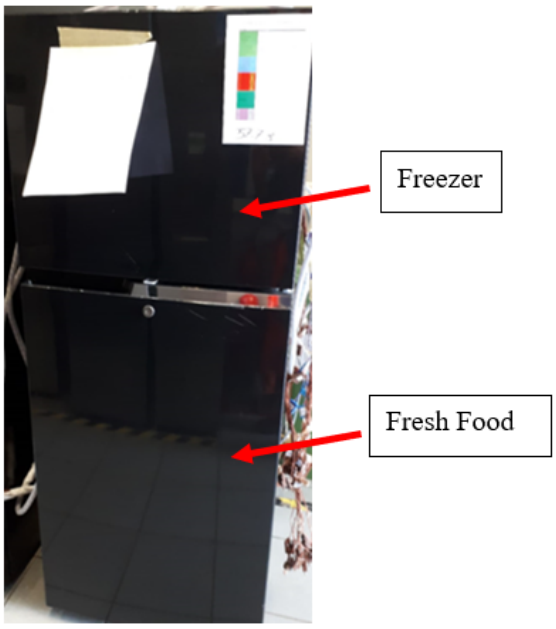

Figure 6.1. Front view of the refrigerator.

Figure 6.2. Inside view of the refrigerator.

Details:

- Freezer Volume: 74 L
- Fresh Food Volume: 190 L
- FF Evaporator type: Plate-on-tube
- FRZ Evaporator type: Skin evaporator wrapped around the top, side and bottom walls
- Condenser type: Wire-on-tube
- Compressor type: Fixed speed; 3000 RPM
- Refrigerant: 61g of R600a (Isobutane)

Note that the compressor listed above is the compressor used to validate the model. Another variable speed compressor was used and run at three different speeds to assess the sensitivity of the model (as descried in Section 7.3). Figures 6.3-6.6 show some other pictures of the refrigerator, with components labelled.

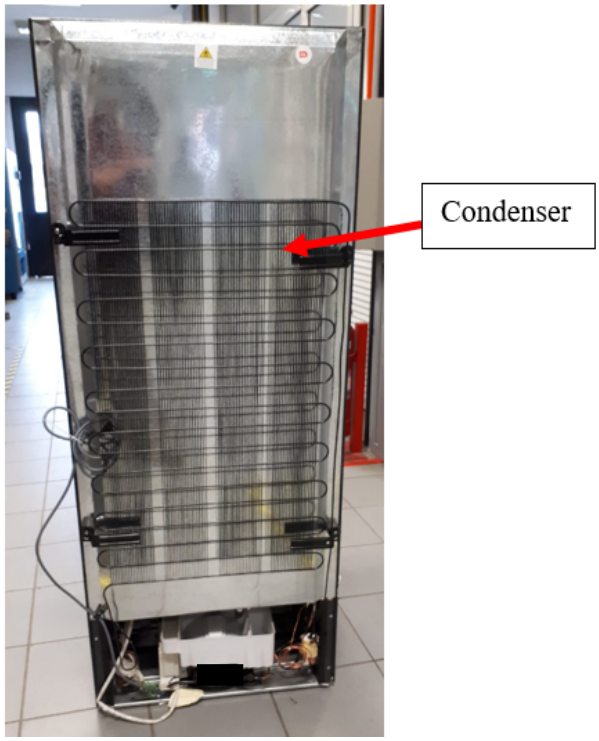

Figure 6.3. Back view of the refrigerator, showing the condenser.

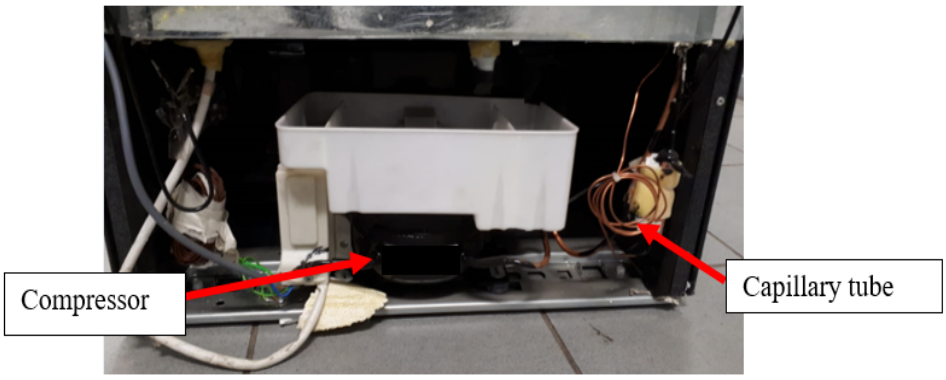

Figure 6.4. Machine room of the refrigerator.

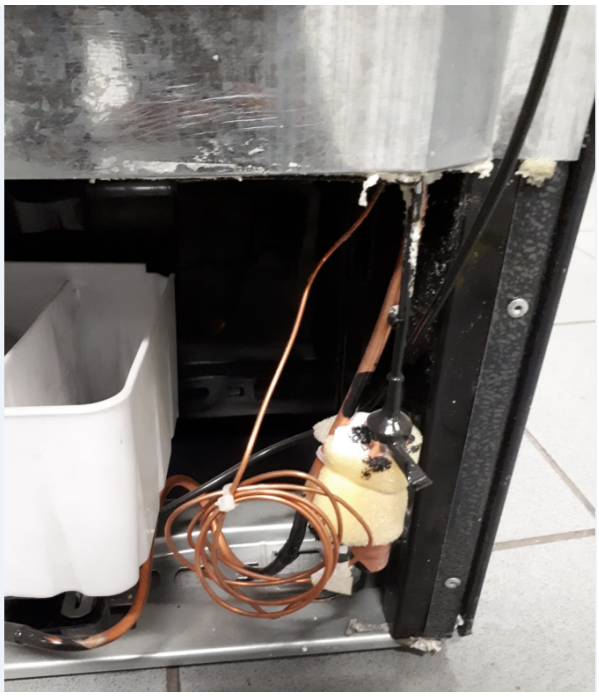

Figure 6.5. Capillary tube.

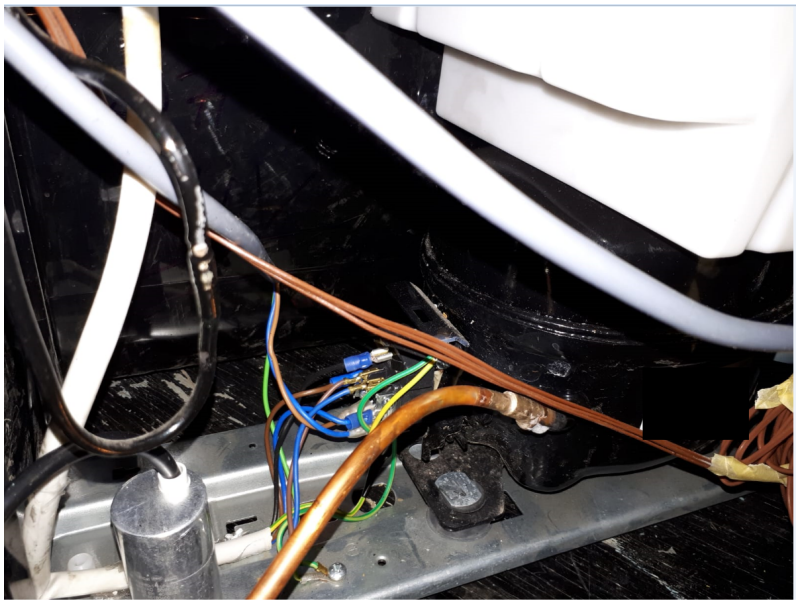

Figure 6.6. Compressor.

6.2. Experimental Setup

6.2.1. Temperature Measurement

The refrigerator was prepared by placing thermocouples at various locations, as listed below. After preparation, the refrigerator was placed inside a climate chamber, on a station made of wood and prepared in accordance with the International Electrotechnical Commission (IEC) Standard for Household Refrigerators (IEC 62552).

The list of thermocouples is as follows. The quantities and location of the thermocouples are written in parenthesis.

Inside the Freezer Compartment:

- Back wall surface (3: top, middle and bottom of surface)
- Left Side wall surface (3: top, middle and bottom of surface)
- Right side wall surface (3: top, middle and bottom of surface)
- Bottom wall surface (1: centre)
- Top wall surface (2: centre)
- Door surface (1: centre)
- Suspended in the air at different positions (5: top left (x 2), centre (x 1), bottom right (x2))
- A thermocouple fitted in a 3-inch diameter copper block (1: centre of the compartment)

Fresh Food Compartment:

- Back wall surface (3: top, middle and bottom of surface)
- Left Side wall surface (3: top, middle and bottom of surface)
- Right side wall surface (3: top, middle and bottom of surface)
- Bottom wall surface (1: centre)
- Top wall surface (1: centre)
- Compressor Front Surface (1: centre)
- Compressor Top Surface (1: centre)

- On each shelf (to measure air temperature above that shelf) and inside the crisper drawer (5: above each shelf (x 4), inside crisper drawer (x 1))
- A thermocouple fitted in a 3-inch diameter copper block (1: centre of the compartment)
- Door surface (x 2)

System Components:

- Compressor suction pipe (1)
- Compressor discharge pipe (1)
- Condenser inlet (1)
- Condenser centre (1)
- Condenser outlet (1)
- FRZ Evaporator Inlet (1)
- FRZ Evaporator Outlet (1)
- FF Evaporator Inlet (1)
- FF Evaporator Outlet (1)

Note that such a large number of thermocouples were used primarily for diagnostic purposes. That is, to detect the cause of any problem which may occur in the refrigerator (for e.g. gas charge leakage leading to an uncooled evaporator). However, the surface temperatures of walls inside the cabinet were taken especially to calculate the temperature difference between the wall and air and thereby calculate the heat transfer coefficient inside both compartments (Section 5.5.2). Also note that thermocouples were also placed on the left and right side of the refrigerator to measure the exact ambient temperature of the area where the refrigerator is placed. Figure 6.7 shows the refrigerator on the platform in the climate chamber. Figures 6.8-6.10 show the thermocouple placement inside the refrigerator.

Figure 6.7. Refrigerator placed on the wooden platform in the climate chamber.

Figure 6.8. Thermocouples placed inside both compartments.

Figure 6.9. Thermocouples (marked with blue circles) inside the FF compartment.

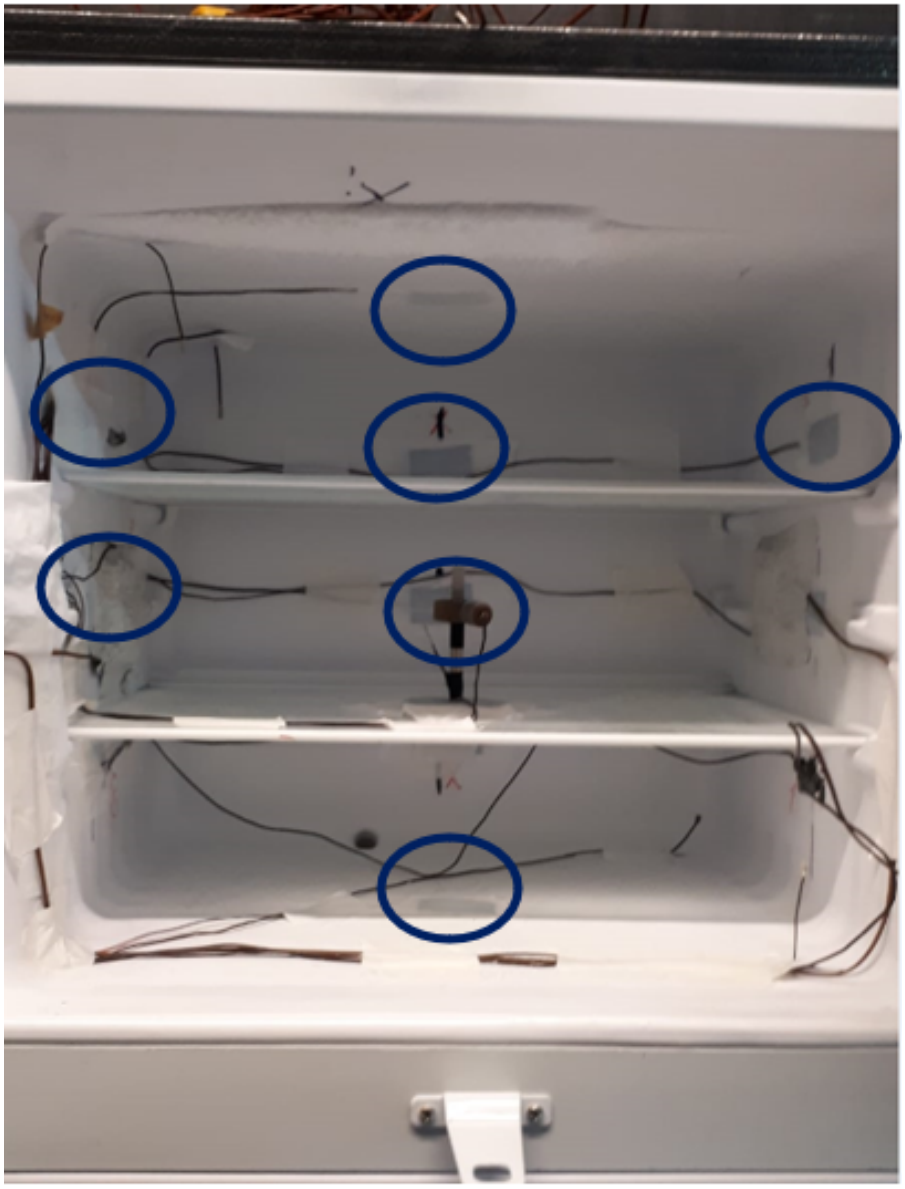

Figure 6.10. Thermocouples (marked with blue circles) in the FRZ Compartment.

6.2.2. Other Measurements

Besides temperature, the voltage, current, power and energy values were also measured during the experiments. The uncertainty values for each sensor is show in Table 6.1.

Table 6.1. Uncertainty values of sensors used in the experiment.

Sensor	Uncertainty
Voltage	0.25 %
Current	0.25 %
Power	0.05 %
Temperature	0.5 °C

To calculate the energy consumption of the refrigerator (Equation 6.2), the run time (given in Equation 6.1) is multiplied by the compressor power, and the product is then multiplied by 24 to get the energy in Wh/24h:

$$Run\ Time\ (RT)\ = \frac{on\ time}{off\ time} \tag{6.1}$$

and

$$E = (24)(P)(RT). \tag{6.2}$$

where E is the energy in Wh/24h and P is the Power in W.

To calculate the uncertainty in the energy value, the classical procedure used by Kline and McClintock (1953) [46] was used. In that paper, the main equation for uncertainty is as follows:

$$w_r = \sqrt{\left(\frac{\partial R}{\partial v_1} w_1\right)^2 + \left(\frac{\partial R}{\partial v_2} w_2\right)^2 + \cdots \left(\frac{\partial R}{\partial v_n} w_n\right)^2} \tag{6.3}$$

where w is the uncertainty in a result R which is a function of the quantities v_1, v_2.. v_n having corresponding uncertainties w_1, w_2.. w_n. Using 6.2 and 6.3, we can then write:

$$w_E = (24)\ (RT)(w_1) \tag{6.4}$$

where w_E is the uncertainty in energy, and w_E is the uncertainty in power. Now, the absolute uncertainty in power is not known; however, Table 6.1 gives the percentage uncertainty in power. Since energy is also best expressed as a percentage uncertainty, we can manipulate Equation 6.4 by dividing it by Equation 6.2 to get:

$$\frac{w_E}{E} = \frac{w_1}{P}.$$

Therefore, the percentage uncertainty in energy is simply equal to that of the power, which is 0.05 %

6.3.Experimental Method

After the refrigerator was prepared with thermocouples and placed on the platform in the climate chamber, data was recorded every minute using a Data Acquisition System. The refrigerator was firstly placed in the room for about 6 hours with doors open to ensure that it reaches the ambient temperature. The doors were then closed, and the refrigerator was plugged in. After pull down, (which lasted about 6 hours), the refrigerator entered into a cyclic "regime". In this regime, the compressor turns on and off, thus performing cycles, according to threshold temperatures (called cut-in and cut-out temperatures). To ensure a sufficient number of cycles are present for validation, data was collected for another 24 hours. This was firstly carried out at 32 °C to validate the model. The model was then simulated at 25 °C for ambient temperature sensitivity, and the experiment was carried out again at 25 °C to ensure that the simulation results are accurate. Moreover, to assess the sensitivity of the model for different compressor and compressor speeds, simulations were carried out at 32 °C by replacing the original fixed sped compressor with a variable one. This variable speed compressor was run at three different speeds (3000 rpm, 2500 rpm and 2000 rpm). Experiments were carried out with this compressor as well, to assess the accuracy of the model's response.

As mentioned in Section 3.2, the second part of this study involved simulation of the "water pot" test, in which a specific amount of warm water is placed in the FF compartment and the water temperature after 6 hours is noted. To validate this model; the refrigerator was

left to cool down at 32 °C. The thermostat was deactivated inside the refrigerator so that it does not enter cyclic mode. After 6 hours of pull down, the door of the FF compartment was opened for 6 minutes and a total of 20L of water at 27 °C was placed inside the FF compartment. This was done in the form of 4 containers filled with 5 L of water. The containers were placed close together on the bottom two shelves. They were placed as close as possible to make the approximation of water as a lumped mass more accurate. Thermocouples were placed inside each container, at the very centre of the volume of water. The refrigerator was then left to cool down the water for another 6 hours. Again, data was recorded every minute. Figure 6.11 shows the FF compartment in the refrigerator filled with water pots.

Figure 6.11. FF compartment filled with water pots for the water pot test.

7. RESULTS AND DISCUSSION

Using the modelling and experimental methods described in the previous chapters, the following simulations were validated:

i) Cyclic operation using a fixed speed compressor (3000 RPM) at 32 °C
ii) Cyclic operation using a fixed speed compressor (3000 RPM) at 25 °C (to test sensitivity of the model to a different ambient temperature)
iii) Cyclic operation using a variable speed compressor operated at different speeds at 32 °C:
    a. At 3000 rpm
    b. At 2500 rpm
    c. At 2000 rpm
iv) Water Pot test at 32 °C

The results and discussion are now presented for each case. Note that the experimental air temperature values in the relevant graphs below are the average of all the thermocouples placed inside the refrigerator to measure the air temperature (see Section 6.2.1). Error bars denoting ±0.5 °C (the thermocouple uncertainty) are also placed on the graphs showing temperatures. Error bars for power consumption are not shown because power has a very low uncertainty of 0.05%; hence, the bars were not visible on the graph.

7.1. Cyclic Operation Using A Fixed Speed Compressor at 32 °C

Figures 7.1-7.4 show the FF and FRZ air temperatures, compressor power consumption, evaporator temperature and condenser temperature respectively.

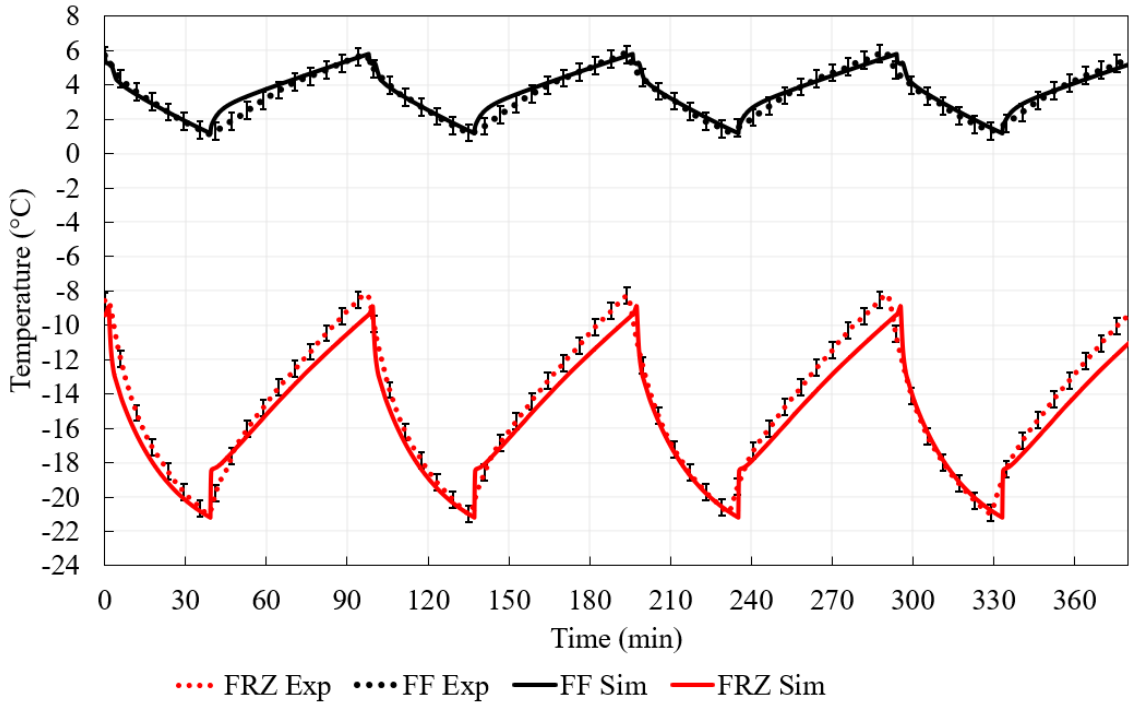

Figure 7.1. FF and FRZ Air Temperatures for 32 °C (fixed speed compressor).

The air temperatures are very close, with a maximum deviation of 2 °C (for both FF and FRZ). This occurs primarily because air is treated as a “lumped” mass in the model, but it is a “distributed” mass in reality. Also note that the steep rise at the onset of the heating period (i.e., when the compressor first switches off) is because of numerical errors as the compressor switches from on to off.

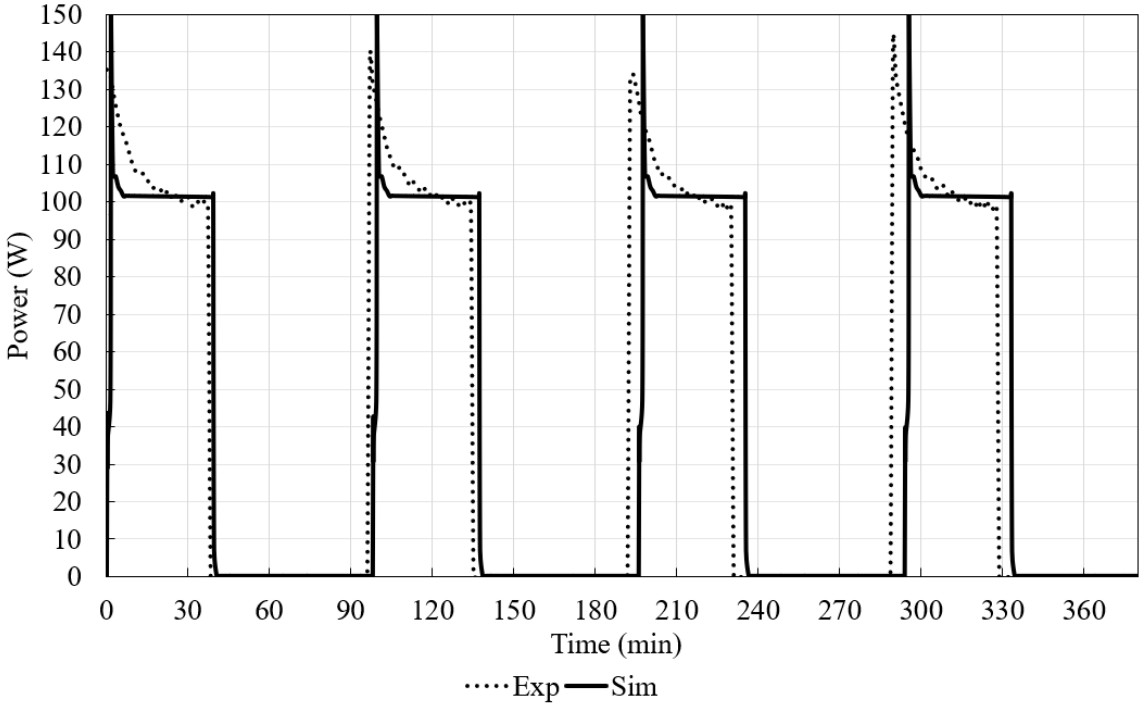

Figure 7.2. Compressor Power Consumption for 32 °C (fixed speed compressor).

Figure 7.2 shows the compressor power consumption. A deviation of 3.7% occurs between the average power consumption values, with the model slightly understating the average value. This happens because compressor power is a function of the evaporation temperature, and the evaporator temperature in the simulation reaches the steady state evaporation temperature (set by the system parameters such as the capillary tube length and diameter) more quickly than in reality (see Figure 7.3). The more gradual drop of the evaporator temperature in reality is because the actual evaporator is attached directly to the walls of the compartments and is therefore directly exposed to heat gain from the outside ambient (which ultimately reaches the inside air). This heat gain opposes the tendency of the evaporator to cool as low pressure refrigerant flows in it. In the model, the evaporator is treated as a separate tube (see Section 5.2) and is not exposed to the heat gain directly. Another cause for the delay is that in reality the refrigerant takes some time to completely fill the evaporator, while in the model, this filling is much more rapid. Due to this lag in evaporator temperature drop, the compressor power in the experiment drops gradually, while in the simulation it reaches the steady state value governed by the system parameters more rapidly.

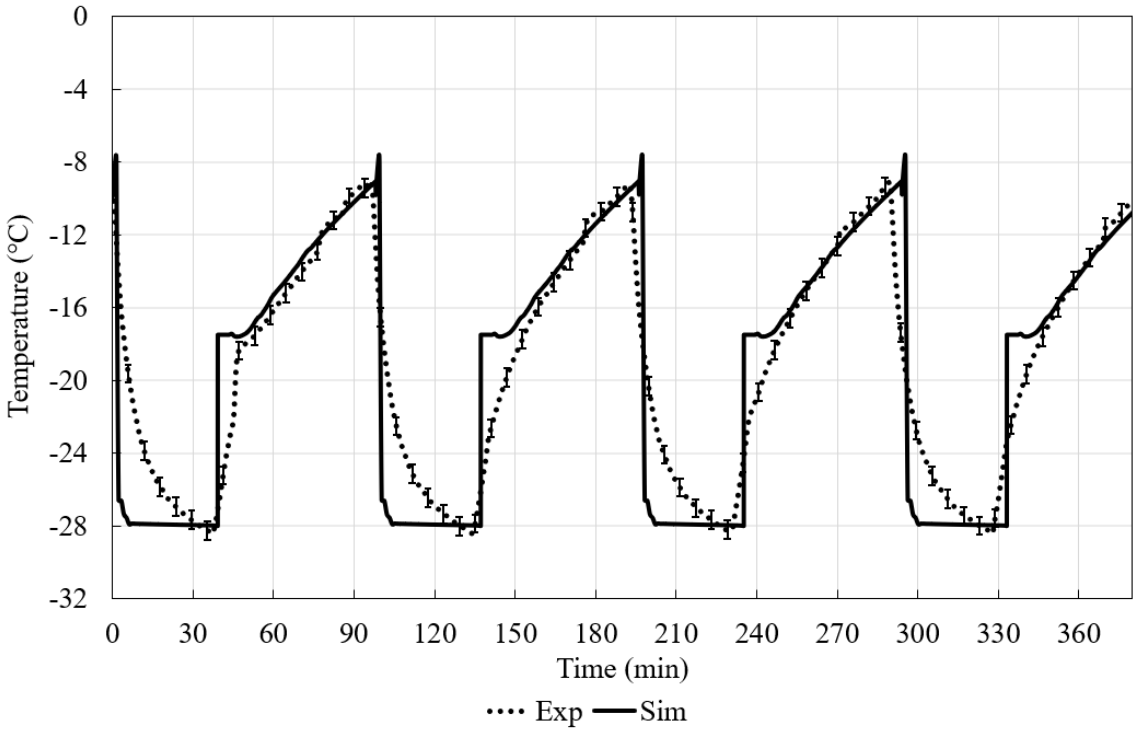

Figure 7.3. Evaporator Temperature for 32 °C (fixed speed compressor).

Figure 7.3 shows that the actual evaporation temperature (i.e., the bottom peak for the experimental values, around -28 °C) differs from the simulated value by a maximum of 0.5 °C. The difference can be attributed solely to experimental uncertainty, since the uncertainty of thermocouples is 0.5 °C. As explained above, in the simulation the steady evaporation value during compressor on-time is reached more quickly compared to that in the experiment. This occurs because of the reasons mentioned above while discussing power, namely, the direct attachment of the evaporator to the wall, and the time taken by the refrigerant to fill the evaporator completely.

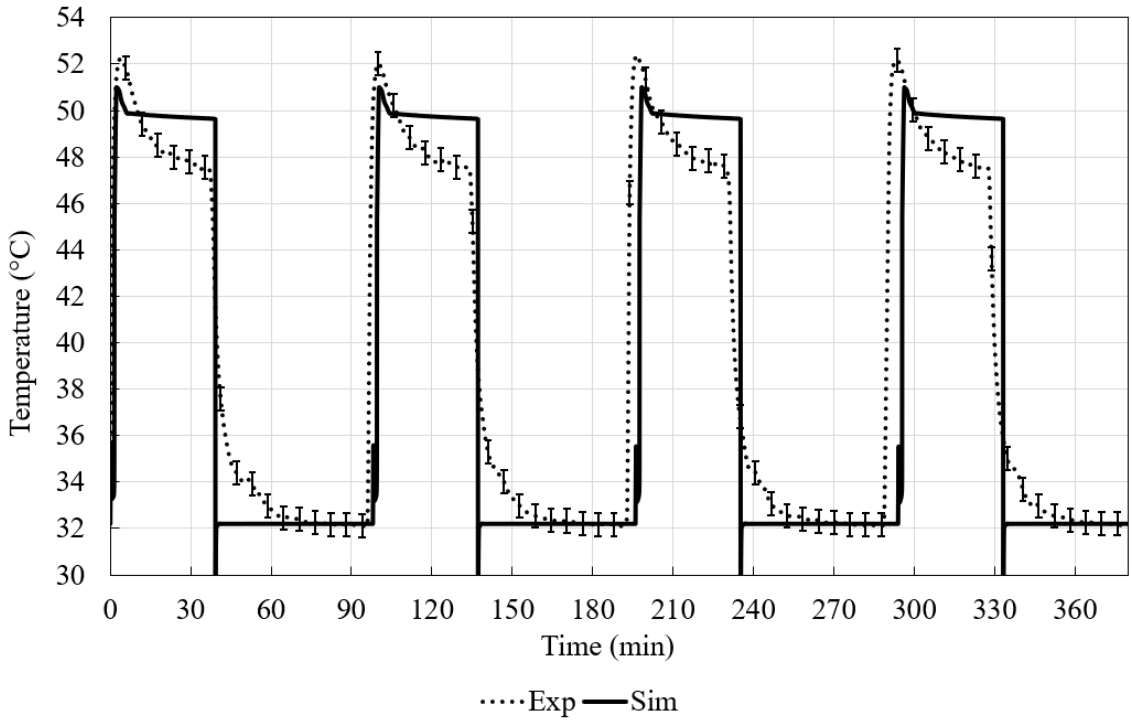

Figure 7.4. Condenser Temperature for 32 °C (fixed speed compressor).

The maximum difference in condensation temperature is 2 °C. Besides experimental uncertainty, another cause is that the combined heat transfer coefficient between the ambient and the condenser was taken as the ASHRAE approved value of 9.26 W/m^{2}K. However, this value does not consider the tubular nature of the condenser, which could lead to greater disturbance in the air flow and therefore enhance the heat transfer coefficient in that region. This translates into increased heat transfer between the condenser and the ambient, and therefore lower condensation temperature. At any rate, the condensation temperature does not severely affect the power values (the evaporation temperature is much more dominant), and 2 °C is quite acceptable.

Table 7.1. Comparison of Runtime, Power and Energy - 32 °C, fixed speed compressor.

		Experiment	Simulation	Difference
Time (min)	ON	37.0	39.3	2.3 min
	OFF	56.5	58.7	2.2 min
Run Time	-	0.395	0.401	1.4%
Power (W)	ON	108	104	-3.7%
	OFF	0	0	0.0%
Energy (Wh/24h)	-	1025.0	1000.9	-2.4%

Table 7.1 presents the run time and power for both experiment and simulation, two essential factors in determining the energy consumption of a refrigerator. Note that the time-averaged power consumption values were compared for both the on and off states. The run time shows very little deviation, with the percentage difference between the two ratios less than 1.5%. The slightly longer cooling times in simulation are balanced by the almost equally longer heating times, thereby cancelling the discrepancy, and leading to nearly equal run times. The power consumption value shows a deviation of 3.7% during on time and is mainly responsible for the 2.4% deviation in the energy consumption (since the energy consumption is given by Equation 6.2). This is quite acceptable, considering that the allowed tolerance in energy consumption as per the EU Ecodesign Regulation is 10%, and thus, the energy consumption from the model can be used to assess the true energy consumption of the refrigerator with decent accuracy.

7.2. Cyclic Operation Using a Fixed Speed Compressor at 25 °C

Figures 7.5-7.9 show the FF and FRZ air temperatures, compressor power consumption, evaporator temperature and condenser temperature respectively.

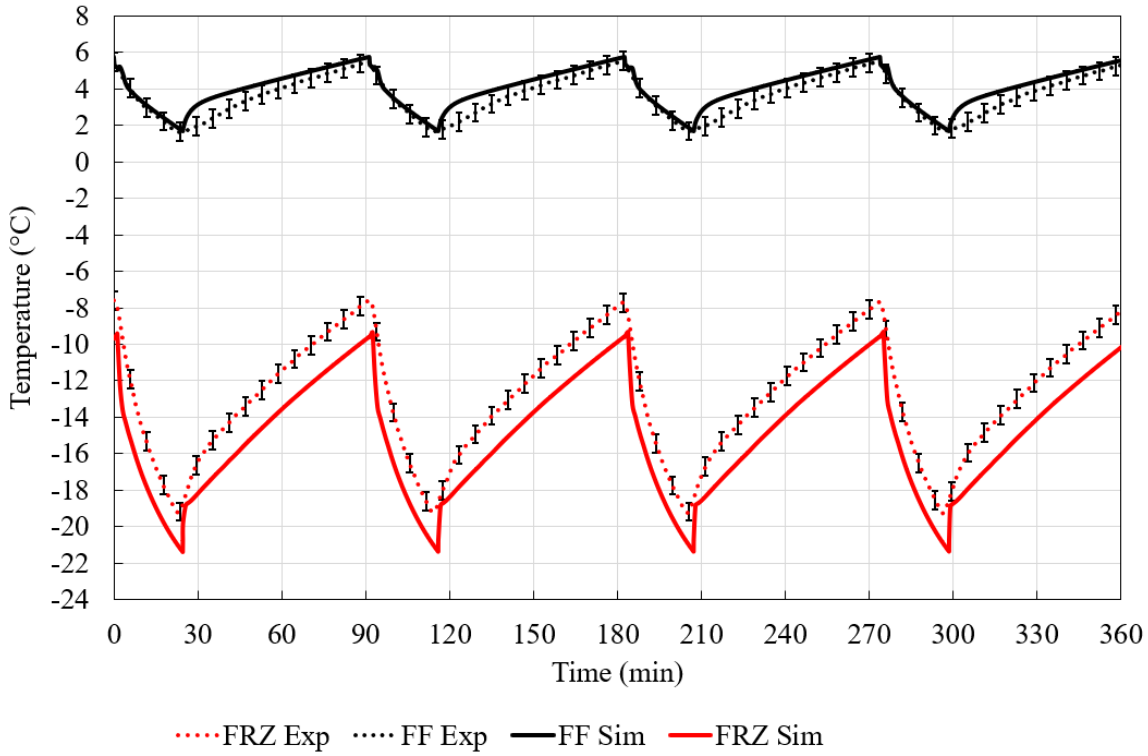

Figure 7.5. FF and FRZ Air Temperatures for 25 °C (fixed speed compressor).

The maximum difference in air temperatures is 3 °C for FRZ and 1.5 °C for FF. The main reason for this deviation is similar to the 32 °C case, namely, the lumped mass approximation.

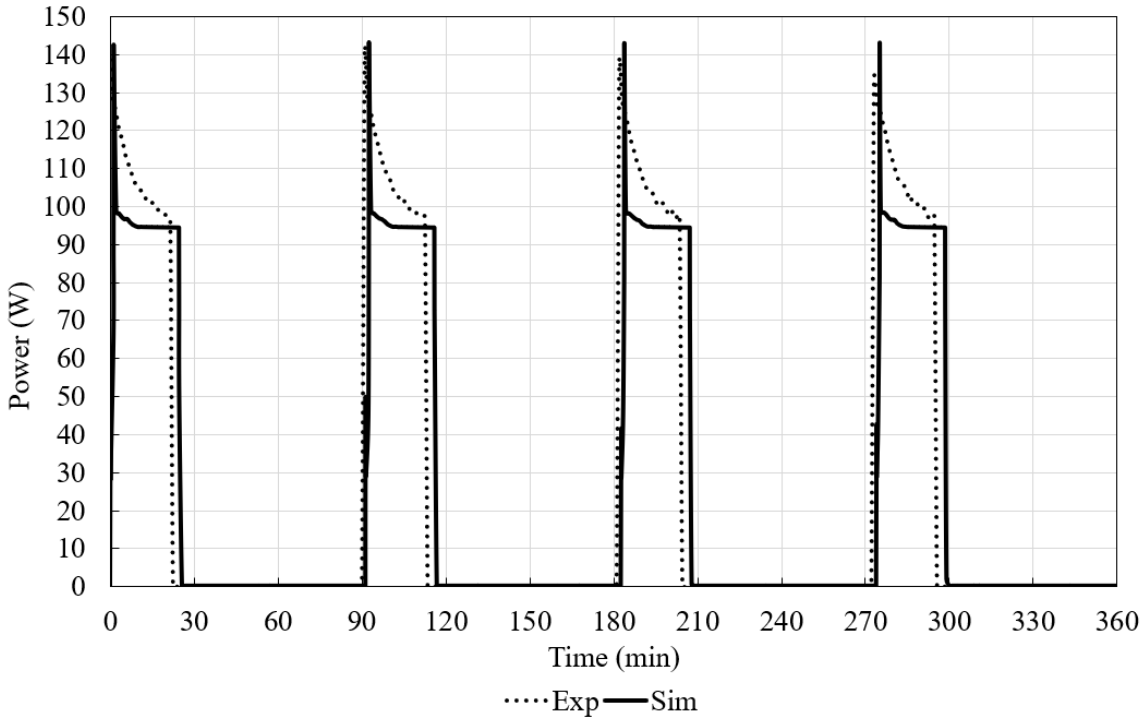

Figure 7.6. Compressor Power Consumption for 25 °C (fixed speed compressor).

Compared to 32 °C, the deviation in power consumption at 25 °C is somewhat larger, with simulation reporting 9% lower values. This occurs in part because of the previously discussed reason, namely, that the evaporator temperature levels-off quicker in the model than in the experiment. But another factor is that the model responds to a change in the ambient temperature by lowering the system evaporation temperature (as can be seen in Figure 7.7), since that is the way most "No-Frost" appliances -operating on a thermostat based on the inner air temperature- work. A lower ambient temperature leads to a lower heat gain, which allows the evaporation temperature to drop. However, the refrigerator used to carry out the experiments has a thermostat attached directly to the evaporator, so that regardless of the ambient temperature, the evaporation temperature can only reach a certain fixed value (around -28 °C) before the compressor operation is cut-off. Since this was not incorporated in the model, simulation showed slightly lower evaporation temperature, and consequently, lower power consumption.

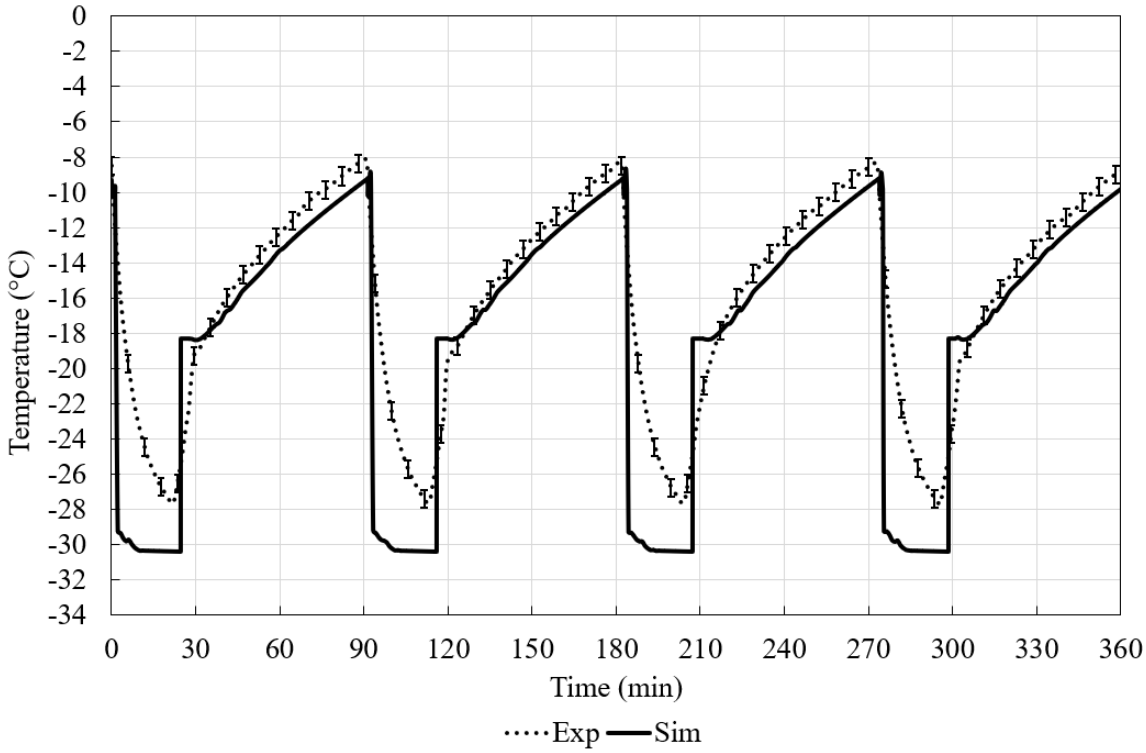

Figure 7.7. Evaporator Temperature for 25 °C (fixed speed compressor).

The evaporation value in simulation is about -30 °C, 2 °C lower than -28 °C in the experiment. The reason has been discussed above, which is that the model responds to the lower ambient by reducing the evaporation temperature, but the real refrigerator does not show that response. That is because it has a thermostat attached to the evaporator, preventing the evaporator temperature from going below a certain set-point temperature.

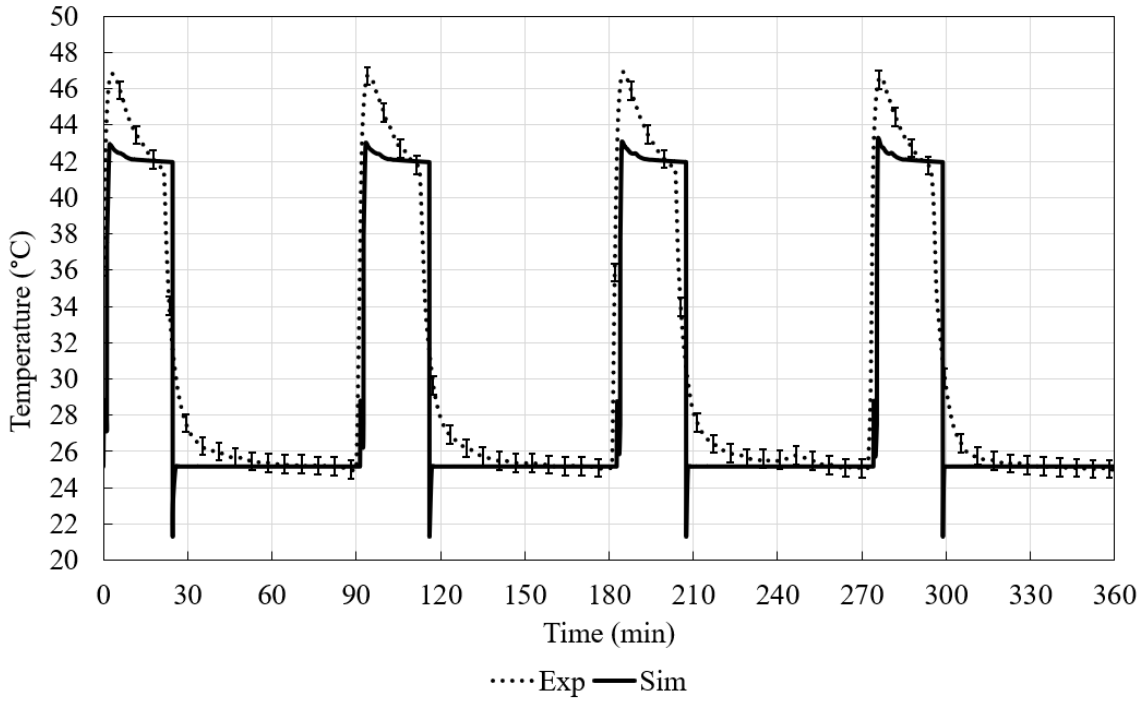

Figure 7.8. Condenser Temperature for 25 °C (fixed speed compressor).

The peak in condensation temperature is not captured by the model (the peaks occur due to greater evaporator temperatures during on time in the experiment). In the simulation, the evaporator temperature drops very quickly, so that the condenser does not get a chance to reach very high peak values. However, the actual condensation temperature towards the end of the compressor on state is almost identical; 42 °C for both simulation and experiment.

Table 7.2. Comparison of Runtime, Power and Energy - 25 °C, fixed speed compressor.

		Experiment	Simulation	Difference
Time (min)	ON	22.3	24.7	2.4 min
	OFF	68	66.6	-1.4 min
Run Time	-	0.247	0.270	9.6%
Power (W)	ON	108.3	98.7	-8.9%
	OFF	0	0	0.0%
Energy (Wh/24h)	-	641.0	640.5	-0.1%

Table 7.2 presents the run time, power consumption and energy consumption for both experiment and simulation. The run time in this case shows a deviation of 9.6%, greater than the negligible value at 32 °C (0.2%). This is because the cooling time in simulation was 2.4 minutes greater than that of the experiment, while the heating time was 1.4 minutes shorter! This led to an overall discrepancy of 3.8 minutes, causing the error in runtime to be greater. The power consumption value, as stated above, shows a deviation of approximately 9%, the reason for which was explained above while discussing the power consumption graph. Despite the larger deviation in both run time and power, the energy consumption discrepancy turned out to be better than for 32 °C, because the error in run time is offset by the error in power consumption. This offsetting behaviour at lower ambient temperatures can be beneficial for optimisation studies which mostly focus on the final energy consumption value.

7.3. Cyclic Operation Using a Variable Speed Compressor

A variable speed compressor was used to test the model's sensitivity to a different compressor and different compressor speeds. The ambient was kept at 32 °C for all simulations (and validation experiments). The air temperatures and power consumption values were recorded for three different compressor speeds: 3000 rpm, 2500 rpm and 2000 rpm. Results for each are presented as follows:

7.3.1. 3000 rpm

Figures 7.9 and 7.10 shows the air temperature and power consumption respectively. Table 7.3 tabulates the run time, power and energy values for both simulation and experiment.

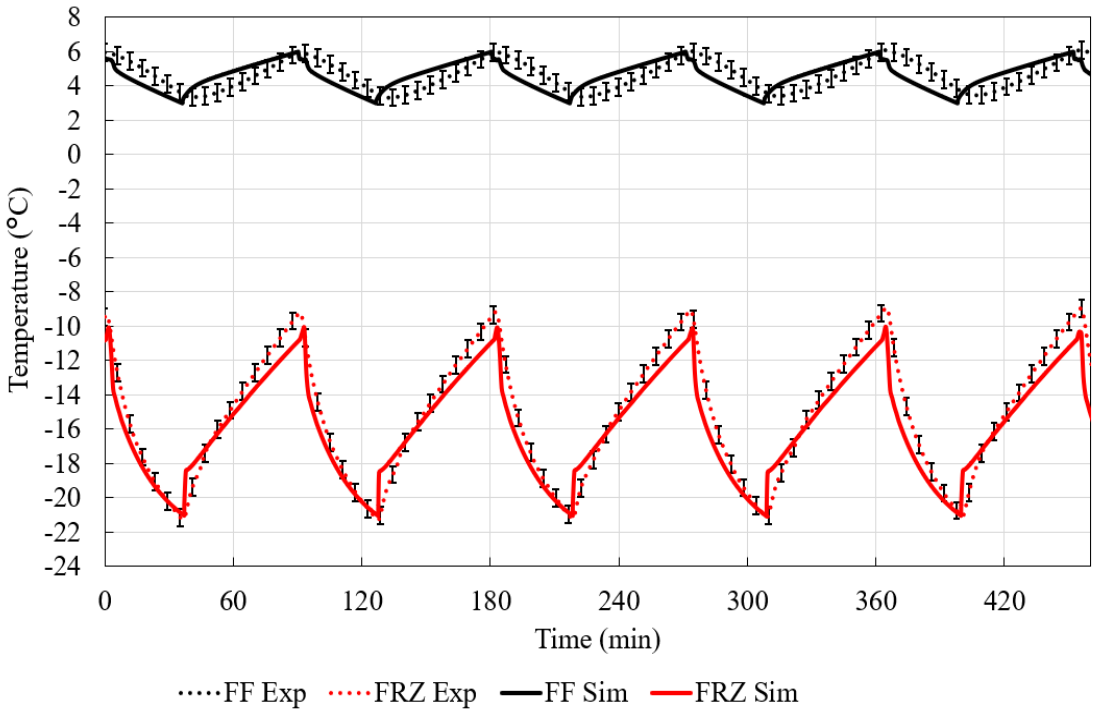

Figure 7.9. FF and FRZ Air Temperatures (variable speed compressor- 3000 rpm).

Figure 7.9 shows that the maximum deviation in air temperature is 1.5 °C and 3 °C for FF and FRZ respectively.

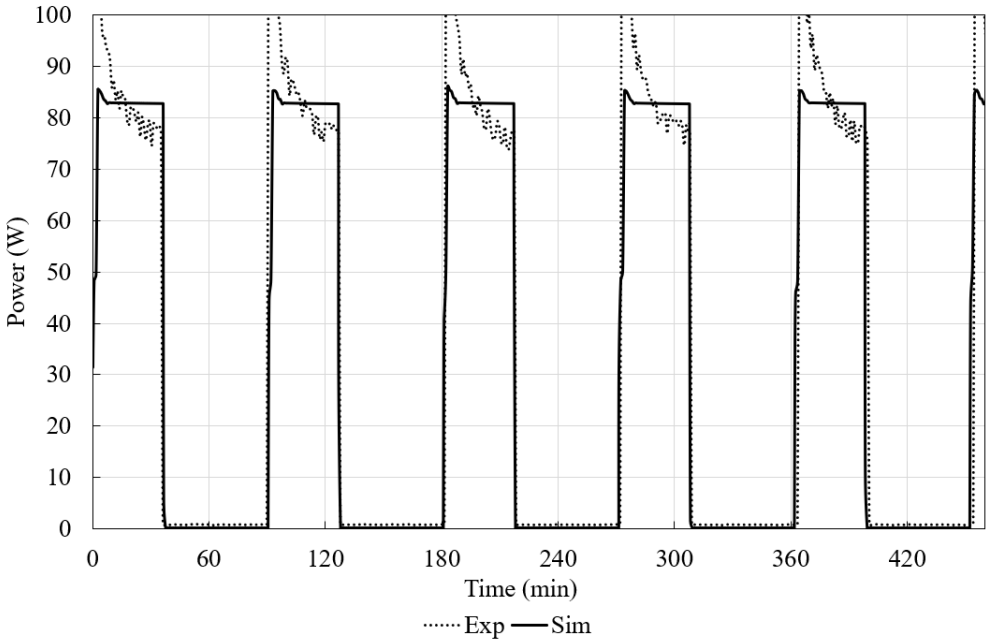

Figure 7.10. Compressor Power Consumption (variable speed compressor- 3000 rpm).

The power consumption graph here shows different values compared to the previous fixed speed compressor. While the average power during on state for the fixed speed compressor was 108 W in experiment and 104 W in simulation (see Table 7.1), the average power here for this new compressor at 3000 RPM is 86.5 W (experiment) and 83 W (simulation). This shows that the model is indeed able to respond to a different type of compressor having a different power consumption value.

Table 7.3. Comparison of Runtime, Power and Energy (variable speed compressor- 3000 rpm).

		Experiment	Simulation	Difference
Time (min)	ON	37.2	36.5	-0.7 min
	OFF	53.8	53.7	-0.1 min
Run Time	-	0.409	0.405	-1.0%
Power (W)	ON	86.5	83	-4.0%
	OFF	0	0	0.0%
Energy (Wh/24h)	-	848.7	806.1	-5.0%

Table 7.3 shows the run time, power and energy values for this compressor at 3000 RPM. As discussed above, the average power consumption is 86.5 W in the experiment, 4% greater than in the simulation. This deviation can be attributed to reasons similar to the ones discussed previously in Section 7.1; namely, due to the difference in evaporator temperatures.

It is noteworthy that despite the lower power consumption for this compressor the run time is very similar to the fixed speed compressor (comparing Table 7.3 with Table 7.1). This implies that the cooling capacity supplied by the compressor is similar in both cases. Since the COP is obtained by dividing the cooling capacity by the compressor power, this directly implies that this new compressor has a greater COP at 3000 rpm compared to the previous one. Due to this, the final energy consumption here (806.1 Wh/24h in the simulation) is 20% lower than the previous fixed speed compressor case (1000 Wh/24h in the simulation).

7.3.2. 2500 rpm

Figures 7.11 and 7.12 shows the air temperature and power consumption respectively. Table 7.4 tabulates the run time, power and energy values for both simulation and experiment

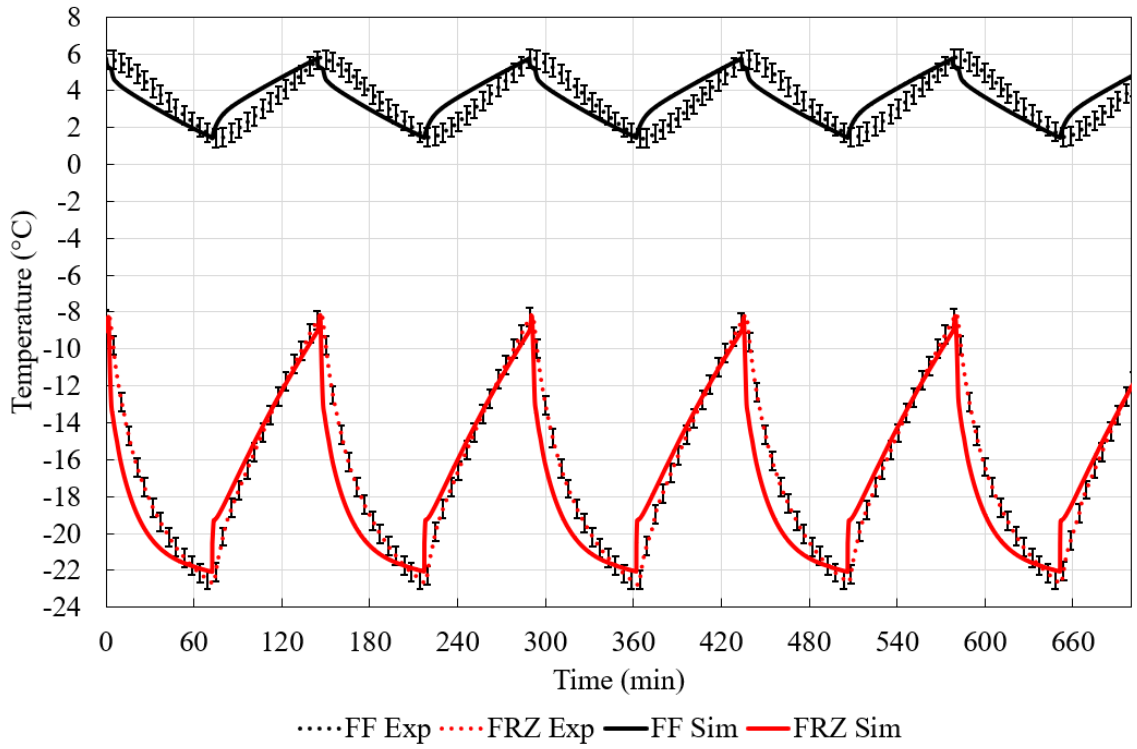

Figure 7.11. FF and FRZ Air Temperatures (variable speed compressor- 2500 rpm).

Figure 7.11 shows that the maximum deviation in air temperature is 1.8 °C and 3 °C for FF and FRZ respectively.

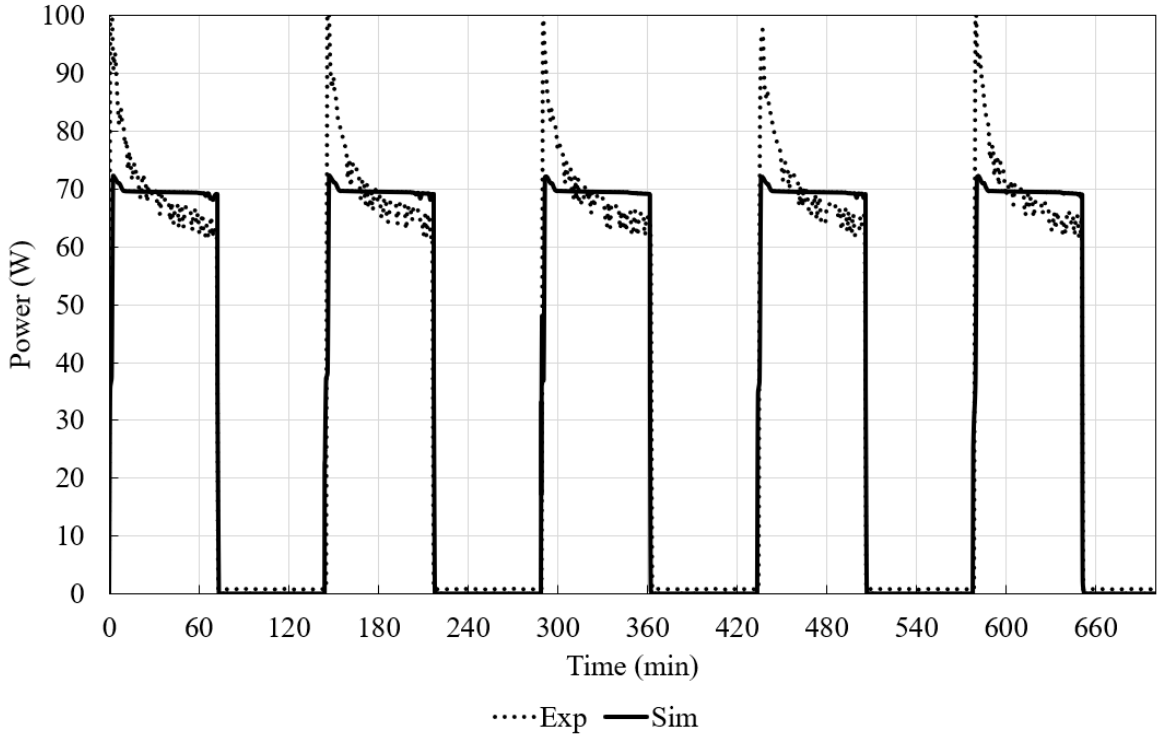

Figure 7.12. Compressor Power Consumption (variable speed compressor- 2500 rpm).

Table 7.4. Comparison of Runtime, Power and Energy (variable speed compressor- 2500 rpm).

		Experiment	Simulation	Difference
Time (min)	ON	71.9	73	1.1 min
	OFF	72.9	71.7	-1.2 min
Run Time	-	0.497	0.504	1.6%
Power (W)	ON	70.7	69.6	-1.6%
	OFF	0	0	0.0%
Energy (Wh/24h)	-	842.5	842.7	0.02%

Once again, Figure 7.12 and Table 7.4 show that the model responds to changes in compressor speed adequately. The power consumption drops from 86 W at 3000 rpm to 70.7 W at 2500 rpm in the experiment, while in the it drops from 83 W to 69.6 W in the simulation.

The deviation in run time is 1.6%, completely offset by the equal deviation in power. This causes almost no difference in the energy consumption values, as Table 7.4 shows.

7.3.3. 2000 rpm

Figures 7.13 and 7.14 show the air temperature and power consumption respectively. Table 7.5 tabulates the run time, power and energy values for both simulation and experiment

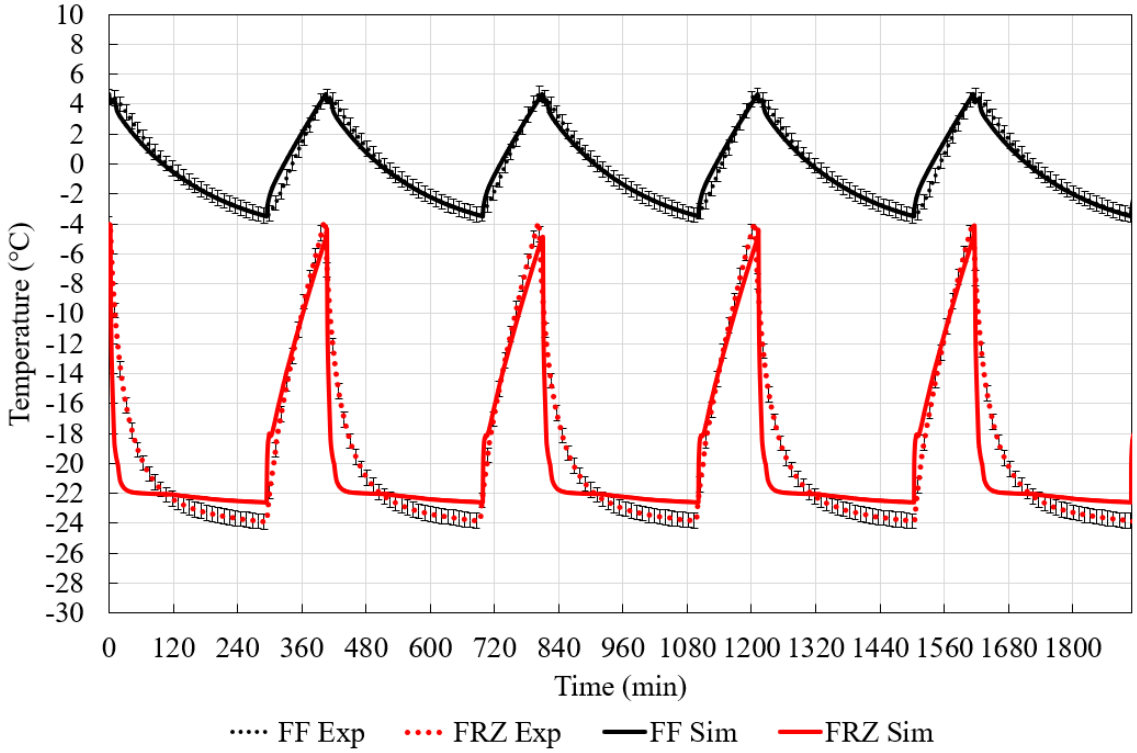

Figure 7.13. FF and FRZ Air Temperatures (variable speed compressor- 2000 rpm).

The air temperature deviation for FRZ in this case is a maximum of 4 °C for FRZ, while it is 1 °C for FF. The air inside the FRZ compartment shows a greater deviation because the lower compressor speed leads to a lower cooling capacity, which means that the evaporator temperature drops even more slowly than in the previous cases. This affects the FRZ compartment more than the FF because the FRZ has a greater heat gain and therefore cannot drop as quickly as it did when the speed was greater. This slower drop is not well captured by the model, leading to the aforementioned 4 °C difference.

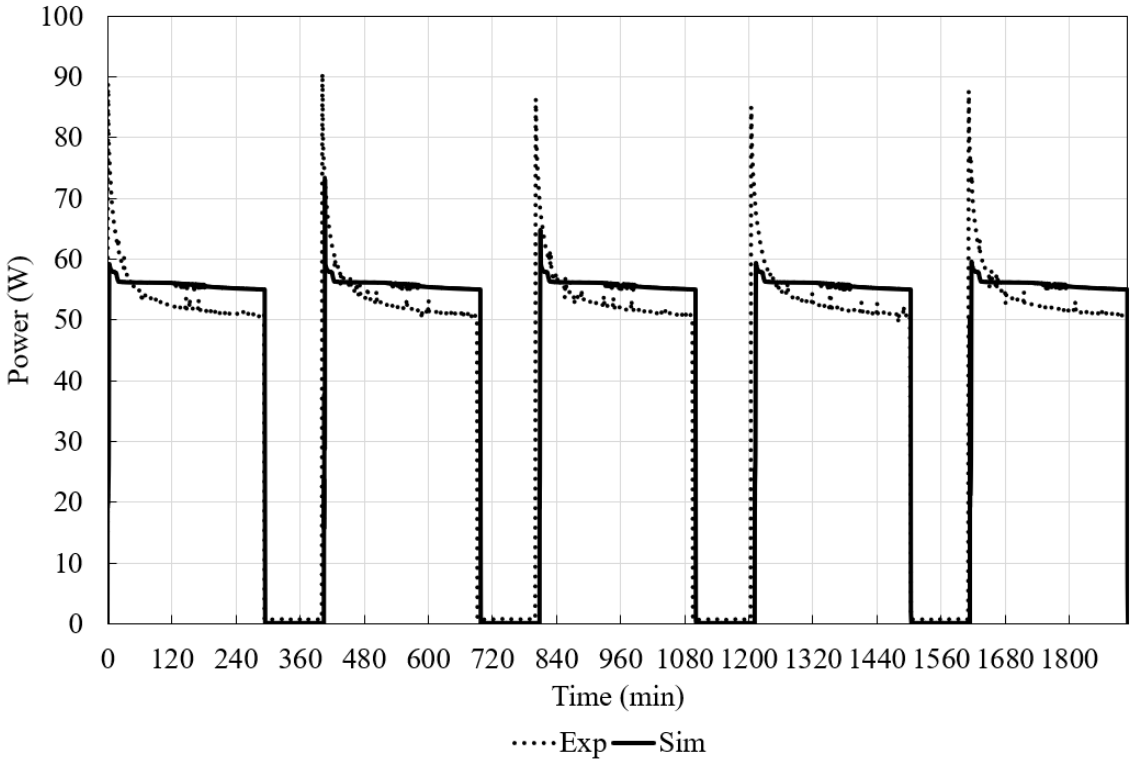

Figure 7.14. Compressor Power Consumption (variable speed compressor- 2000 rpm).

Table 7.5. Comparison of Runtime, Power and Energy (variable speed compressor- 2000 rpm).

		Experiment	Simulation	Difference
Time (min)	ON	296.7	293.8	-2.9 min
	OFF	108.7	110.3	1.6 min
Run Time	-	0.732	0.727	-0.7%
Power (W)	ON	53.9	55.8	3.5%
	OFF	0	0	0.0%
Energy (Wh/24h)	-	946.7	973.6	2.8%

The model shows a run time of 72.7%, only 0.7% lower than the experimental value of 73.2%. At this low a speed, it is not a surprise that the run time is very high. This occurs due to the long compressor on time (110 minutes!) caused by the lower cooling capacity at the lower compressor speed. The power consumption is also lower, with the simulation

reporting 55.8 W (deviating by 3.5% from the experimental value of 53.9 W). The final energy values are 946.7 Wh/24h and 973.6 Wh/24h for experiment and simulaiton respectively.

7.4. Water Pot Test Results

Figures 7.15-7.18 show the FF air temperature, FRZ air temperature, FF water temperature and power consumption graphs for the test.

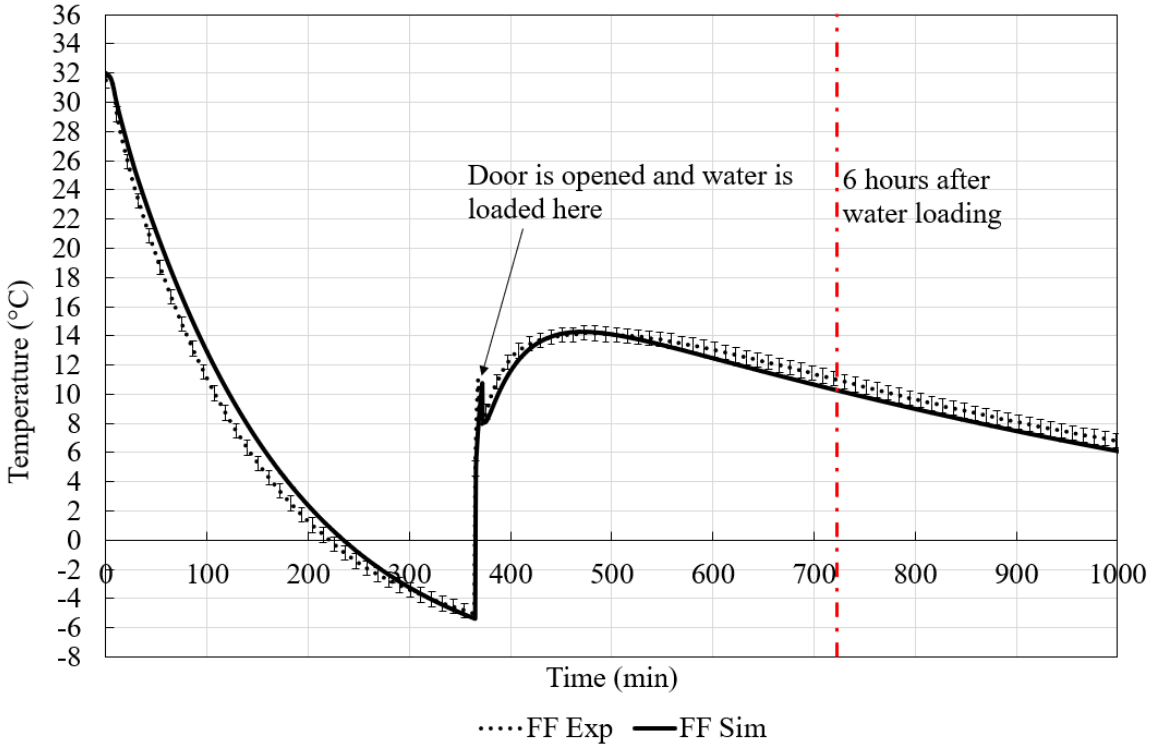

Figure 7.15. FF Air Temperature for the Water Pot Test.

It can be seen from the graph above that the refrigerator is left to cool down until 365 minutes (~6 hours), upon which the door of the FF compartment is opened, and water load is placed inside. A peak is reached, which is also captured by the simulation, as heat is gained rapidly by the Fresh Food compartment. The door is closed, and the warm water load then causes the air temperature to rise further. The temperature peaks at 14 °C, whereafter it starts to cool down again. After 6 hours, the air temperature in the simulation is 10.2 °C, while that

of the experiment is 10.9 °C. Also, the overall deviation throughout the test is 2 °C, occurring during the initial unloaded pull down. Considering the thermocouple uncertainly of 0.5 °C, these results are quite acceptable.

Again, as with the air temperatures for the cyclic case, this deviation can be mainly attributed to the lumped approximation of the air inside the FF cabinet.

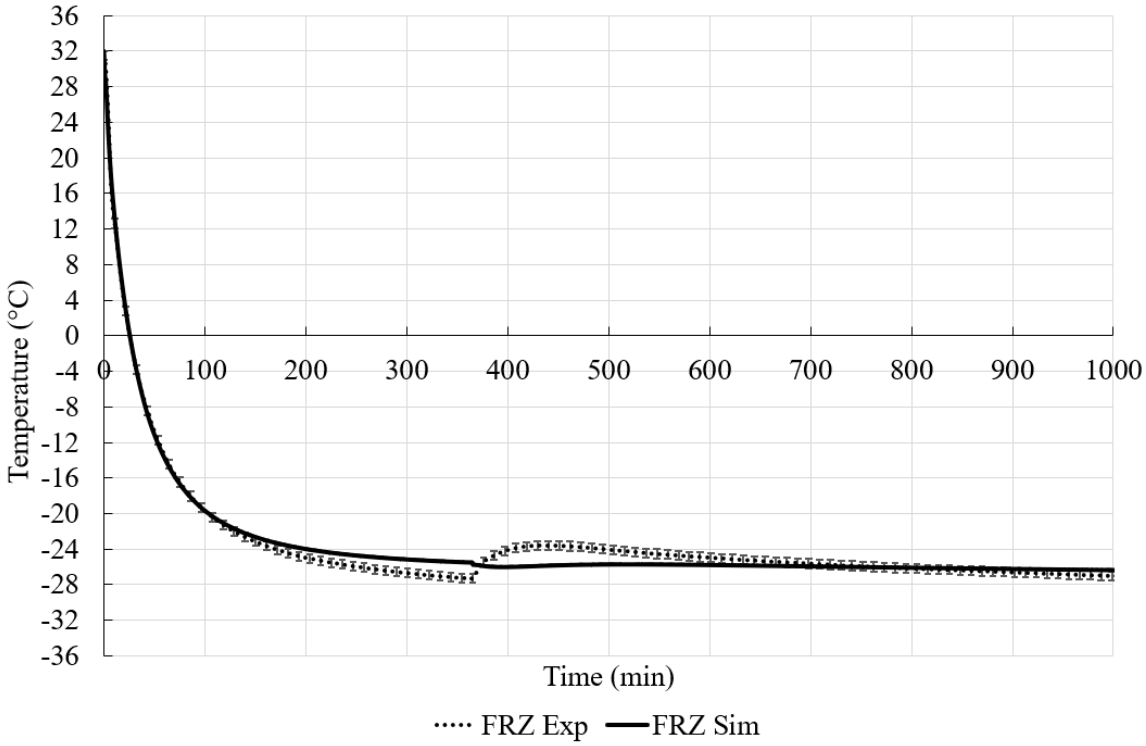

Figure 7.16. FRZ Air Temperature for the Water Pot Test.

Figure 7.16 shows the results for the FRZ air temperature. Up until approximately 150 minutes, the two curves are almost exactly the same. Then the curves start to diverge, with the experimental values being colder than those in the simulation by a maximum of 1.6 °C at the 365th minute. This can be attributed to the lumped air approximation in the model, as the bottom area of the cabinet does become colder due to buoyancy upon reaching steady state (cold air sinks towards the bottom). This colder bottom area causes the overall average temperature to drop.

After 6 hours, as mentioned above, water is placed inside the Fresh Food compartment. Although the door of the FRZ compartment is not opened, the FRZ air temperature starts to rise. This happens because the evaporator temperature in the FF compartment rises, and since the refrigerator is based on a serial cooling system, the temperature of the refrigerant in the FRZ compartment rises too, since the same refrigerant flows in both the compartments. In the real case, the evaporator in the FRZ is directly attached to the walls of the FRZ, which causes the walls and consequently the air inside to rise steeply. In the simulation, the evaporator is treated as a separate tube, causing no rise in the temperature.

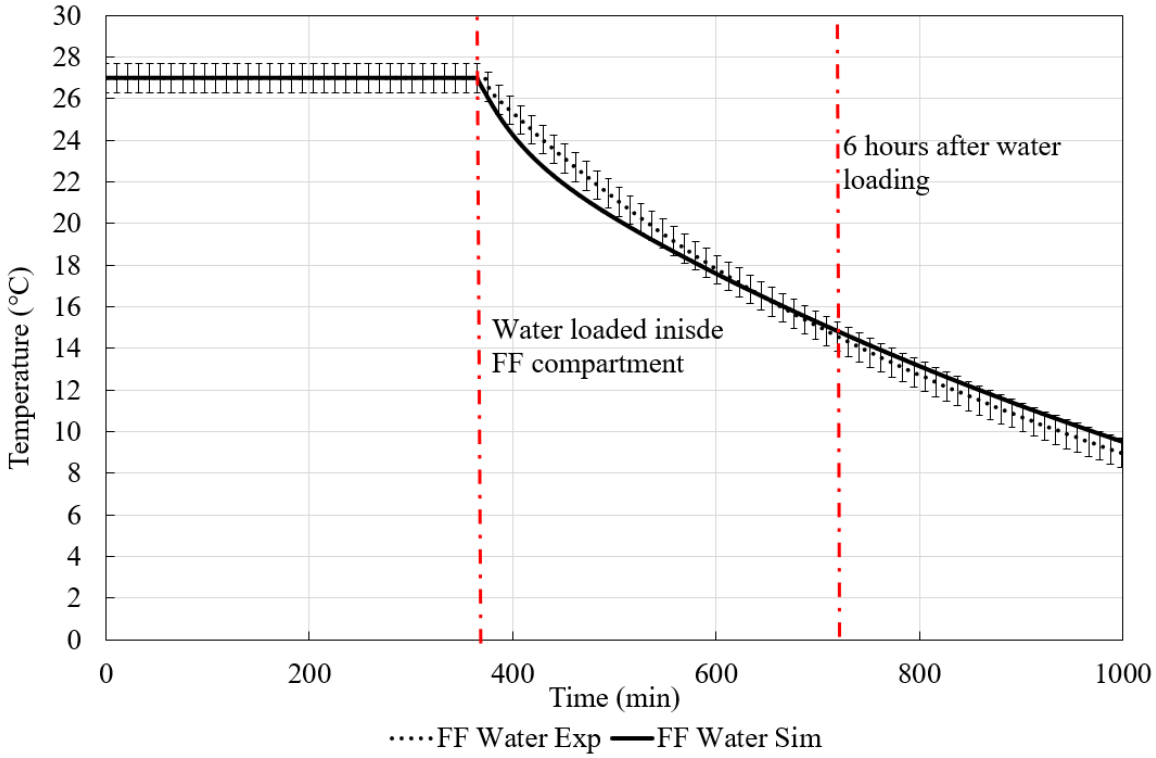

Figure 7.17. FF Water Temperature for the Water Pot Test.

At the 365th minute, that is, after about 6 hours of unloaded pull down, water at 27 °C is placed inside the cabinet. The maximum deviation in water temperature is 1.2 °C for the whole test. After 6 hours, the experimental and simulation values are exceedingly similar, being 14.2 °C and 14.7 °C respectively, the difference being exactly equal to the thermocouple uncertainty!

The maximum deviation of 1.2 °C occurs around the 450th minute. The primary cause of this is once again the lumped mass approximation used in the simulation. As Figure 6.11 showed, 4 water containers are placed close together inside the refrigerator. Nevertheless, some variation of temperature is to be expected, both within each container as well as across all the containers. This slight deviation, however, is hardly a problem, especially while evaluating the cooling performance using this test, in which the temperature after a predefined time (for example 6 h) is more important.

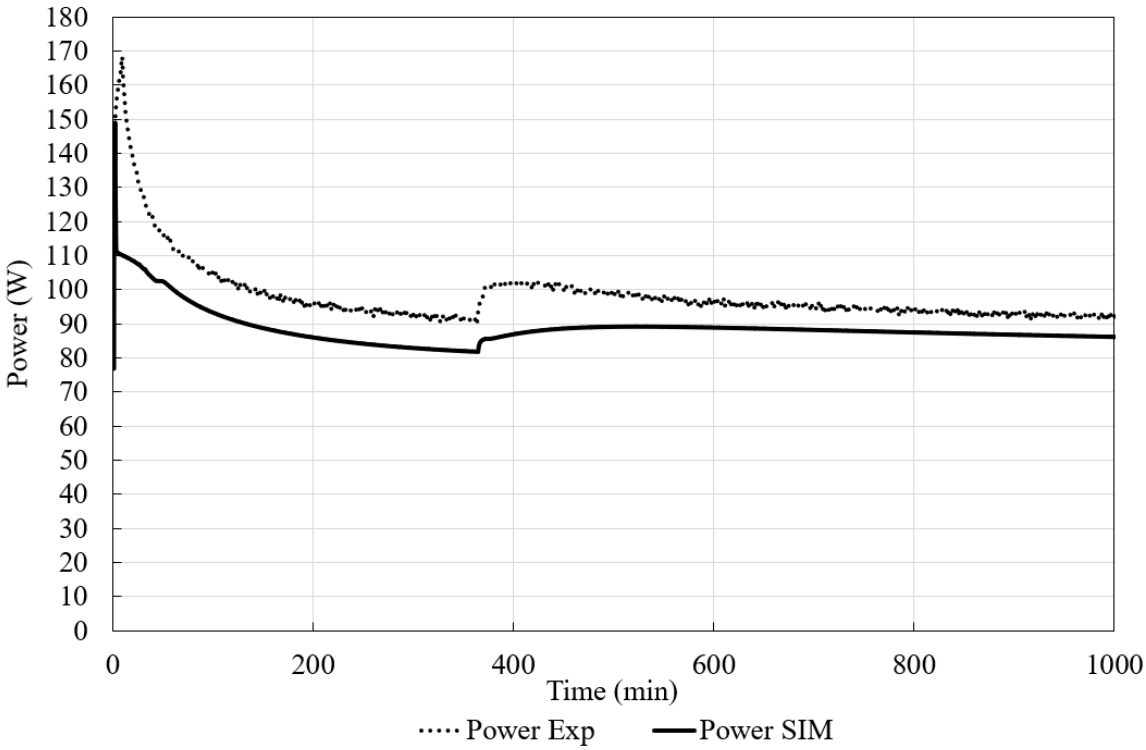

Figure 7.18. Compressor Power Consumption for the Water Pot Test.

Finally, the graph in Figure 7.18 shows the compressor power consumption. Note that the same fixed speed compressor as the one used in the initial cycle validation was used in this water pot experiment too. The simulation does capture the general characteristic, with the maximum deviation in the average power consumption during unloaded pull down (first 6 hours) being 12.5%. In the next stage (loaded pull down; from 365 minutes to 1000 minutes) the deviation is 5.5%. However, a striking feature is that the simulation is constantly understating the power value compared to the experiment. This happens because of the lower evaporation temperature. As explained in the previous discussion for cyclic

tests, the evaporation temperature develops much quicker in the model compared to the experiment, since the evaporator is treated as a tube in the model, which allows the evaporator to reach the final evaporation temperature very quicky. This causes the power consumption to decrease as well (recall: lower evaporation temperature leads to lower mass flow rate, which in turn leads to lower power consumption). Another point to note is the peak at the 365th minute. The peak in the dotted curve for experiment is steeper compared to the one in the simulation. This happens because the evaporator temperature rises more quickly compared to the simulation (again, due to the direct heat gain the evaporator faces in the experiment).

8. CONCLUSION

A top-mounted, serial system convectional refrigerator was modelled in this study by creating a sub-model for each component present in the refrigerator and then combining all the models into a refrigeration cycle. The TIL library in Dymola, based on the programming language Modelica, was used to carry out the modelling.

The cyclic state of the refrigerator was simulated for two different ambient temperatures and validated using experiments carried out in a climate chamber. To test the sensitivity of the model to a different compressor run at different compressor speeds, a variable speed compressor was used to simulate the model at three different speeds. Validation was carried out again, and the results were indeed very close.

As a second part of the thesis, the cabinet model was modified to take into account the effect of loading a warm load of water into the Fresh Food compartment and simulate the "loaded pull down". The effect of door opening was also included in the model. Again, validation was carried out by performing experiments, and the results showed less than 2 °C difference in the air and water temperatures.

Some key takeaways from this study, which were elaborated upon in Chapter 7 are listed as follows:

- The slight difference in air temperatures and water temperature (~2-3 °C) occurs due to the lumped approximation method
- The evaporator temperatures in the model reaches the actual steady state evaporation value almost instantaneously, compared to the real case, in which there is a time lag. This lag occurs because the real evaporator is attached directly to the wall of the compartments, causing a rapid heat gain through the wall and thus a more gradual temperature drop. Another cause is the time taken by the refrigerant to completely fill the evaporator.

- This difference in evaporation causes the power values in the model to reach the final value much quicker compared to the experiment and leads to the slight deviation in power
- The run time is very well captured by the model for all cases (except at 25 °C, where the maximum deviation is 9.6%). The energy values are also in very good agreement, with a maximum deviation of 5% which occurred for the variable speed compressor operated at 3000 rpm.
- The loaded pull down simulation is also in excellent agreement with experiment, with a deviation of 1.2 °C for water temperature. The major cause can be attributed to the lumped mass approximation of water.

This model can be used as a basis for future studies in which the evaporator may be modelled in more detail, so that the lag in evaporator temperature may be captured. Also, a discretised cabinet model may be created, so that the spatial variation in air temperature can be modelled as well. The model may also be used to optimise the algorithm of a refrigerator. Finally, frost accumulation on the evaporator and cabinet inner walls (especially the Freezer compartment) may also be studied in the future by extending this model to create more sophisticated ones.

REFERENCES

1. Choi, S., U. Han, H. Cho and H. Lee, “Review: Recent advances in household refrigerator cycle technologies”, *Applied Thermal Engineering* 132, pp 560–5746, 2018.

2. Diniz, M.C., C. Melo and C.J. Deschamps, “Experimental performance assessment of a hermetic reciprocating compressor operating in a household refrigerator under on–off cycling conditions”, *International Journal of Refrigeration* 88, pp 587-598, 2018.

3. Yan, G., G. Liu, M. Zhou and J. Yu, “Experimental research on configuration optimization of a frost-free refrigerator-freezer with the parallel circuit cycle”, *International Journal of Refrigeration,* 2020.

4. Tosun, T. and M. Tosun, “Heat exchanger optimization of a domestic refrigerator with separate cooling circuits”, *Applied Thermal Engineering* 168, pp 114810, 2020.

5. Fatouh, M. and H.A. Ziyan, “Energy and exergy analysis of a household refrigerator using a ternary hydrocarbon mixture in tropical environment – Effects of refrigerant charge and capillary length”, *Applied Thermal Engineering* 145, pp 14–26, 2018.

6. Fatouh, M. and H.A. Ziyan, “Transient and cyclic characteristics of a household refrigerator using ternary hydrocarbon mixture – An experimental investigation”, *Applied Thermal Engineering* 129, pp 446–462, 2018.

7. Harrington, L., L. Aye and B. Fuller, “Impact of room temperature on energy consumption of household refrigerators: Lessons from analysis of field and laboratory data”, *Applied Energy* 211, pp 346–357, 2018.

8. Choi, Y., B. Min, H. Kim and G.M. Choi, "Experimental Study on Effects of Lubricant Oil in a Domestic Refrigerator-Freezer", *17th International Refrigeration and Air Conditioning Conference at Purdue,* 2018.

9. Azzouz, K., D. Leducq and D. Gobin, "Performance enhancement of a household refrigerator by addition of latent heat storage", *International Journal of Refrigeration* 31, pp 892-901, 2008.

10. Ding, G., "Recent developments in simulation techniques for vapour-compression refrigeration systems", *International Journal of Refrigeration* 30, pp 1119-1133, 2007.

11. Flores, J.M.B., J.M.B. Maldonado, A.P.R. Muñoz and G.C. Vázquez, "Enhancements in domestic refrigeration, approaching a sustainable refrigerator – A review", *Renewable and Sustainable Energy Reviews* 51, pp 955–968, 2015.

12. Davis, L. and T.C. Scott, "Component, Modeling Requirements for Refrigeration System Simulation", *International Compressor Engineering Conference*, Paper 221. https://docs.lib.purdue.edu/icec/2211976, 1976.

13. Chen, L., F. Sun, C. Wu and R.L. Kiang, "A Generalized Model of a Real Refrigerator and its performance", *Applied Thermal Engineering* 17, pp 401-412, 1996.

14. Gupta, J.K., M.R. Gopal and S. Chakraborty, "Modeling of a domestic frost-free refrigerator", *International Journal of Refrigeration* 30, pp 311-322, 2007.

15. Hermes, C.J.L., C. Melo, F.T. Knabben and M. Gonçalves, "Prediction of the energy consumption of household refrigerators and freezers via steady-state simulation". *Applied Energy* 86, pp 1311–1319, 2009.

16. Gonçalves, J.M., C. Melo and C.J.L. Hermes, "A semi-empirical model for steady-state simulation of household refrigerators", *Applied Thermal Engineering* 29, pp 1622–1630, 2009.

17. Ding, G., C. Zhang and Z. Lu, "Dynamic simulation of natural convection bypass two-circuit cycle refrigerator–freezer and its application. Part I: Component models", *Applied Thermal Engineering* 24, pp 1513–1524, 2004.

18. Lu, Z., G. Ding and C. Zhang, "Dynamic simulation of natural convection bypass two-circuit cycle refrigerator–freezer and its application. Part II: System simulation and application", *Applied Thermal Engineering* 24, pp 1525–1533, 2004.

19. Hermes, C.J.L. and C. Melo, "A first-principles simulation model for the start-up and cycling transients of household refrigerators", *International Journal of Refrigeration* 32, pp 1341-1357, 2008.

20. Hermes, C.J.L. and C. Melo, "Assessment of the energy performance of household refrigerators via dynamic simulation", *Applied Thermal Engineering* 29, pp 1153–1165, 2009.

21. Bruno, B., C. Hermes, C. Melo and G. Goncalves, "Transient Simulation of Household Refrigerators: A Semi-Empirical, Quasi-Steady Approach". *International Refrigeration and Air Conditioning Conference*. Paper 1018. http://docs.lib.purdue.edu/iracc/1018, 2010.

22. Lin, E., G. Ding, D. Zhao, Y. Liao, N. Yua and J. Yamashita, "Dynamic model for multi-compartment indirect cooling household refrigerator using Z-transfer function based cabinet model", *International Journal of Thermal Sciences* 50, pp 1308-1325, 2011.

23. Bergera, E., S. Poscha, M. Heimela, R. Almbauera, M. Eichingera and A. Stupnik, "Transient 1D heat exchanger model for the simulation of domestic cooling cycles working with R600a". *Science and Technology for the Built Environment*, DOI: 10.1080/23744731.2015.1057084, 2015.

24. Heimel, M., E. Berger, S. Posch, A. Stupnik, J. Hopfgartner and R. Almbauer, "Transient cycle simulation of domestic appliances and experimental validation", *International Journal of Refrigeration* 69, pp 28-41, 2016.

25. Egger, A., B. Zuber, M. Rohrhofer, J. Hopfgartner, R. Almbauer and E. Perz, "Dynamically Calibrated Simulation of a Refrigeration Cycle for Household Freezers", *17th International Refrigeration and Air Conditioning Conference at Purdue*, July 9-12, 2018.

26. Heinrich, C. and K. Berthold, "A Modelica Library for Simulation of Household Refrigeration Appliances Features and Experiences", The Modelica Association, *Modelica 2006*, September 4th – 5th, 2006.

27. Avcı, H., D. Kumlutaş, Ö. Özer and M. Özşen, "Optimisation of the design parameters of a domestic refrigerator using CFD and artificial neural networks", *International Journal of Refrigeration* 67, pp 227-238, 2016.

28. Bayer, O., R. Oskay, A. Paksoy and S. Aradag, "CFD simulations and reduced order modeling of a refrigerator compartment including radiation effects", *Energy Conversion and Management* 69, pp 68–76, 2013.

29. Laguerre, O. and D. Flick, "Temperature prediction in domestic refrigerators: Deterministic and stochastic approaches", *International Journal of Refrigeration* 33, pp 41-51, 2010.

30. Arsenjev, S.L., I.B. Lozovitski and Y.P. Sirik, "The Flowing System Gasdynamics Part 3: Saint-Venant–Wantzel's formula modern form", Retrieved from https://arxiv.org/ftp/physics/papers/0302/0302038.pdf, 2003.

31. Gavin, H.P., *The Levenberg-Marquardt algorithm for nonlinear least squares curve-fitting problems,* Department of Civil and Environmental Engineering, Duke University, 2020.

32. Shah, M.M., “A General Correlation for Heat Transfer During Film Condensation Inside Pipes”, *International Journal of Heat and Mass Transfer* 22, pp 547-556, 1979.

33. ASHRAE Handbook of Fundamentals, Ref. 1, Chap. 22, Table 1.

34. Colebrook, C.F. and C.M. White, “Experiments with fluid friction in roughened pipes”, *Proceedings of The Royal Society A Mathematical Physical and Engineering Sciences* 161(906), pp 367-381, 1937.

35. Swamee, P.K. and A.K. Jain, “Explicit equations for pipe flow problems”, *Journal of Hydraulics Division* 102, pp 657-664, 1976.

36. Xu, B. and P.K. Bansal, “Non-adiabatic capillary tube flow: a homogeneous model and process description”, *Applied Thermal Engineering* 22, pp 1801–1819, 2002.

37. Wongwises, S and P. Chan, “Two-phase separated flow model of refrigerants flowing through capillary tubes”, *International Communications in Heat and Mass Transfer* 27-3, pp 343-356, 2000.

38. Khan, M.K., R. Kumar and P.K. Sahoo, “Flow characteristics of refrigerants flowing through capillary tubes – A review”, *Applied Thermal Engineering* 29, pp 1426-1439, 2008.

39. Apaydın, T., *Modelling for Refrigerant Flow Of R600a Through Diabatic Capillary Tube In Vapor Compression System*. Yıldız Technical University, 2016.

40. VDI Heat Atlas, 2nd Ed. 2010.

41. Ostrach, S., “Natural Convection in Enclosures”, *Advances in Heat Transfer* 8, pp 161-227, 1972.

42. Karatas, H. and T. Derbentli, “Natural convection and radiation in rectangular cavities with one active vertical wall”, *International Journal of Thermal Sciences* 123, pp 129-139, 2018.

43. Laguerre, O., S.B. Amara and D. Flick, “Experimental study of heat transfer by natural convection in a closed cavity: application in a domestic refrigerator”, *Journal of Food Engineering* 70, pp 523–537, 2005.

44. Laguerre, O. and D. Flick, “Heat transfer by natural convection in domestic refrigerators”, *Journal of Food Engineering* 62, pp 79–88, 2004.

45. Laguerre, O., S. Ben Amara, M. C. Charrier-Mojtabi, B. Lartigue and D. Flick, “Experimental study of air flow by natural convection in a closed cavity: Application in a domestic refrigerator”, *Journal of Food Engineering* 85, pp 547–560, 2008.

46. Cengel, Y., *Heat Transfer- A Practical Approach*, 2nd Edition, McGraw-Hill, New York, 2002.

47. Zhang, C. and Y. Lian. “Conjugate heat transfer analysis using a simplified household refrigerator model”, *International Journal of Refrigeration* 45, pp 210-222, 2014.